Università
Ca'Foscari
Venezia

Scuola Dottorale di Ateneo
Graduate School

Dottorato di ricerca
in Scienza e Gestione dei Cambiamenti Climatici
Ciclo 28
Anno di discussione 2016

A recent past temperature reconstruction based on oxygen and hydrogen stable isotopes in Alpine ice cores

SETTORE SCIENTIFICO DISCIPLINARE DI AFFERENZA: GEO/08
Tesi di Dottorato di Giuliano Dreossi, matricola 956001

Coordinatore del Dottorato

Prof. Carlo Barbante

Tutore del Dottorando

Prof. Carlo Barbante

Co-tutore del Dottorando

Prof. Barbara Stenni

INDEX

CHAPTER 3: THE STUDIED AREA

CHAPTER 4: INSTRUMENTAL DATA

CHAPTER 5: MATERIALS AND METHODS

Prologue

Climate change has become the major environmental concern on world scale of the last decades, threatening economy, health and safety, food production, security and other dimensions. The Alps have experienced a significant warming trend, roughly double the world average, and are particularly vulnerable to the consequences of a further temperature increase (EEA, 2009). Ice cores have been drilled in the Alpine region since the 1970s, but almost exclusively in the Western Alps, while the Eastern Alps potential remains virtually unexploited. To fill this gap, four ice cores were drilled at 3859 m on Mt. Ortles (South Tyrol, Italy) in autumn 2011, while several snow pits and two shallow firn cores were obtained from 2008 to 2014 in the same area. The estimated accumulation rate for the last fifty years is ~850 mm w.e./a; this datum, coupled with the discovery of a 2600-year old larix leaf at the bottom of the glacier, suggests the presence of a very long climatic record stored in the ice, made possible by the low accumulation rate and the exceptional thinning of the deep ice layers. Core #1 was processed and analyzed for water stable isotopes in the framework of this PhD project, while core #2 was processed and analyzed at the Byrd Polar and Climate Research Center (BPCRC) of the Ohio State University (Gabrielli, personal communication). The two 2014 snow pits were also analyzed during this PhD, while all the other Ortles glacial archives were analyzed at the BPCRC. The aim of this study is to reconstruct the climate variations of the region by means of water stable isotopes measurements in the Ortles cores, compared to other isotopic records from the Alps. An extensive temperature coverage is available for this area (Gabrielli *et al.*, 2010), starting from 1864, while an Automatic Weather Station (AWS) was installed in proximity of the drilling site in autumn 2011. Two temperature records from gridded-datasets (Palazzi, personal communication) were also compared to local temperatures to test the reliability of large-scale temperature reconstructions applied to Mt. Ortles. The isotopic records from deep cores shows a significant increase in the upper part, most probably due to the steep temperature increment. The availability of a good age scale for the deep cores, and the understanding of the temperature-isotope relation for this area, are the key factors to attempt a climatic reconstruction based on water stable isotopes in ice cores.

INTRODUCTION

I The state of the climate

Climate change is no longer just a scientific curiosity, and no longer just one of several environmental and regulatory concerns, but the major environmental issue of our time, and the biggest challenge facing environmental regulators (UNEP, 2010). It is extremely likely (95 % confidence) that human activity is the dominant cause of observed warming since the mid-20th century. Warming of the climate system is unequivocal and many of the observed changes are unprecedented over decades to millennia. The combined land and ocean surface temperature has increased by 0.85 °C (0.65-1.06 °C) over the period 1880-2012 (fig. I-1), the era for which reliable measurements are available. Each of the last three decades has been sequentially warmer at the Earth's surface than any preceding decade since 1850 (IPCC, 2014). 2014 was probably the warmest or at least tied-for-warmest year since temperature records began in the second half of the 1800s, depending on the minor differences between different datasets: global average surface temperature (land plus ocean) was 0.27-0.29°C above the 1981-2010 average, a period already affected by global warming. Concerning the land, the global average annual temperature for 2014 was 0.37-0.44°C above the 1981-2010 average, while oceans experienced an increment of 0.21-0.27°C compared to the same reference period (American Meteorological Society, 2015).

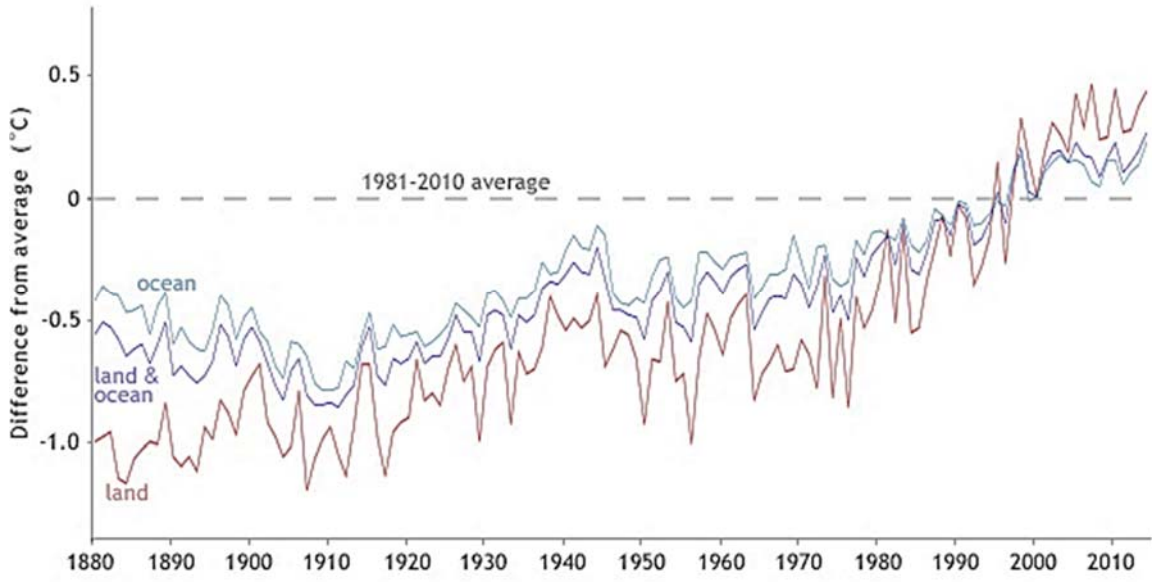

Fig. I-1 Land, ocean and combined global average annual temperature trend (1880-2014), credit to American Meteorological Society (2015)

Human activities have impacted on the Earth's energy budget by increasing the emissions and the resulting atmospheric concentrations of radiatively important gases (greenhouse gasses, GHG), aerosols and by changing land surface properties (IPCC, 2014).

Regardless of a growing number of climate mitigation measures, global anthropogenic GHG emissions have increased continuously between 1970 and 2010, reaching the highest level in the history of humanity in the decade 2000-2010. In 2010, CO_2 accounted for 76 % of total GHG emissions (65 % due to fossil fuel combustion and industrial processes and 11 % associated to land use), CH_4 for 16 %, 6 % came from N_2O and 2 % from fluorinated gases (IPCC, 2014). Ice core measurements suggest that present-day carbon dioxide concentration is the highest of the last 800,000 years; other proxies indicate that CO_2 last approached 400 ppm about 3 to 5 million years ago, when global average surface temperature is estimated to have been about 2 to 3.5°C higher than in the pre-industrial period. (NAS and RS, 2014). Since the Industrial Revolution, human activities have caused the atmospheric carbon dioxide concentration to increase by more than 40 %. Globally, the growth rate of carbon dioxide has dramatically raised from about 0.6 ppm/a in the early 1960s to an average of 2 ppm/a during the last 10 years, reaching a mean annual value, for 2014, of 398.6 ppm. On April, May and June 2014, mean monthly carbon dioxide concentrations topped 400 ppm (American Meteorological Society, 2015).

It is important to understand the difference between weather and climate: weather is defined by the atmospheric conditions (temperature, pressure, humidity, wind, and other parameters) at a certain place and time; climate is normally defined as the average weather, or more rigorously, as the statistical description in terms of the mean and variability of relevant quantities (temperature, precipitation, wind) over a period of time ranging from months to thousands or millions of years (IPCC, 2014).

Climate change is a complex issue, spreading among economic, health and safety, food production, security and other dimensions. Climate change is also a serious threat to poverty reduction and could nullify decades of development efforts. Poor countries are more vulnerable because of their high dependence on natural resources and inadequate capacity to cope with climate variability and extremes (UNEP, 2010). Climate change is "the defining challenge of our generation".

Climate change has been one of the most discussed topic of the last decades, with an increasing attention given by both the masses and the scientific community. 7.37 billion people live today on our planet, and some of the most densely populated areas are highly vulnerable to the effects of increasing temperatures. Many developing countries do not have the needed resources to adapt to the changing climate, while the first world is still struggling to find an agreement concerning an effective plan of emission reduction in order to mitigate the warming.

II Present time and future scenarios

The observed temperatures from instrumental records (fig. II-1) have been increasing throughout the last century in the most part of the earth (IPCC, 2014).

Regarding the European continent, a higher-than-the-global-mean increase in annual mean temperature is predicted by model projections: the most consistent warming is expected during winter in Northern Europe and during summer in Southern Europe (IPCC, 2007). Precipitation would probably intensify in Northern Europe and decrease in the Mediterranean region, increasing the frequency of summer droughts. Concerning the snow season, an overall shortening is expected, and snow depth should decrease over most Europe (IPCC, 2007).

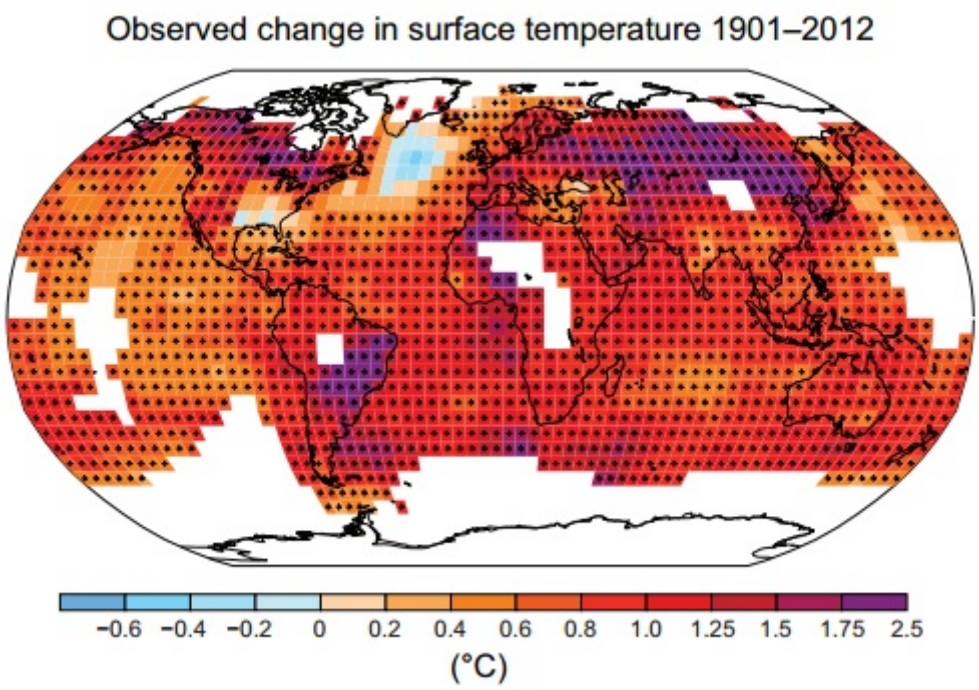

Fig. II-1 Map of the observed surface temperature changes from 1901 to 2012, obtained from temperature trends determined by linear regression. White areas were excluded for having less than 70 % complete records or less than 20 % data availability in the first and last 10 % of the time period. The + sign indicates grid boxes in which the trend is significant at the 10% level (IPCC, 2014)

Giorgi and Coppola (2007) discovered the "European climate-change oscillation" (ECO) under the IPCC Fourth Assessment Report A1B scenario (CO_2 reaching 700 ppm by 2100). Between 2071 and 2100 (reference period: 1961-1990), mean surface air temperature should show a mild-to-severe increase during wintertime, more pronounced in eastern continental Europe and less in the Atlantic and Mediterranean sectors. During summer months temperature should increase more

in southern Europe and less in the central-northern part, but an overall increment is predicted for the whole continent in each time of the year. For mean precipitation, predictions show a bipolar behavior between southern Europe (decrease) and northern Europe (increase) during winter, while in summertime, the equilibrium line (no change) should move northward and most of the continent is expected to experience less precipitation.

An altitudinal amplification of the warming trend has been observed in different mountain regions, with an average decrease of the surface mean temperature lapse rate of 0.2°C per km of altitude over the last 50 years; this effect is likely associated to the effective moist convection (Wang *et al*., 2014).

During the last decades, changes in climate have impacted on natural and human systems on all continents and oceans. Changes in extreme weather and climate events have been observed since about 1950 (IPCC, 2014).

III Climate change vulnerability

In the map below (fig. III-1), 192 world countries are ranked considering their vulnerability and readiness to cope with climate change for the year 2013; the higher the score, the better they would fare. It has been created by the London-based company Eco Experts, using the ND-GAIN (the Notre Dame of Indiana Global Adaptation) index.

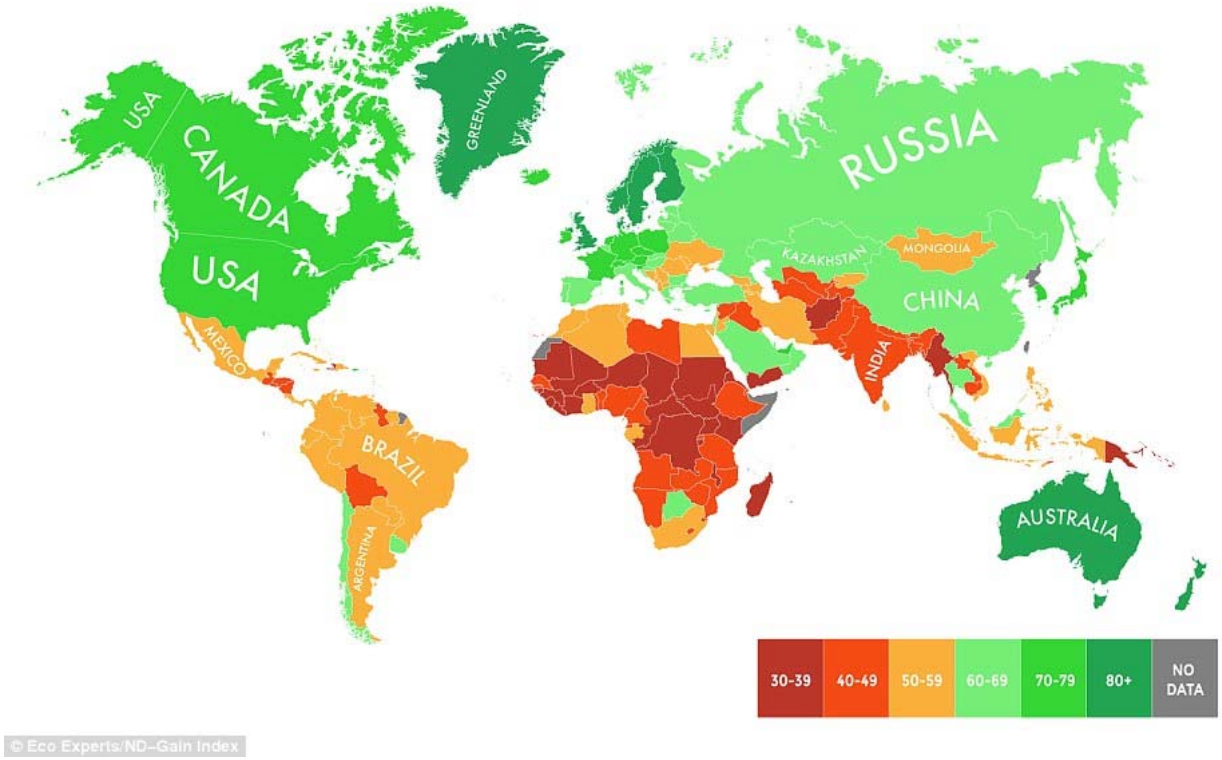

Fig. III-1 Ranking of 192 countries based on how well they would cope with climate change (Eco Experts)

Europe, on average, scores pretty well, and so does North America, but almost the entire African continent and South Asia seem prone to warming-induced natural disasters, being also poorly equipped to face the consequences.

The ND-GAIN index map looks quite similar to the 2013 gross domestic product (GDP) per capita world map (fig. III-2), showing how individual wealth plays a role regarding the capacity to cope with climate change; conversely, the total 2013 GDP world map (III-3) does not correlate as well with the ND-GAIN index map.

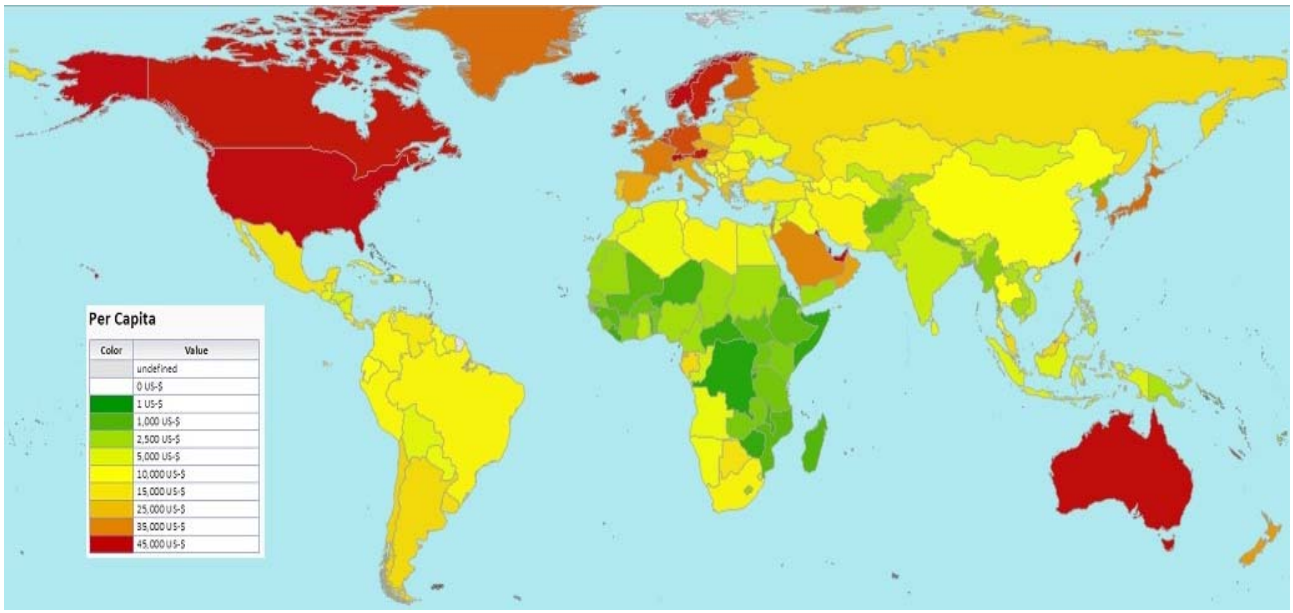

Fig. III-2 2013 Gross domestic product per capita (http://world.bymap.org/)

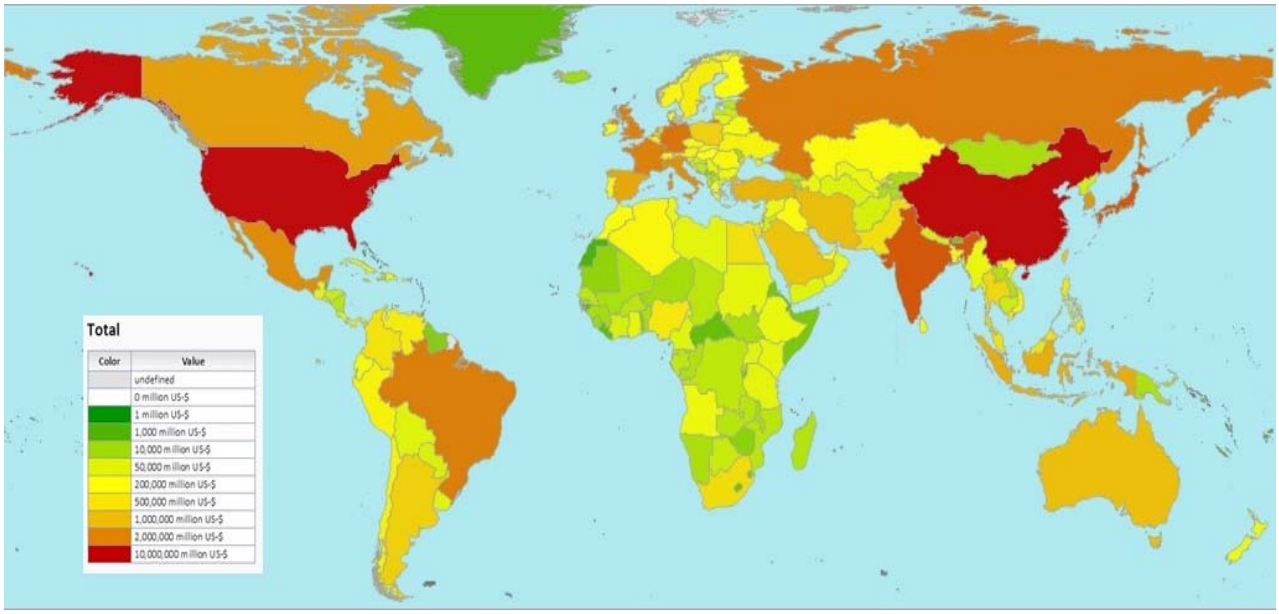

Fig. III-3 2013 Total gross domestic product (http://world.bymap.org/)

IV Instrumental data and natural archives

Most instrumental observations of meteorological parameters have started in the mid-19th century, contemporary to the supposed beginning of the anthropogenic forcing (IPCC, 2007). In order to

lengthen the climatic information further back in time, and to better separate human influence from nature-induced variability, additional data have to be obtained using climate proxies: parameters extracted from natural archives that are linked to climate variables and can be used to indirectly measure those variables. Proxies obtained from natural archives can provide information about past temperature, humidity, precipitation, greenhouse gas concentrations and solar radiation. Each natural archive and its proxies has advantages and disadvantages. In paleoclimate research, the study of the past temperature is among the most investigated aspects.

Many natural archives can be used to reconstruct the climate of the past: tree rings, speleothems, corals, marine and lacustrine sediments and ice cores are commonly utilized for this purpose. Each of these archives contains one or more climate proxies. The time span covered by these proxies ranges from few decades to millions of years, and it is usually inversely proportional to the temporal resolution that they provide. The proxy record distribution, similar to the instrumental record, is strongly non-uniform, with more data coming from the northern hemisphere.

The main goal of this study is to extend the climate information of the high-elevation Eastern Alps beyond the instrumental data era, providing a qualitative reconstruction of temperature variations interpreting the isotope records from the Ortles ice cores, and comparing these data to other records from the Alpine region and to a temperature dataset for the entire Alps mountain range, with the intent to test the spatial representativeness of this climate archive. The aim of this work is also to understand the effects of post-depositional processes on the isotope signal of settled snow, and how the pristine isotopic content of precipitation is modified by them. Classically, stable isotope records from ice cores are interpreted as reflecting precipitation-weighted temperature signals, ignoring the exchanges between the surface snow and atmospheric water vapor (Persson *et al*., 2011), as well as the exchanges between snow and meltwater. However, the impact of these processes on the isotope-temperature reconstruction is not yet adequately understood, but fundamental to constrain (Ebner *et al*., unpublished).

CHAPTER 1: ISOTOPE GEOCHEMISTRY

1.1 The hydrological cycle

Water constitutes 0.4 % of the Earth's mass, and about 17 % of the total H_2O is free; of this free water, 96 % is salty water forming the oceans. Considering the remaining 4 % of freshwater, almost 70 % is stored in form of ice: this is the biggest sink of freshwater by far. Glacier ice now covers about 10 % of land surface on earth, but the figure was three times higher during ice ages. Only 1 % of glaciated areas are not far away from human settlements, while the most part sits in Greenland and Antarctica (Paterson, 1994).

The hydrological cycle (fig. 1.1-1) is driven by solar radiation and it is responsible for the moderate temperature on our planet, permitting the spread of life on it. This is due to the extraordinary heat capacity of water, higher than any other liquid or solid substance. The cycle also provides water for carbon fixation by photosynthetic organisms and plays an important role in distributing the nutrients and making them available for the uptake.

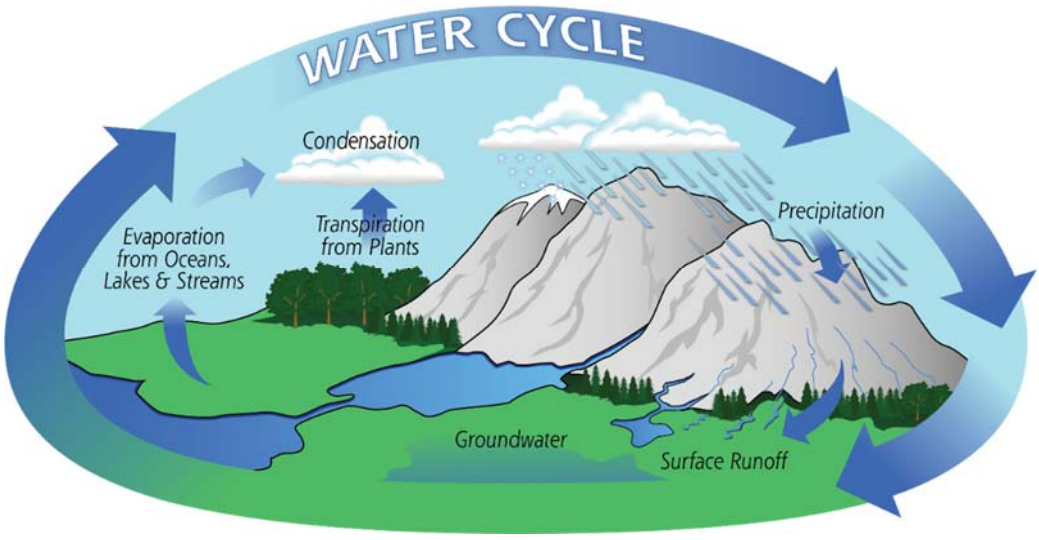

Fig. 1.1-1 The water cycle scheme (credit: www.nasa.gov). The shape reproduces the form of a falling raindrop

Solar energy is the key factor of the water cycle, being the force behind water phase changes, such as evaporation, condensation and sublimation; since solar radiation heats the Earth's surface dishomogeneously, it creates energy unbalances, leading to temperature gradients that are behind air/moisture mass and ocean currents. The evaporation from the ocean surfaces constitutes the major part of the surface-to-atmosphere exchange; oceans cover over 70 % of the Earth's surface,

giving the opportunity for such large-scale evaporation to occur. Evapotranspiration includes evaporation from the ground and transpiration from plants, in the latter, moisture flows through plants from the roots to the photosynthetic part, evaporating from the small pores called stomata, placed on the downside of leaves.

1.2 Isotopes

Atomic nucleus is made by protons and neutrons bound together by the residual strong force. Since protons have a positive charge, they repel each other. Neutrons, which have a neutral charge, act as stabilizers of the nucleus in two ways: pushing protons slightly apart, reducing the electrostatic repulsion between them, and exerting the attractive nuclear force on each other and on protons. At least one neutron is necessary for two or more protons to bind into a nucleus. As the number of protons increases, so does the neutrons to protons ratio necessary to ensure stability.

Isotopes are atoms of the same element characterized by an identical numbers of protons and electrons but having a different amount of neutrons; different isotopes of an element occupy the same position on the periodic table. The difference in the neutron number between the various isotopes of an element implies they have similar charges but different masses.

Nuclear processes occurring within the stars are the cause of the original isotopic content of the universe. On Earth, isotope abundance is the result of the processes of radioactive decay, cosmic ray interactions, as well as anthropogenic activities like nuclear fuels processing, reactor accidents, and nuclear weapons testing.

Radioactive isotopes have unstable nuclei that spontaneously decay over time to form other atoms. During the process, radioactive isotopes emit radiations in form of alpha or beta particles or gamma rays. The so-called stable isotopes are nuclei that do not appear to decay on geological timescales. The different isotopes of a certain element have slightly different chemical and physical properties thanks to their mass differences. When the atomic number is low, such mass differences are enough for many physical, chemical, and biological processes to "fractionate" or change the relative proportions of various isotopes. Two different types of processes, equilibrium and kinetic isotope effects, cause isotope fractionation.

In 1914, J. J. Thomson discovered the first proof for multiple stable isotopes of an element. He channeled streams of neon ions through a magnetic and an electric field and measured their deflection by placing a photographic plate on their path; each stream produced a glowing patch on the photographic plate at the point of the impact. Thomson noticed two separate patches on the photographic plate, suggesting two different trajectories of deflection: he eventually found out that

some of the atoms in the neon gas had higher mass than others. The reason why isotopes exist was, however, not clear until by Chadwick discovered the neutron, in 1932.

After hydrogen and helium, oxygen is the third most abundant element in the universe and the most abundant in the Earth's crust (SAHRA, 2005). Oxygen presents three natural stable isotopes. Oxygen-16 (or ^{16}O) is the most abundant (99.762 %) and contains eight neutrons; oxygen-18 has ten neutrons and constitutes the 0.201 % of total oxygen, while oxygen-17 possesses nine neutrons and is quite rare: 0.039 %. Other than these stable isotopes, fifteen other short-lived oxygen radioisotopes exist; most of them have a half-life of few seconds, the most stable among these radioisotopes is oxygen-15, with a half-life of 122 seconds (EnvironmentalChemistry.com, 2007). The most part of ^{16}O is formed in massive stars at the end of the helium fusion process, while a smaller portion is produced in the neon burning process. ^{17}O is mainly produced by the burning of hydrogen into helium, hence it is common in the hydrogen burning zones of stars. Oxygen-18 is produced by ^{14}N capturing a ^{4}He nucleus; ^{18}O is therefore common in the helium-rich zones of evolved massive stars (Meyer, 2007). Any compound that incorporates oxygen into its chemical structure is characterized by a ratio of ^{18}O:^{16}O. We can measure the ratio of these isotopes.

Hydrogen is the lightest element on the periodic table and the most abundant of the universe. It has two stable isotopes: hydrogen (^{1}H or protium, given its single proton in the nucleus) and deuterium (^{2}H or D); the most common hydrogen atom, ^{1}H, has a relative abundance of 99.985 % and contains no neutrons. Deuterium is quite rare (0.015 %) and has one neutron. Tritium (^{3}H or T), with two neutrons, is only presents in traces on Earth and has a half-life of 12.32 years; it decays in helium-3 via β^- decay (EnvironmentalChemistry.com, 2007). On planet Earth it is produced by cosmic rays interacting with atmospheric gases; the most frequent reaction involves a fast neutron (its energy has to be greater than 4.0 MeV) interacting with atmospheric nitrogen (^{14}N), forming $^{12}C + {}^{3}H$. The global production of tritium from natural sources is quite constant: around 148,000 terabecquerels/a (Young and Foster, 1972). Tritium is artificially produced during nuclear reactions, as a by-product in nuclear reactors: an uncommon product of the nuclear fission of uranium-235, plutonium-239, and uranium-233, or when deuterium captures a neutron in heavy water-moderated reactors. It can be created on purpose in special production reactors, where the isotope lithium-6 (or lithium-7) is bombarded with neutrons to produce tritium (Serot *et al*., 2005).

Heavier and highly unstable isotopes, such as ^{4}H or ^{7}H, can be artificially produced but does not exist in nature (Gurov *et al*., 2004). Atomic mass differences lead to different physicochemical properties; the effect is stronger for elements having a low atomic number, like hydrogen: the mass ratio of D/H is equal to 2, while oxygen $^{18}O/^{16}O$ mass ratio is equal to 1.125.

The existence of oxygen-17 and oxygen-18 was discovered by Johnston and Giauque in 1929, while few years later (1939) Urey discovered deuterium. Physicists Ernest Rutherford, M. L. Oliphant, and Paul Harteck discovered tritium in 1934.

These oxygen and hydrogen isotopes form water molecules characterized by different isotopic composition, called "isotopologues". $^{1}H_2{}^{16}O$ is the most abundant (99.78 %), followed by $^{1}H_2{}^{18}O$ (0.20 %), $^{1}H_2{}^{17}O$ (0.03 %), $^{1}H^{2}H^{16}O$ (0.0015 ‰), $^{2}H_2{}^{16}O$ (0.022 ppm) and $^{1}H^{3}H^{16}O$ (trace); water molecules containing more than one heavy isotope do not form in nature but can be artificially created. Heavier water molecules require more energy to evaporate, and therefore have lower vapor pressures (Fig. 1.2-1), making them less prone to evaporate compared to lighter water isotopologues. When the temperature increases (and thus the energy of the system), the vapor pressure increases too, leading to more evaporation. During condensation heavier isotopologues tend to aggregate to the liquid phase quicker; the difference in relative abundance of different isotopologues during phase change processes is known as isotope fractionation.

Property	$H_2{}^{16}O$	$D_2{}^{16}O$	$H_2{}^{18}O$
Density (20 °C, in g cm^{-3})	0.997	1.1051	1.1106
Temperature of greatest density (°C)	3.98	11.24	4.30
Melting point (760 Torr, in °C)	0.00	3.81	0.28
Boiling point (760 Torr, in °C)	100.00	101.42	100.14
Vapor pressure (at 100 °C, in Torr)	760.00	721.60	
Viscosity (at 20 °C, in centipoise)	1.002	1.247	1.056

Fig. 1.2-1 Characteristics of different water molecules, from Hoefs, 2009

The chemical bond strength involving different isotopes of an element is slightly different: the heavy isotopes forms a lower energy bond that does not vibrate as violently; the vibrational energy depends from the mass of the atoms. Therefore, it forms a stronger bond in the compound, while the bond involving the lighter isotope is usually a little weaker and easier to break.

The vibrational energy (E_v) equation is

$$E_v = {}^{1}/_{2}\, hv \qquad v = \frac{1}{2\pi}\sqrt{\frac{k}{m}}$$

where h is the Plank's constant (6.63 x 10-34 Js), while k is the Boltzman's constant (1.38 x 10-23 J/K); m is the mass.

The heavy isotopes will favor that part of the system in which they are more strongly bound, according to the general thermodynamic principle that equilibrium systems tend toward a minimum energy state (Gat, 1996); heavier isotopologues tend to stay more in the lower energy state (liquid phase versus gas phase) whereas the lighter tend to evaporate more (Mariani, 2013).

1.3 The equilibrium fractionation

When isotopes redistribute between two different phases or two different compounds until the forward and backward exchange rates become equal, we have an equilibrium fractionation; once the equilibrium is reached, the isotopic abundance in both phases (or compounds) remains constant. The theory of equilibrium fractionation is well understood (Bigleisen, 1961) and has been studied in laboratory experiments (Horita and Wesolowski, 1994). The equilibrium time and position are both temperature dependent. While it is relatively easy to recreate equilibrium fractionation in the laboratory, it is very unlikely to observe it in nature (van Trigt, 2002).

1.4 Non-equilibrium and kinetic fractionation

Kinetic fractionation is unidirectional (SAHRA, 2005), occurring when the reaction product is removed from the reactant before equilibrium is established. Fully kinetic fractionation only happens when the product is immediately isolated from the reactant; in natural environment, the majority of processes are partially kinetic and partially at equilibrium, and are hence called "non-equilibrium processes" (van Trigt, 2002).

In both equilibrium and kinetic fractionations, the scale of the fractionation is expressed using the fractionation factor. The isotope fractionation factor (α) represents the partition of isotopes between two substances or two phases, and is expressed by the ratio of the relative abundance (R) of a given isotope (the ratio of the rarest isotope over the most common one) in two different phases or compounds.

$$\propto = \frac{R\ (reactants)}{R\ (products)}$$

$$H_2O\ (water) \leftrightarrow H_2O\ (vapor)$$

$$\propto [^{18}O\ (water - vapor)] = \frac{\frac{^{18}O}{^{16}O}\ water}{\frac{^{18}O}{^{16}O}\ vapor}$$

It varies with temperature, diminishing with increasing T; ideally, at very high temperatures, no fractionation occurs. In equilibrium fractionation, temperature is the main factor driving α magnitude, while during kinetic fractionation other factors can be just as much important.

Since the air layer exchanging with the sea surface below is under-saturated in terms of water vapor content, the seawater evaporation is in part a non-equilibrium process (Gat, 2001). A very thin air layer (micrometer-thick) lays on water surface, having ideally a 100% saturation, dominated by equilibrium conditions. However, between this layer and the well-mixed air column above there is a transition zone where diffusion dominates since the air is undersaturated with water (Clark and Fritz, 1997). The higher the relative humidity the more diffusion will take place, augmenting the kinetic fractionation.

Enhancing and diminishing effects on the fractionation can be caused by the presence of dissolved salts, which decreases the overall vapor pressure and changes the isotope fractionation in the water-vapor equilibrium, due to an isotope effect in the binding of water in the hydration sphere of the ions (Gat, 2001). At sea water concentration, dissolved NaCl does not noticeably affect the isotopic ratios (Craig and Gordon, 1965), unlike electrolyte solutions as HCl, LiCl, $MgCl_2$, $AlCl_3$ and others (Horita, 2005).

During condensation in clouds, rain is close to equilibrium with the moisture in surface air (Gat, 2001).

1.5 Setting the scale

The absolute concentration of a given isotope in a sample is difficult to measure individually with enough precision; therefore, by comparing a sample ratio to a standard ratio, the difference between the two can be determined more precisely. Utilizing the isotope ratio, the isotope content is expressed in term of departure from an internationally accepted standard (VSMOW), by using the "isotopic composition", reported in δ (‰) units

$$\delta^{18}O = \left[\frac{R\ (sample) - R\ (standard)}{R\ (standard)}\right] \times 10^3$$

The VSMOW standard (Vienna Standard Mean Ocean Water), promulgated by the International Atomic Energy Agency in 1968, reflects the mean isotopic composition of the world oceans (0 δ ‰) and was chosen as the reference standard for the scale of oxygen and hydrogen isotopes in water samples since it constitutes the largest water reservoir and it is fairly homogeneous (Craig, 1961). The ratios of the isotopic species in VSMOW are listed below (NIST, 2005)

$^{2}H/^{1}H = 155.76 \pm 0.1 \times 10^{-6}$

$^{3}H/^{1}H = 1.85 \pm 0.36 \times 10^{-11}$

$^{18}O/^{16}O = 2005.20 \pm 0.43 \times 10^{-6}$

$^{17}O/^{16}O = 379.9 \pm 1.6 \times 10^{-6}$

Before VSMOW there was SMOW (Standard Mean Ocean Water), created by the U.S. National Bureau of Standards in the 1960s, but its reliability was questioned and it was quickly abandoned in favor of VSMOW, which is a recalibration of the original SMOW and was originally prepared by R. Weiss and H. Craig in 1967 (NIST, 2005).

1.6 Enrichment and depletion of the heavy isotope content

Positive δ (‰) values mean an enrichment of the heavy isotopic species with respect to the VSMOW standard, while negative values signify their depletion (Gat, 1996). Where evaporation is higher than precipitation (E/P>1), seawaters are slightly positive, while at polar latitudes and in estuaries are slightly negative. Evaporative basins, like the Red Sea and the Mediterranean Sea, display the highest enrichment, up to 2 ‰ for $\delta^{18}O$ (Craig, 1966; Pierre *et al*., 1986).

The temperature is the main control on the isotopic composition of precipitation; with increasing temperature, precipitation becomes enriched in ^{18}O and ^{2}H content, following a linear relationship (SAHRA, 2005). This relation was first quantified for $\delta^{18}O$ by Dansgaard (1964), finding the following equation based on North Atlantic stations: $\delta^{18}O = 0.695*T - 13.6$ ‰.

Altitude, latitude and distance from moisture origin all affects the isotopic composition of meteoric water (Dansgaard, 1964). Each one of these effects is basically related to the consecutive condensation of moisture by cooling of the air mass and so the correlation with temperature seems to be the overriding factor.

-Altitude effect: a progressive heavy isotope depletion with increasing altitude; it lowers the temperature effect since with the diminished air pressure (pressure gradient: ≈-1.2%/100 m) a

larger temperature decrement is required for the water vapor to condensate. For Siegenthaler and Oeschger (1980) the altitude effect causes a $\delta^{18}O$ decrease of -0.2‰/100 m (also confirmed by Schürch *et al*., 2003, for the Swiss National Network for the Observation of Isotopes in the Water Cycle, NSIOT), but the observed effect on $\delta^{18}O$ normally ranges between -0.1‰ and -0.6‰/100 m often decreasing with increasing altitude (Vogel *et al*., 1975). Similar values have also been found for mountains in Czechoslovakia (Dinçer *et al*., 1970), Nicaragua (Payne and Yurtsever, 1974), Greece (Stahl *et al*., 1974), Cameroon (Fontes and Olivry, 1977), Italy (Bortolami *et al*., 1978) and Switzerland (Siegenthaler and Oeschger, 1980). The pseudo-altitude effect (Moser and Stichler, 1974) consists in the raindrops evaporative enrichment of ^{18}O and D during their fall, and it is larger at low altitudes where the cloud base is usually higher with respect to the ground level.
-Latitude effect: a progressive heavy isotope depletion with increasing latitude; the effect is roughly -0.6‰ for each degree of latitude for $\delta^{18}O$ in Europe and USA, but can grow up to 2‰ for each degree in Antarctica (Gat, 2001).
-Continental effect (distance from the coast): a progressive heavy isotope depletion with increasing distance from the sea; affected by significant geographical and seasonal variations. An example is given by the 7 ‰ average $\delta^{18}O$ decrement during the precipitation route over Europe, from the Irish coast to the Urals: the effect in summer is significantly lower (about one fourth) compared to winter; summer rain re-evaporation could be the main cause (Eichler, 1965).
-Amount effect: compared to the later precipitation, the early liquid phase of rain is enriched in $\delta^{18}O$ and δD; as a consequence, in long rain events, the precipitation gets lighter as the rain continues. This effect is particularly relevant in strong tropical rainfall (SAHRA, 2005). The amount effect is also expressed by a negative correlation between the δ (‰) of precipitation and the precipitation amount over a given time period (Gonfiantini *et al*., 2001, Sharp, 2007); this negative correlation is valid for tropical regions, but can be disappear or even be weakly positive at higher latitudes (Kendall and Coplen, 2001).
The most comprehensive network of direct observations of isotopes in precipitation is GNIP (Global Network of Isotopes in Precipitation), operated by IAEA (International Atomic Energy Agency) jointly with the World Meteorological Organization (WMO). The GNIP database offers precipitation stable isotope (and tritium) data with monthly resolution from several places around the world, starting from 1961. Unfortunately the network coverage is limited and not homogeneously distributed. Fig. 1.6-1 shows the global map of observed present-day mean annual $\delta^{18}O$ in precipitation, obtained with a spatial data interpolation of 231 GNIP stations that recorded at least one year of monthly $\delta^{18}O$ values (open circles) (Werner *et al*., 2011).

Other networks of precipitation for isotope analysis exist on a local scale, but they usually cover a limited time period and are not suitable for interpreting long time trends.

Considering the interpolations of precipitation data, the isotopic content looks quite homogeneous on wide areas (fig. 1.6-1), but on a local scale there could be a significant variability, often determined by the orography of the area. In the Italian map (Longinelli and Selmo, 2003; fig. 1.6-2) the altitude effect (Alps and Apennines) is evident.

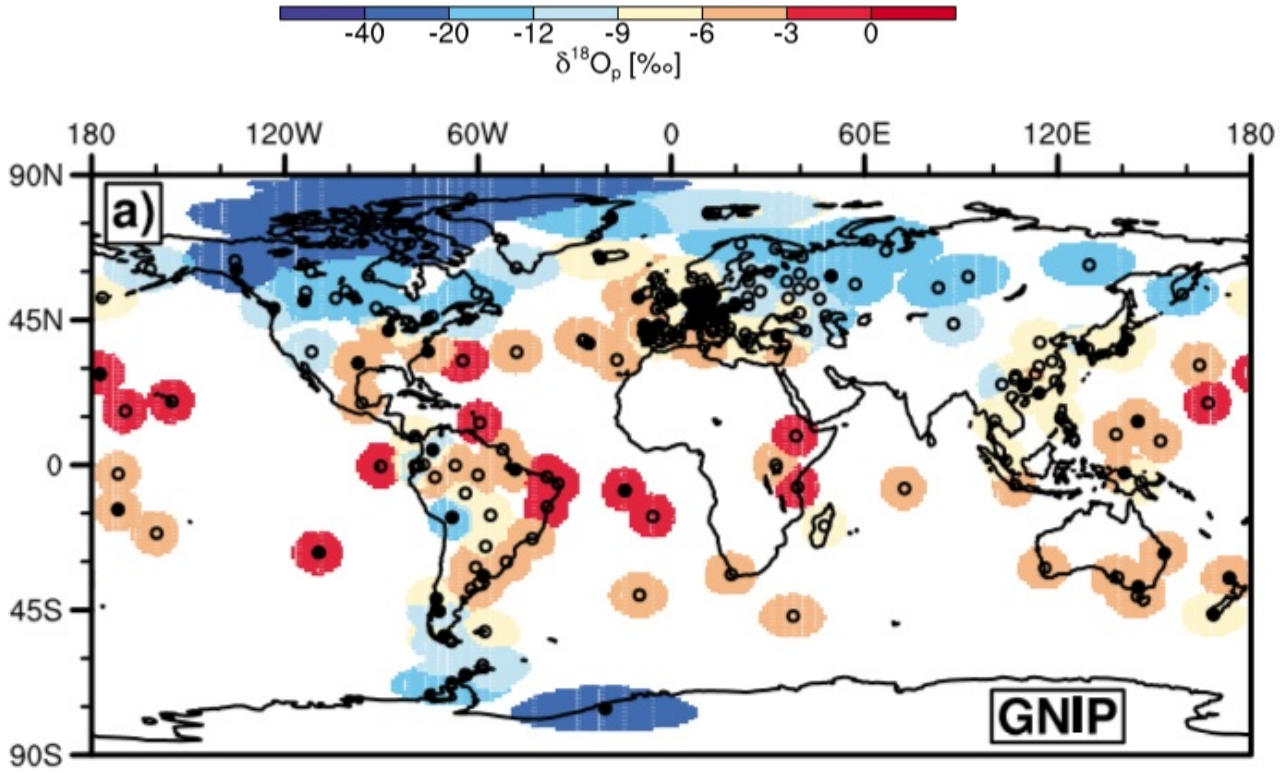

Fig. 1.6-1 Global map of present-day mean annual $\delta^{18}O$ in precipitation. From Wernet *et al*. (2011)

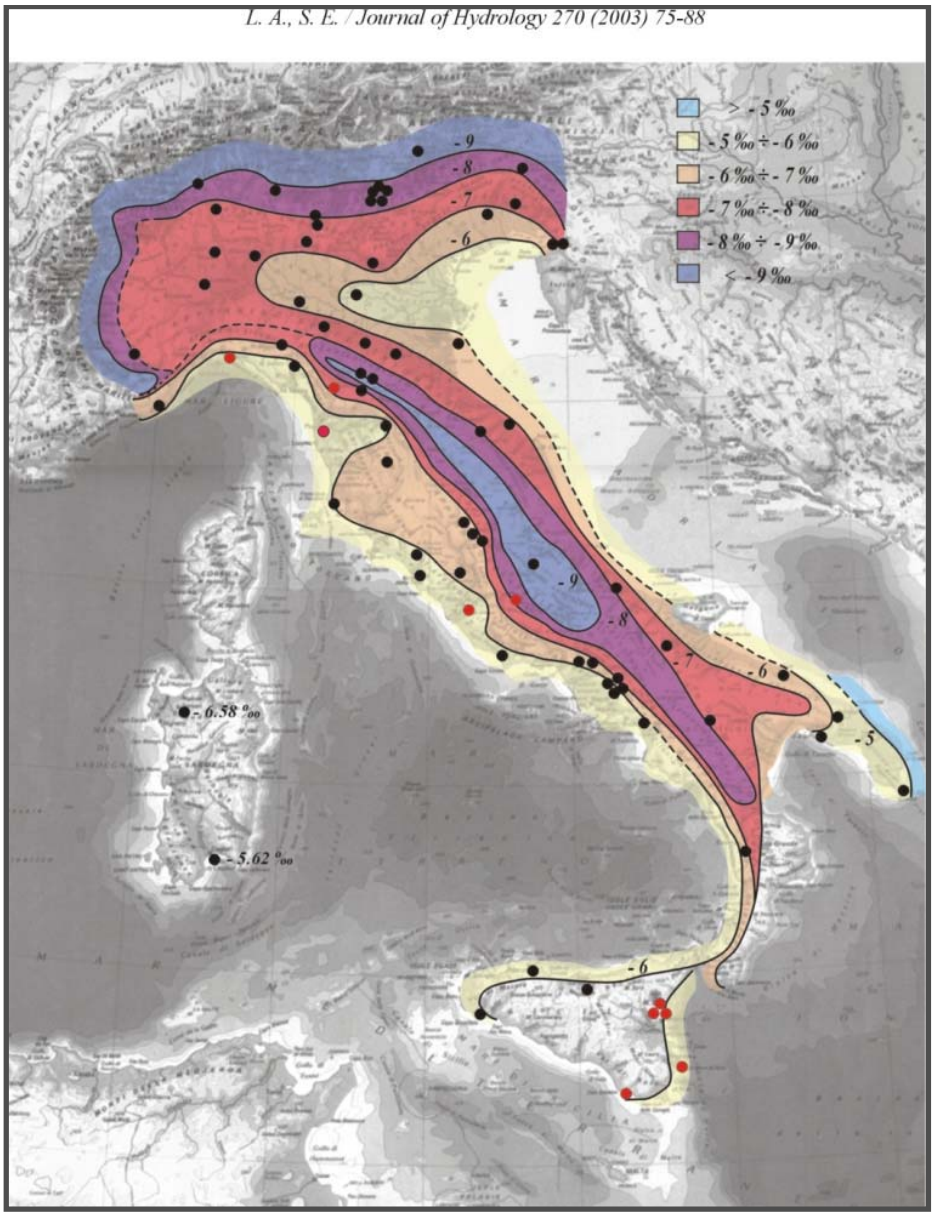

Fig. 1.6-2 Mean annual $\delta^{18}O$ content of precipitation in Italy (Longinelli and Selmo, 2003)

The evaporation phase occurs at non-equilibrium: the vapor formed above the water surface is constantly removed by wind and diffusion; despite the difference regarding sea surface temperature, incoming solar radiation, relative humidity and wind conditions, vapor originating from sea water shows similar values worldwide, around -10 ‰ for $\delta^{18}O$. This value is much lower than expected considering an equilibrium fractionation, due to kinetic effects (Hoefs, 2009). Since condensation mostly happens at thermodynamic equilibrium between vapor and water, the liquid phase is enriched in $\delta^{18}O$ and δD, with the grade of enrichment depending on temperature, as α is a function of T. As condensation continues, the remaining vapor is progressively depleted in its heavy isotopes.

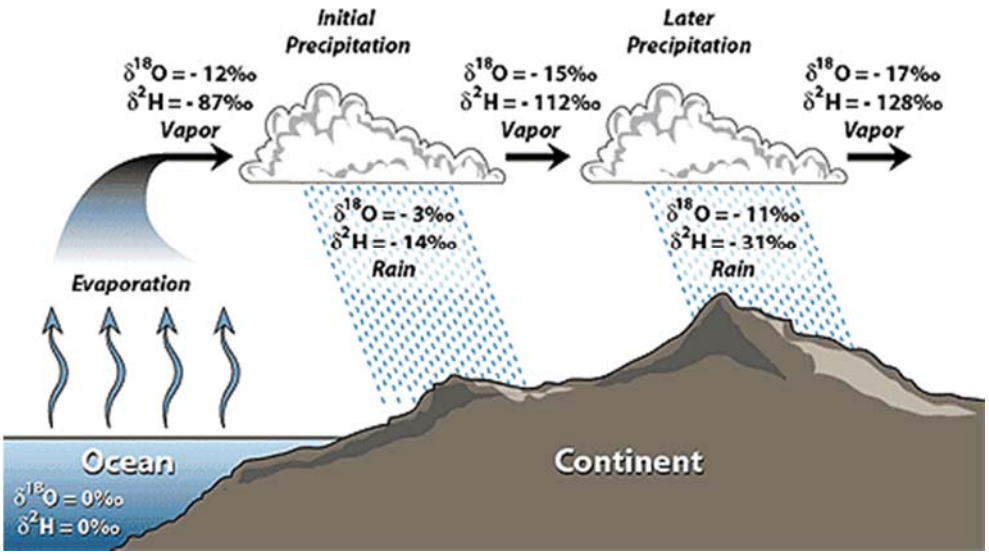

Fig. 1.6-3 Isotope fractionations in the water cycle, based on Hoefs, 1997 and Coplen *et al*. (2000)

While liquid precipitation normally occurs at equilibrium with the surrounding vapor, snow and hail get more depleted in heavy isotopes because the exchange between the air moisture and solid precipitation does not occur; also rain originating from strong convective systems can displays lower $\delta^{18}O$ and δD values, since raindrops only interact with in-cloud air moisture (Gat, 2001).

1.7 The deuterium excess

The deuterium excess (*d*) is a second-order isotope parameter, defined by Dansgaard (1964) and expressed by the equation $d = \delta D - 8*\delta^{18}O$, derived from the Global Meteoric Water Line (GMWL) $\delta D = 8*\delta^{18}O + 10$, in which 10 is the global average deuterium excess of precipitation (Craig, 1961). This relationship is principally a reflection of differences in oxygen and hydrogen isotopic equilibrium fractionation factors; the slope of the GMWL represents this ratio, which is eight times bigger for hydrogen than oxygen (SAHRA, 2005). The relation expressed by Craig (1961) was later confirmed by Rozansky *et al*. (1993) using the GNIP data around the world finding a very similar equation: $\delta D = 8.13*\delta^{18}O + 10.08$.

The deuterium excess is due to the slower mobility of the $H_2{}^{18}O$ molecule compared to $HD^{16}O$ during diffusion, resulting in higher diffusivity of the latter and causing a relative enrichment of $HD^{16}O$ molecules in the weaker bound phase (the gas phase); if there is not enough time for the

two phases to reach the equilibrium, the slower movement can lead to quantifiable differences. Non-equilibrium conditions are caused by a strong gradient in relative humidity above the water surface, or by winds transporting the moisture away from the surface. Both sea surface temperature (SST) and relative humidity (RH) at moisture source affect the deuterium excess: *d* becomes higher with increasing SST and decreasing RH, with proportionality constants of similar magnitude. Nonetheless, the effect of SST on *d* is considerably weaker than RH, because the variability of RH in percentages is normally much larger than the variability of SST in Kelvin/Celsius degrees (Pfahl and Sodemann, 2014). It can be noticed that the SST effect could be a masked RH effect instead, because lower SST leads to higher RH in the air mass close to the sea surface.

Unlike evaporation, condensation and transpiration essentially do not affect *d* (Gat, 2005).

There are also secondary effects influencing the deuterium excess, like the isotopic fractionation during the progressive cooling of an air mass, during ice cloud formation and during the raindrops and soil water evaporation (Jouzel and Merlivat, 1984; Jouzel *et al*., 2007). Secondary effects are more relevant at high latitudes or altitudes, where snow constitutes the major part of precipitation (Pfahl and Sodemann, 2014). In very cold areas, the dominant phase change process is given by water vapor condensing directly into ice, leading to super-saturated clouds. The isotopic fractionation is hence mainly kinetic, due to diffusion of water vapor toward the ice crystals; this causes a marked difference between *d* in the moisture and *d* in the newly formed precipitation (Fisher, 1991). The non-equilibrium condensation during the growth of ice particles causes higher *d* values in the solid precipitation (Jouzel and Merlivat, 1984). The partial evaporation of raindrops, causing an enrichment in ^{18}O and D content of precipitation, leads to a decrease of deuterium excess and hence leaving a mark in precipitation (Moser and Stichler, 1974). For the Alpine region, Froehlich *et al*. (2008) demonstrated that the sub-cloud evaporation can cause a significant decrease in *d* of precipitation for valley stations, but the effect is negligible for mountain stations (over 1600 m a.s.l.), resulting in a *d* variation of less than 2 ‰.

With the exception of some extreme locations, we can assume with good approximation that, within the water cycle, the only process significantly influencing *d* is evaporation; that is why it is possible to use deuterium excess to trace the moisture origin.

On a local scale, the deuterium excess of precipitation is believed to be primarily determined by the seasonal and spatial variation of moisture sources (Sodemann *et al*., 2008; Sodemann and Zubler, 2010).

Part of the air moisture is originated from stagnant water pools and not from the oceans: it is named "recycled moisture". H_2O is reintroduced into the atmosphere via evaporation or plant transpiration (evapo-transpiration); in the first case, given that the same portion of water underwent

two consecutive evaporations, one from the ocean and the second from the stagnant pool, a double kinetic fractionation affects the deuterium excess of the consequent recycled precipitation. The largest share of the evapo-transpiration flux is given by plant transpiration, but also evaporation from the water trapped on the canopy accounts for an important share: up to 35 % in the tropical rain forest (Molion, 1987). The total amount of recycled moisture can constitute the major part of the incoming precipitation, especially in arid areas. While plan transpiration does not lead to any noticeable fractionation, since plants utilizes soil water on a seasonally selective basis, and given the seasonal variations in the precipitation isotopic content (at least at mid-high latitudes), transpiration contribution can alter the isotopic composition of precipitation (Gat, 2001).

CHAPTER 2: ICE CORES: A DETAILED CLIMATE ARCHIVE

2.1 Ice cores

Ice cores are essentially ice cylinders extracted from glaciers or ice sheets. New layers of snow deposit each year, burying and compressing the older layers. Each layer of snow is characterized by its texture and chemistry. Particulates and dissolved chemicals that were contained in precipitation or were deposited by air transport (dry deposition), become a part of the snow. The weight-induced compression forces the snow to re-crystallize in grains with size and shape comparable to sugar grains. Progressively the grains grow larger and the air pockets between them become smaller, causing a density increment. The snow usually turns into firn, an intermediate state between snow and ice, after two winters. When this point is reached, firn has about two-third of the water density. Larger ice crystals become increasingly so compressed over time that the air pockets between them decrease in size (NSIDC). When the ice density is reached (0.83 g/cm^3), the air contained in the porous snow is trapped into ice bubbles (close-off). The close-off depth is very variable, ranging from 20-30 m in temperate mountain glaciers to over 100 m in the inner part of polar ice sheets. Layers of ice (and bubbles) accumulated over the years create a continuous record of the climate conditions at the time of formation, like snow accumulation, local temperature, chemical composition of the atmosphere including greenhouse gas concentrations, volcanic activity, and solar activity.

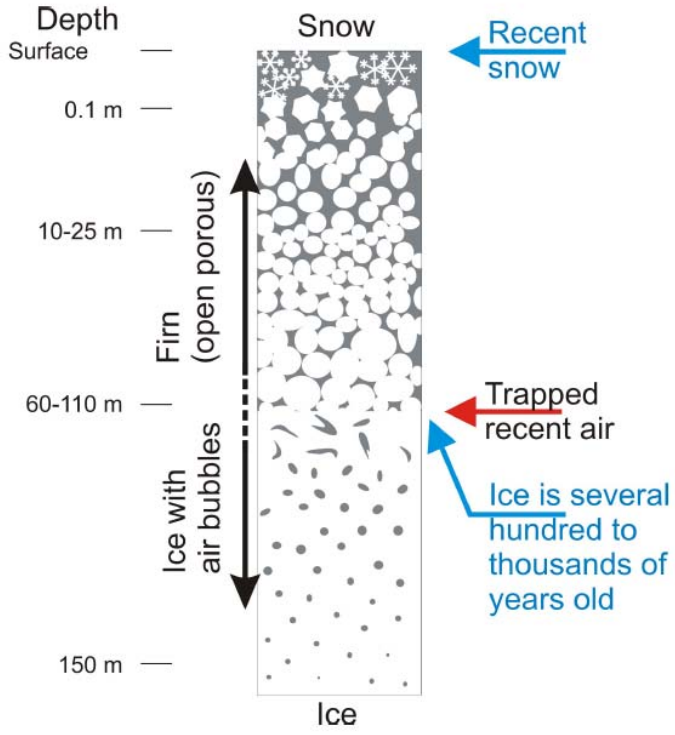

Fig. 2.1-1 Typical metamorphism of the snow-to-ice formation of a glacier/ice sheet (credit to Niels Bohr Institute)

Ice cores can be retrieved in ice sheets or glaciers by means of a mechanical or a thermal drill; they both have a cylindrical shape. The mechanical drill can be operated by hand force (hand auger) or, more frequently, by an electromechanical motor drive; it is essentially a rotating pipe with cutters on the head and it is more suitable to drill cold glaciers in which the englacial temperature is well below the melting point. The thermal drill contains a ring-shaped heater and no cutters; it is more suitable for drilling temperate glaciers, where the ice temperature is at the pressure melting point. Hand augers are the simplest drills available, composed by a barrel with a cutting head and handlebars. They are normally used to retrieve shallow cores in the snow and upper firn portion of the glacier/ice sheet.

Ice cores are among the most used and powerful climate archives, furnishing a good compromise between the temporal resolution (this parameters is dependent from the snow accumulation rate of the area) and the time span they cover. Annual layers, when detectable, allow the interpretation of how the climate changed from year to year. Ice cores are also the only archives that store the atmosphere of the past in the air bubbles trapped in the ice. Thanks to the kilometric thickness of the ice sheet, deep cores from polar regions (mainly Greenland and Antarctica) usually offer a long timescale, especially in the Antarctic plateau, where the record-breaking Epica Dome C core (depth: 3270.2 m) goes all the way back to 800,000 years before present (BP) (Jouzel *et al*., 2007).

The Dome C drilling reached the bedrock in January 2005, disclosing eight glacial-interglacial transitions. In accordance with the very low precipitation rate of these regions (Dome C has a mean annual long-term accumulation rate, from 1815 to 1998, of 25.3 kg/a; Fujita *et al*., 2011), the temporal resolution has necessarily to be quite low (around 7 years for 10-cm samples in the upper part). Only few deep ice cores goes back to the last interglacial period (Eemian), and, besides two, are all located in Antarctica. When the ice that was buried under kilometers of overlaying firn and ice is taken to the surface during the coring, the decompression causes a volume expansion, which could lead to ruptures if handled incorrectly. Currently, the "oldest ice" drilling project is being discussed; this record breaking core would take place in the Antarctic plateau, to reach 1.5 Ma before present (BP), going back to the mid-Pleistocene transition. Several chemical and physical parameters are recorded and analyzed in ice cores: at least for the Holocene, oxygen and hydrogen stable isotope long-term records from cold polar glaciers provide the most reliable atmospheric paleothermometer, which can be reasonably well calibrated in terms of changes in local temperature (Wagenbach, 2003).

In 1935, the first attempt to investigate the inner part of an ice sheet was carried out by Sorge (1935), consisting of the study of a 15 m-deep pit dug in Greenland, at Station Eismitte. About twenty years later, the first ice cores were drilled in Dronning Maud Land (Antarctica), by a Norwegian, British and Swedish team (Langway, 2008). The first scientist to investigate the linkage between the temperature and isotopic content of polar snow (oxygen-18 and deuterium) at the precipitation site was Willem Dansgaard (Dansgaard, 1953, 1964). Together with his Copenhagen team, he was the first to recover continuous isotopic records from deep ice cores (Dansgaard *et al*., 1969; Johnsen *et al*., 1972). The first ice core covering an entire glacial-interglacial cycle was the Vostok core drilled in the 1980s; before that, only sediment cores could cover such a long time scale (Jouzel, 2013).

Also many others natural archives are found at remote latitudes, far away from human settlements, and while it can be considered an advantage, since they have laid undisturbed for all this time, they usually reflect just particular climate conditions of that specific region, which can be very different from the climatic trends that have been affecting Europe or other densely populated, and anthropogenically influenced, areas.

Mountain glaciers from mid and low latitudes retains climate information covering a shorter time, but are crucial for recording the local climate variability being close to human settlements. The vicinity to anthropogenic settlements and activities permits to study the impact of pollution and of the human-induced climate forcing by measuring substances with a dishomogeneous global

distribution and increasing concentration close to the source, like dust and several molecules and elements emitted by human activities.

Whether polar or mid-to-low latitude glaciers retain the most well-preserved temperature archives remains questionable: polar ice sheets (Greenland and Antarctica) are characterized by much lower temperature during the entire year, and melting is negligible when not completely absent, but the lower accumulation rate and the lower snowfall density allow some post-depositional processes to interact more with the uppermost snow layers between separate precipitation events. Phenomena such as wind scouring, diffusion and isotopic exchange between vapor and surface snow can alter the pristine isotope signal of precipitation and erase the delicate seasonality given by the barely sufficient accumulation rate (Stichler *et al*., 2001; Steen-Larsen *et al*., 2014).

The first researcher to believe in the scientific importance of drilling tropical glaciers was Lonnie G. Thompson; he overcame the issues of drilling at very high altitude by using light solar-powered mechanical drills, retrieving ice cores from several glaciers at risk of disappearing because of the warming trend (Jouzel, 2013).

2.2 Dating the ice cores

One of the most difficult part in studying ice cores is creating a reliable age scale; several different approaches are available, but most of the times they should be merged together in order to generate a consistent chronology.

- Annual layer counting is based on the identification of seasonal oscillation (i.e. winter minima and summer maxima), or presence/absence of some parameters/species: ^{18}O, ^{2}H, deuterium excess, NH_4^+, dust content and acidity content (electrical conductivity method, ECM). Some biological species have been used lately for dating ice cores. Snow algae can be useful for identifying the seasonality (Uetake *et al*., 2006), but their applicability is limited: after eight years they have been proven to undergo autolysis and bacterial decomposition (Yoshimura *et al*., 2000). Bacteria, cyanobacteria and fungi could be useful too, but are easily transported downwards by meltwater seepage due to their small size. Bacteria and fungi have also shown growth after they had deposited, altering the seasonal signal (Uetake *et al*., 2006). The feasibility of the annual layer counting relies primarily on a sufficiently high accumulation rate and thus is not possible in dry areas, such as inland Antarctica. This method provides a high accuracy thanks to the identification of single years, but leads to uncertainties due to the sometimes only visual recognition of annual cycles, which can be very subjective (the possibility of missing some years characterized by

unclear and incomplete oscillations is always present). The counting of annual layers becomes more difficult with depth, due to the strong thinning of the ice strata.

- Reference horizon identification:
  - signs of nuclear weapons tests (^{3}H, ^{137}Cs, β emissions),
  - Saharan dust events,
  - volcanic eruptions (tephra layers and sulfate peaks).

Unfortunately, these events are documented for a relatively short time and cannot be used to date very old ice; plus, they are not always found in every ice core.

- ^{210}Pb: this lead isotope has a half-life of 22.20 years, and assuming a sufficiently high concentration in ice core layers, permits the dating only back to roughly 100 years.
- ^{14}C: this dating methodology can be carried out only on organic matter contained within the firn/ice; it is possible to date single organic remains trapped within the glacier (leaves, insects) or the particulate and dissolved carbon contained in the firn/ice. One of the problems regarding this method is that part of the particulate or dissolved carbon comes from old soils and therefore could be older than the time in which it deposited on the snow.

Cold and temperate mountain glaciers from summit areas located at mid-low latitudes are characterized by complex ice flow patterns and show a strongly non-linear age-depth relation, making the dating very difficult and leading to significant uncertainties within 10-50 years and to a basically unknown chronology beyond 1000 years ago (Wagenbach, 2003).

CHAPTER 3: THE STUDIED AREA

3.1 The Alps

The Alps are the most important European mountain system, approximately 1200-km long, stretching across several countries.

The first official partition of the Alps was presented in 1926 (fig. 3.1-1). The European mountain range system was divided into three parts: Western, Central and Eastern Alps, with the latter extending from the Brennero Pass to the Croatian city of Fiume (Comitato Geografico Nazionale, 1926); according to this subdivision the highest peak of the Eastern Alps was Mt Marmolada (3342 m a.s.l.), while Mt Bianco (4810 m a.s.l.) was the highest summit of the Alps.

The *Suddivisione Orografica Internazionale Unificata del Sistema Alpino* (SOIUSA) has been officially adopted in 2006, dividing the Alps into Western and Eastern Alps and in other sub-categories (fig. 3.1-2). The Western Alps range from the line Savona-Colle di Cadibona-Montezemolo-Mondovì to the line Reno-Spluga Pass-Lario Lake, the Eastern Alps go from the latter line to the one between Wien-Neusiedl Lake-Graz-Maribor-Zagreb. Western Alps are further divided into Northern and Southern Western Alps; Eastern Alps are further divided into Northern, Central and Southern Eastern Alps (Marazzi, 2006). According to the actual partition, the highest peak of the Eastern Alps has become Mt Bernina (4049 m a.s.l.).

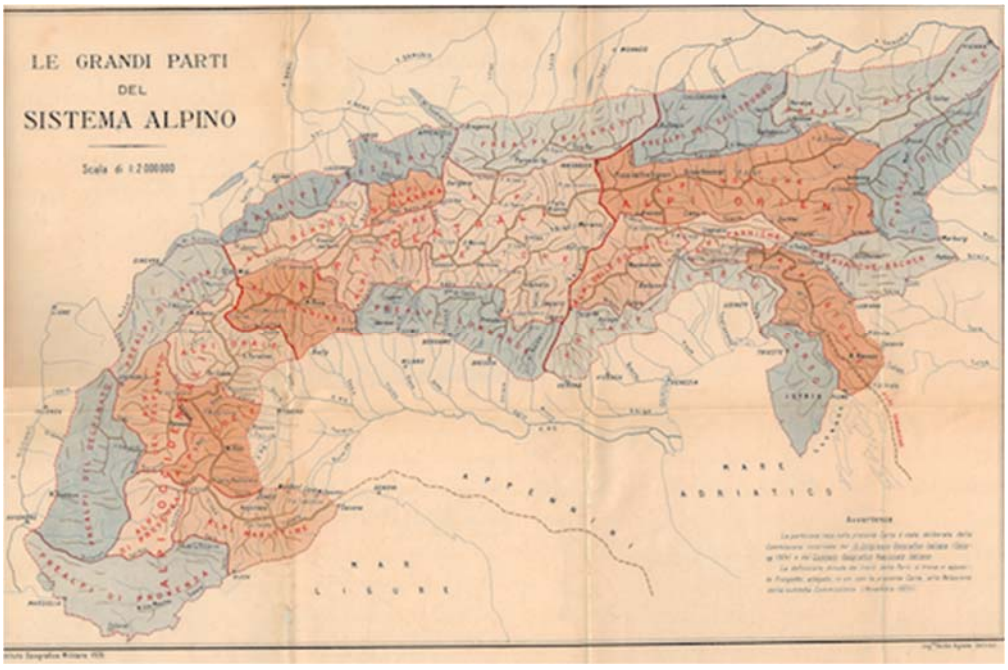

Fig. 3.1-1 First partition of the Alpine system, from Comitato Geografico Nazionale (1926)

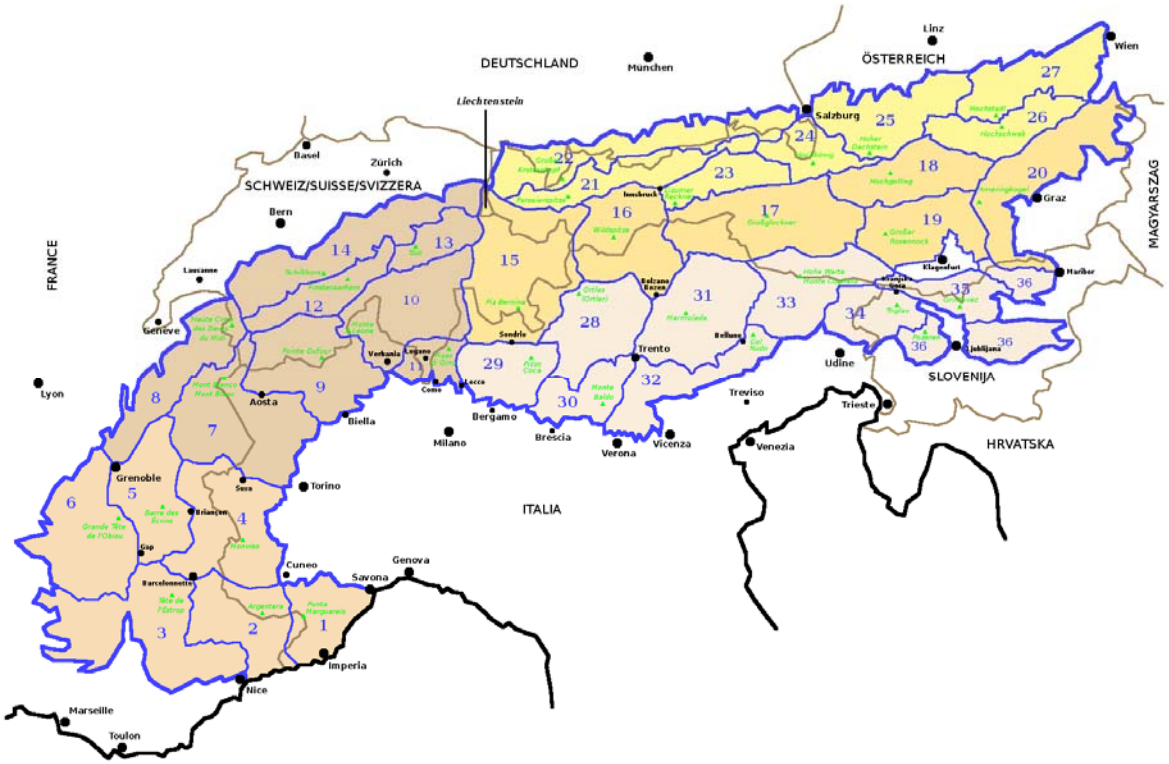

Fig. 3.1-2 SOUISA Alps Partition, dividing the Alps in Eastern and Western Alps and other sub-categories. From Marazzi, 2006

Few climate studies have been conducted on Eastern Alps glaciers; these glaciated areas are characterized by lower elevations (always below 4000 m a.s.l.) compared to Western Alpine glaciers, and the majority of them can be defined as "temperate", meaning that glacier temperature can exceed the pressure melting point during the warm season.

Many low elevation Eastern Alps glaciers are very small and does not present a sufficient thickness to allow deep coring, permitting only to retrieve shallow cores.

3.2 The Alpine climate

The Mediterranean cryosphere is a particularly delicate system, very vulnerable to environmental and climatic changes. It is formed by the glaciated areas of the Southern Alps, the Apennines and the Pyrenees. Beside the Alpine glaciers, the ice-covered areas of the other Mediterranean mountain systems are very limited and have dramatically shrank during the last century (Trueba *et al*., 2008; Hughes, 2011).

The air mass circulation over the Mediterranean basin is very complex, but it is influenced by the positioning of the Azores High (also known as the Azores anticyclone): a semi-permanent

anticyclonic region with fairly consistent high pressure. During summer, the Azores High tends to remain on the Mediterranean, leading to high temperatures and dry conditions: this is the cause of the extremely dry and hot climate of North Africa and the surrounding areas. During winter, the Azores High moves back to the Atlantic Ocean, allowing low-pressure to enter the Mediterranean, permitting the entrance of cold air masses from the north. The central pressure is around 1024 mbar (or hPa) in both winter and summer (WeatherOnline). This meteorological situation was quite stable during the past, but it has changed in the recent period, leading to differences in the distribution and frequency of precipitation over the Mediterranean area (Pecci *et al*., 2005).

The North Atlantic Oscillation (NAO) is one of the main teleconnection patterns, consisting of a north-south dipole of anomalies: the low-pressure center is located over Greenland (Icelandic low) and the high-pressure center spans the central latitudes of the North Atlantic between 35°N and 40°N (Azores high). The NAO shows significant inter-seasonal and inter-annual variability, as well as prolonged periods (several months) of both positive and negative phases. The wintertime NAO can display significant multi-decadal variability (Hurrell 1995, Bell and Chelliah, 2005). The NAO index is adopted to quantify the oscillations: a positive NAO index indicates a stronger than usual Azores High and a deeper than normal Icelandic Low, a negative NAO index indicates a weaker than usual Azores High and a shallower than usual Icelandic Low. During a positive NAO index, the humid Atlantic air is deflected toward central and northern Europe, leading to dry conditions in the Mediterranean; during a negative NAO index, more humid air enters the Mediterranean basin, leading to more precipitation in Southern Europe (fig. 3.2-1).

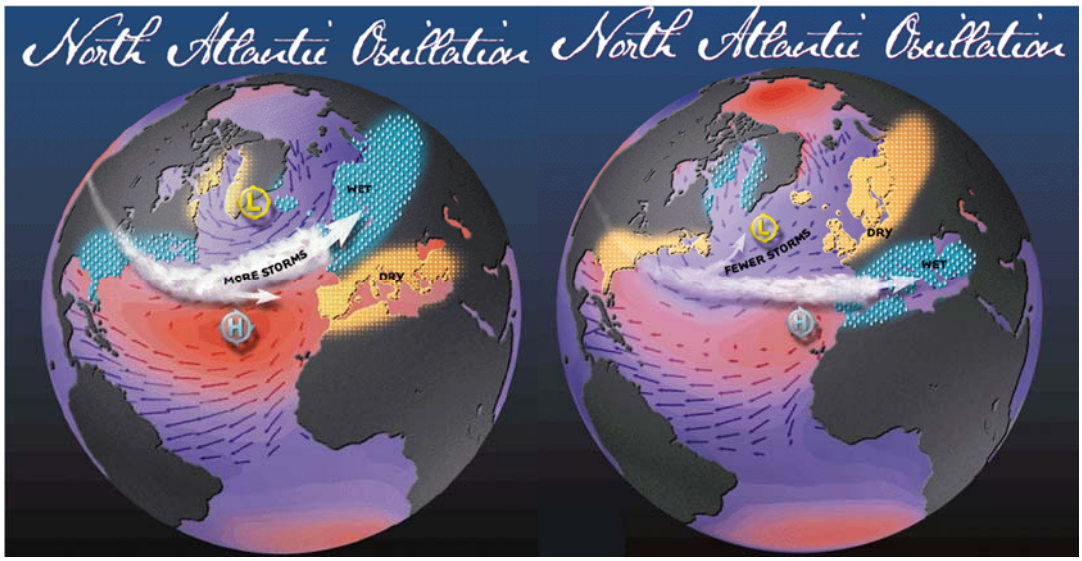

Fig. 3.2-1 Positive (left) and negative NAO index (right). Source: http://www.ldeo.columbia.edu/

Several mountain areas around the world have lost a significant portion of their glaciated areas during the last 150 years, and the loss rate has severely increased during the past two decades (Haeberli *et al*., 2005a, 2005b); this is the clearest indication of how fast climate change is affecting our environment. Alpine glaciers lost 35% of their area in the period 1850-1970s, and close to 50% by the year 2000. Total glacier volume is believed to be close to one third of what it was at its recent peak, around 1850. With a 5°C temperature increment, the Alps would be almost ice-free (Zemp *et al*., 2006).

Fig. 3.2-2 The tongue of Grosser Aletschgletscher (Bernese Alps), the longest glacier of the Alps (23 km), in 1856 (left) and 1996 (right). From Swiss Federal Institute of Technology Zurich

Sunshine duration is characterized by the shortest observation period among climate indicators. The first observations took place in the 1880s, limiting the comparative analysis of sunshine and cloudiness series to roughly the last 110 years, although cloudiness series alone are longer. Temperature shows the longest observation period; coupling temperature with sunshine duration at high elevation Alpine sites, it is evident that both have increased significantly since 1900. (Auer *et al*., 1998).

The Alps are densely populated, and present a high susceptibility to climate-related hazards; this territory plays a crucial role in water supplying, also essential for energy production (hydropower): the Alps are considered the "Water towers of Europe" (EEA, 2009). The tourism sector is of major importance in both winter and summer, constituting one of the main income source of the region.

Other than being particularly vulnerable to climate change, the Alps also contribute to GHG emissions more than other areas, consuming around 10% more energy per capita than the European average; this is mainly due to house heating. The Alpine tourism is also a crucial source of greenhouse gasses, considering that motor cars are used for 84 % of holiday travels to the Alps (Alpine Convention, 2013). Future changes in climate could heavily affect key economic sectors such as water supplying, energy production, tourism and agricultural and dairy production. In particular, the shrinkage of the ski season, coupled with the snow-reliable ski resort shortage, will cause significant damage to the winter tourism sector. The snow-reliability line of ski areas, considering the 100-day rule (having at least 100 days of snow cover characterized by a snow depth of 30 cm or more), will rise by 150 m for each Celsius degree of warming (Haeberli and Beniston, 1998). Precipitation pattern changes are likely to influence the abundance and geographic distribution of snow, but several studies have stated that temperature is expected to be the dominant control on snow cover in a warmer climate, and the increase in winter precipitation, projected for the Alps by many models, will not compensate the elevate temperature-induced large losses in snow volume (Gobiet *et al*., 2014).

During the last decades many parts of Europe have experienced remarkable changes in climate conditions. Mountain areas, in particular the Alps, are indicated in the EU White Paper on Adaptation (Commission of the European Communities, 2009) as among the most vulnerable areas to climate change in Europe. Between the late 19th and early 21st century, the Alps have experienced a remarkably high temperature increase of around 2°C, more than twice the rate of the Northern hemisphere, leading to extensive glacier melting, raising of the snowline, changes in the run-off regime of rivers and water availability (Auer *et al*., 2007). This temperature increment has involved the entire Alpine region, and has been particularly marked between 1980 and 2000 (EEA, 2009).

The significant regional warming is believed to be due to a systematic northward shift of the global subtropical high-pressure bands. The increased mean air pressure in the region (Auer *et al*., 2007) has significantly extended sunshine duration in the Alps. Coupled with a general reduction of wind speed in central Europe during the 20th century (Matulla *et al*., 2007), this has caused the climate to be more influenced by local forces, mainly influenced by incoming solar radiation, due to the geographical location in the mid-latitudes, the west-east orientation and the altitude.

A surface air temperature reconstruction for a high elevation area (~4300 m a.s.l.) of Mt Blanc, based on multiple englacial temperature profiles (Gilbert and Vincent, 2013), showed a warming of 2.0 ± 0.6°C for the period 1900-2004, in accordance with other Alpine temperature trends

detected at lower elevations or at regional scale; this indicates that warming in the Alps is not amplified at high elevations.

Considering the entire Alpine mountain range, the contribution of the different moisture sources to the annual mean precipitation has been diagnosed using a Lagrangian moisture source diagnostic and data from the ERA-40 European Centre for Medium-Range Weather Forecasts (ECMWF) reanalysis: North Atlantic ocean 39.6 %, Mediterranean 23.3 %, European land surface 20.8 %, North Sea and Baltic Sea 16.6 %. A strong seasonal variability is observed: moisture transport to the Alps changes from being dominated by North Atlantic moisture sources during winter to a continental mode during summer with a significant contribution from Central Europe lands (Sodemann and Zubler, 2010).

The Alps form an orographic barrier, dividing the region in different climatic zones. The region north of the Alps presents a continental climate, dominated by the influence of North Atlantic air masses in winter and land evaporation in summer, while the Southern Alps are more influenced by the Mediterranean (Frei and Schär, 1998; Eichler *et al*., 2004; Barry, 2008; Sodemann and Zubler, 2010). The Mediterranean seems to be a major source for precipitation extremes, both floodings and droughts. Since the Southern Alps have roughly double the fractional precipitation from the Mediterranean than the Northern Alps, the Southern Alps would be more prone to precipitation extremes than the Northern Alps (Sodemann and Zubler, 2010).

The spatial distribution of precipitation in the Alps is heterogeneous; some areas are characterized by very high precipitation rate, more than 2000 mm w.e./a: the northern Alpine rim, extending over 600 km and some zones in the southern rim, like Ticino, North-Eastern Italy and Slovenia. The St. Gotthard pass connects the northern and southern wet anomalies in Switzerland. On the other hand, some dry inner Alpine areas such as the Valais and South-Eastern Switzerland receive just around 600-700 mm w.e./a (Frei and Schär, 1998). The precipitation amount normally increases with altitude.

In general, the precipitation amount is higher over the Southern Alps, with maxima in spring and autumn, and lower over the Northern Alps, with a large peak in summer (Frei and Schär, 1998; Eichler *et al*., 2004; Sodemann and Zubler, 2010).

The Alpine sub-region characteristic precipitation regimes cannot be solved by either GCMs or higher-resolved regional models (Mariani *et al*., 2014).

Two antagonistic centennial precipitation trends have been detected (Auer *et al*., 2005): the north-west of the Alps (Eastern France, Northern Switzerland, Southern Germany and Western Austria) shows a wetting trend (since the 1860s), while the south-east (Slovenia, Croatia, Hungary, South-Eastern Austria and Bosnia-Herzegovina) shows a drying trend (since 1800s). While the

uncertainty remains high, several future projections agree on increasing drought events for the near and long-term future for the Alpine area. Until the end of this century, the annual cycle of precipitation is projected to change significantly with decrements in summer, especially in the southern regions, and increments in winter (Gobiet *et al*., 2014).

Alpine glaciers advanced in the last part of the Little Ice Age, between 1760 and 1830, despite mean summer temperatures that were higher than the 20th century average (Bohm *et al*., 2001; Luterbacher *et al*., 2004), thanks to increased winter precipitation (at least 25% higher than the 20th century average); when winter precipitation decreased, the glaciers started to retreat, long before the observed 20th century warming (Vincent *et al*., 2005). Observations clearly show that glaciers all over the world are retreating and losing mass. Both glaciological and geodetic methods reveal a globally observed mass loss rates in the early 21st century that is unmatched in the period of observations. The rate derived from the glaciological mass balances for this period is considerably more negative than the average rate for the second half of the 20th century (-0.54 m w.e./a vs -0.33 m w.e./a). The rate derived from the geodetic method is much more impressive: four times the average rate for the period 1851-1900, three times the rate for 1901-1950 and two times the rate for 1951–2000. Summer balances are the main drivers behind the increment of mass loss of recent decades (ablation processes), while winter balances appear to be of inferior importance (Zemp *et al*., 2015).

3.3 Ice cores in the Alps

Climate change concern has stimulated interest towards an extension of climate variability indices beyond the instrumental era to differentiate natural variability and anthropogenic influence on longer time scales. Water stable isotopes are suitable for the purpose given that some European glaciers, mainly in the Alps, offer such a possibility, having stored the precipitation history of several hundred years, often with a reasonably high temporal resolution. However, in most cases post-depositional processes alter the originally accumulated isotopic values. The Alps are located at mid latitude, characterized by a temperate climate, and usually it is possible to extract well-preserved ice cores only above 4000 m a.s.l., where the mean annual temperature is below -10°C (Orombelli, 2004). More recently, even low latitude mountain sites have been utilized for ice coring, at very high altitude, like on Mt Kilimangiaro, Caucasus and the Andes.

The paleoclimatic potential of the Alpine region is still largely unexploited, even if the ice coring began in the 1970s, the Eastern Alps have been left behind in the process, because of the scarcity of suitable glaciers, due to lower elevation and smaller glacier dimensions.

Alpine glaciers are usually limited in size and located in a complex topography, with hardly understandable flow patterns (Schwikowski *et al*., 1999). Ice caps and saddles are preferable for drilling, in order to avoid fast horizontal advection of ice caused by steep slopes and to better understand and model the glacial flow (Funk, 1994).
To my knowledge, these are the ice core sites of the Alps that were already exploited (fig. 3.3-1).

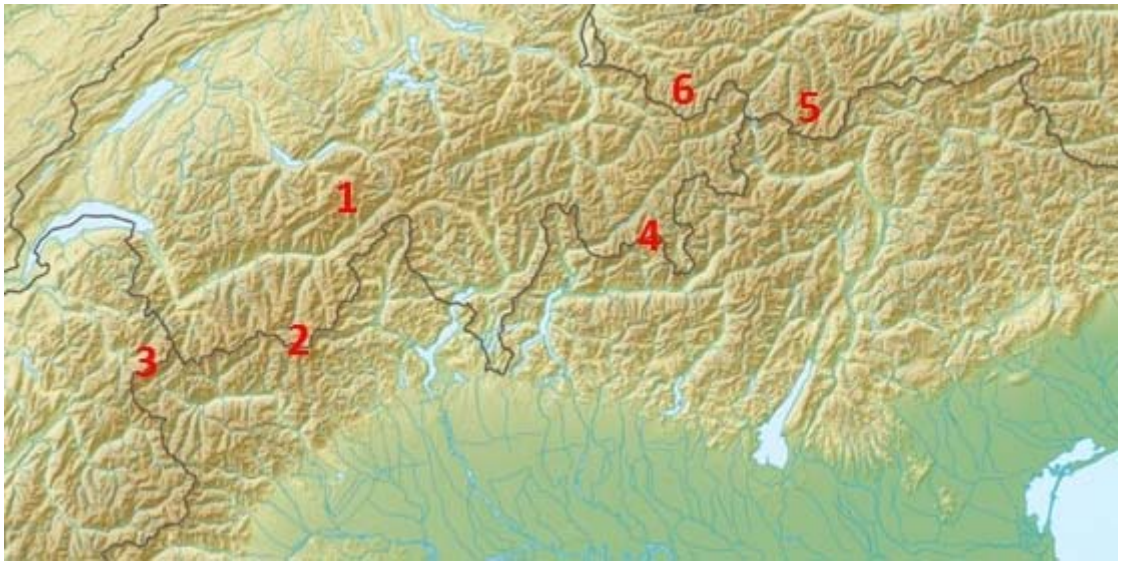

Fig. 3.3-1 Drilling site locations in the Alps; the numbers correspond to the enumeration in the list below

1. Bernese Alps

- Fiescherhorn (two cores: 1989 and 2002) (Schotterer *et al*., 1997, 2002; Schwikowski *et al*., 1999; Jenk, 2006)
- Ewigschneefeld (2010) (Paul Scherrer Institut)
- Plain Morte (three cores in 1972) (Rufli *et al*., 1976)
- Jungfraujoch (three cores, 1972 and 1974)

2. Mt Rosa massif

- Colle Gnifetti (several cores from 1976 to 2005) (Oeschger, 1977; Schotterer *et al*., 1978; Schotterer *et al*., 1985; Lüthi and Funk, 2001, Jenk, 2006)
- Colle del Lys (several cores from 1996 to 2012) (DISAT-UNIMIB)
- Grenzglescher (1994) (Eichler *et al*., 2000)

3. Mt Bianco massif

- Col de Brenva (1986) (Ronseaux and Delmas, 1988)
- Col du Dome (several cores from 1973 to 2004) (Jouzel *et al*., 1984; De Angelis and Gaudichet, 1991; Vincent *et al*., 1997; Preunkert *et al*., 2000)
- Dome du Guter (1998) (Van de Velde *et al*., 1998)
- Mt Bianco summit (1973) (Jouzel *et al*., 1977)

4. Bernina massif

- Piz Zupo (two cores in 2002) (Palmer *et al*., 2003)

5. Ötzal Alps

- Vernagtferner (three cores in 1979, two in 1983) (Oerter and Rauert, 1982; Oerter *et al*., 1985)

6. Silvretta (one core in 2011) (Paul Scherrer Institut)

Only few of these drilling sites are located in the Eastern Alps: Piz Zupo, Vernagtferner and Silvretta.
Isotopic records were obtained just for some of these ice cores.
Other than traditional ice coring, other ice samplings were carried out in Alpine ice caves, at lower altitudes compared to surface glaciers, such as Moncodeno, on the northern side of Mt Grigna (Citterio, 2005) and Mt Canin (Colucci, 2014).
While most of the Alpine glaciers cover relatively short time periods of few hundred years, some are believed to retain climatic information up to 10,000 years, covering almost the entire Holocene (Jenk *et al*., 2006). These extremely long records can be found in low-accumulation sites, and only if the glacier thickness is sufficient. The extremely heterogeneous distribution of precipitation and the significant melting rate occurring at elevation below 4000 m a.s.l., make it very difficult to retrieve ice cores covering such a long time span. The complex ice-flow dynamics affect the preservation of a continuous temporal record, and the ice layers, especially close to the bedrock, might be significantly inclined, and folding of the strata could also occur.
Climate information from the last millennia can also be inferred by historical climatology: the use of historical documentation can provide useful evidence on climate change during the recent part of the Holocene.

Mountains over 4000 m of altitude usually host glaciers in which the temperature is low enough throughout the year to minimize melting, water percolation and refreezing in deeper layers (cold glaciers). Most of the times these sites are exposed to strong winds, favorably eroding light winter snow; depleted in heavier isotopes. Winter precipitation normally sticks better to the surface of sheltered places, but increased summer melting affects the snow seasonal preservation. Since seasonal variations in the isotopic values are much larger than those expected to indicate a climate anomaly (inter-annual variations), any post-depositional change lowers the possibilities of detecting climate variability (Schotterer *et al*., 2002). Even in the hypothetical case in which the precipitation was perfectly archived and the climate noise absent (no changes in air-mass circulation and precipitation pattern), the long-term temperature reconstruction based on oxygen and hydrogen stable isotopes would not be straightforward, considering that the long-term variability could be lower by more than one order of magnitude compared to seasonal variations (Hoffmann *et al*., 2005; Wagenbach *et al*., 2012).

High-altitude Alpine glaciers are characterized by a higher accumulation rate than polar ones, in accordance with a precipitation amount ranging from 500 to 3000 mm per year. Several alpine drilling sites are characterized by an accumulation rate higher than 1 m w.e./a: Ortles (Festi *et al*., 2015), Fiescherhorn, Col du Dome, Colle del Lys; while an accumulation rate reaching ~2.6 and ~2.7 m w.e./a has been recorded at Piz Zupo and Grenzgletscher, respectively (Schwikowski, 2006). The higher accumulation usually permits the preservation of annual layers, characterized by the seasonal oscillation of several chemical species. Post-depositional effects, as well as seasonal distribution of precipitation, can compromise the presence of those oscillations.

Ice core layers, especially in Alpine cores, show a significant thinning along with depth, therefore the depth-age relationship is strongly non-linear. The weight of the overlying firn/ice mass produces a plastic deformation of the ice, causing a horizontal ice flow that stretches the layers proportionally with depth. Thinning rates are higher in cold glaciers compared to temperate glaciers. Given this significant thinning, in the upper part of the core the annual layers may consist of several meters of firn, while in the deeper part the annual layer thickness is reduced to a few centimeters of ice or less. The discontinuity of ice core records can be very high at sites characterized by a high inter-annual variability of precipitation. In many cases, the seasonal distribution of precipitation is known only for the recent times, while remains unknown for the most part of the time span covered by the ice core. Hence, using precipitation weighted parameters, such as precipitation weighted temperature, while strongly suggested, cannot be always achieved (Schwicowsky *et al*., 2014).

Temperature trends derived from isotopic records from cold mountain glaciers often showed supposed long-term variations exceeding by far the real local temperature increment (Wagenbach, 2003).

3.4 Snow, firn, ice and albedo

Different density levels characterize snow precipitation and the different layers of glaciers. The fresh snow (immediately after falling calmly) is comprised between 30 and 100 kg/m^3, while very wet snow, with a significant liquid water content, has a high density, up to 700-800 kg/m^3 (Paterson, 1994). Once the snow has settled, the deconstructive metamorphism changes the crystal forms from complex to more rounded shapes, making them losing their branches and fuse together to form bigger rounded crystals, uniform in size. If there is a strong negative temperature gradient (bottom to top) the vapor, which sublimates in the deeper and warmer part, travels vertically through the air pores to the upper part, encounters cooler temperatures and condenses and refreezes, forming typical big crystals which increase the density of the layer (Hindelang, 2004). Melting increases the rate at which grains become rounded, because the grains melt first at their extremities.

The original strict definition of firn is “snow that has survived one summer without being transformed to ice” (because of melting and refreezing); however, this meaning is not commonly used anymore and there is some ambiguity because of the lack of a clear distinction between firn and snow (Paterson, 1994). Firn turns into glacier ice when the interconnections between the air pockets are sealed off (density: 830 kg/m^3); for example, in Vallée Blanche in the western Alps the firn-ice transition is at 32 m of depth (age: 13 years). The firn density ranges between 400 and 830 kg/m^3. The Glacier ice density goes from 830 to 917 kg/m^3 (Paterson, 1994).

When meltwater percolates downward through the snow/firn column it can refreeze if the temperature is sufficiently low, forming characteristic ice bodies: ice lenses are the (almost) bubble-free (sub) horizontal ice layers, ice glands are pipe-like structures that form when water percolating vertically refreezes.

The so-called superimposed ice is formed when a conspicuous amount of meltwater is produced and the ice layers merge to a continuous mass. Refreezing is the most important factor in warming the snow; during this process the energy is released in the form of latent heat (Cuffey and Paterson, 2010).

All these processes lead to isotopic fractionation between the solid, liquid and gas phase within the snow (Arnason, 1969), the magnitude of which remains largely unknown, but they surely alter, to some extent, the pristine isotopic signal of precipitation (Zhou *et al*., 2000).

In dry-snow zones measuring firn temperature at 10 m of depth allows to infer the mean annual air temperature (Loewe, 1970).

In a temperate glacier the ice is at the melting point throughout, except for a surface 10-m thick layer, in which temperature is below 0°C for part of the year. A temperate glacier has only wet-snow and ablation zones; speaking about zones in a glacier is usually better than classifying the entire glacier as cold or temperate. Some glaciers may lose ice by melting at base but the amount is usually negligible compared to surface ablation (Paterson, 1994).

Albedo is a non-dimensional, unitless quantity indicating how well a surface reflects solar radiation (NSIDC, 2015). The Albedo can be calculated from short-wave radiation measurement; albedo is extremely important and it represents the amount of solar radiation that is reflected back to the atmosphere and does not concur to the increase of the heat of the glacier. It is presented as a percentage (%) or a value from 0 (no albedo) to 1 (all the incoming radiation is reflected by the surface).

The albedo characterizing a glacier shows significant variations, depending on the reflective surface; the typical values are the following: dry snow = 80-97 %; melting snow = 66-88 %; firn = 43-69 %; clean ice = 34-51 %; dirty ice = 15-25 % (Paterson, 1994).

The snow albedo is much higher than the one related to ice; snow covers the glaciers surface, but in temperate glaciers, usually at very low latitudes, the snow cover is increasingly removed until it disappears completely; the increase of the albedo can thus aggravate the melting rate. The lower the albedo, the higher the heat content increment of the glacier and the consequent melting; even with stable temperature, an increased albedo can influence the mass loss of a glacier or snow surface.

As snow gets older, impurity particles (organic remains from plants, particulate matter from pollution, …) accrue within the snow. These darkened particles decrease the snow albedo, causing a temperature increment, and increasing the melting.

3.5 The Ortles Project

The Ortles-Cevedale Group is one of the main massifs of the Alpine region and its summit, Mt Ortles (3905 m a.s.l.) is the second highest peak of the Eastern Alps (fig. 3.5-1). The group hosts

one of the largest glaciated regions of the Southern Alps: 76.8 km^2, about 3.5 % of the total Alpine glacier area (Carturan *et al*., 2013).

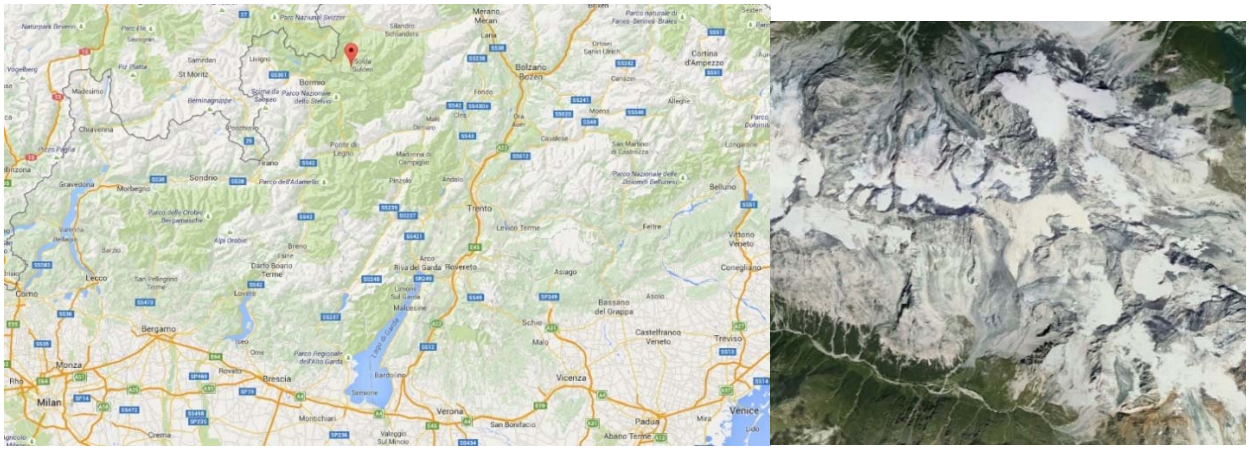

Fig. 3.5-1 Mt Ortles location (left) and the Ortles massif (right) from Google Earth

The Alto dell'Ortles glacier (3870-3018 m a.s.l.) is the most elevated glacier of the mountain, gently sloping (8-9°) for the upper 300 m and then flowing on steeper bedrock, splitting into two major "tongues" down to its lowest elevation point; the total surface area is 1.34 km^2 (Carturan *et al*., 2012) of which ~10% constitutes the upper, gentle slope.

The Ortles-Cevedale glaciers have been retreating since the end of the Little Ice Age (LIA); more recently, between 1987 and 2009, these glaciers lost 23% of their area and under current climate condition, they will need to lose about 50% of their area to reach the equilibrium (Carturan *et al*., 2013).

Under the actual climatic phase most of the glaciers of the Ortles-Cevedale group lie below the snowfall limit (i.e. ~3300 m) during the warmest part of the summer, but the upper part of the Alto dell'Ortles glacier still receives solid precipitations in that period. Nonetheless, prolonged heat waves with dry conditions, like those experienced during the summers of 2003, 2006, 2015 and the first half of summer 2010, are able to ablate these glaciers at all the elevations.

The average snow accumulation, calculated between 2003 and 2009, is ~1200 mm w.e./a, with a minimum of ~1000 mm in 2005 and a maximum of ~1350 mm in 2009. The average reconstructed ablation for the same period, is ~400 mm w.e./a, with a minimum of ~250 mm in 2004 and a maximum of ~600 mm in 2003. The mean annual net mass balance between 2003 and 2009 is ~800 mm w.e./a (Gabrielli *et al*., 2010). A more recent estimation of the accumulation rate, for the last ~5 years, derived from the pollen dating of the Ortles shallow core 2009, is ~1070 mm w.e./a (Festi *et al*., 2015).

The historical documents, such as the painting showed here (fig. 3.5-2), can give us a qualitative estimation of the magnitude of the glacier shrinkage during the last century.

Fig. 3.5-2 The Ortles glaciers seen from the Stelvio pass, in a century-old painting (on the left) and in a recent photograph (on the right)

Since 2007, during every summer, at least one survey was conducted at the top of the glacier, in the framework of a climate reconstruction project, The Ortles Project (www.ortles.org), which culminated with the drilling of four deep cores during autumn 2011 (Gabrielli *et al*., 2012). Since the first visual observations, the lamination of the exposed ice appeared excellent down to bedrock (Gabrielli *et al*., 2010)

Since 2008, at least one snow pit was dug each summer; during more recent years (2012 and 2013) two snow pits were excavated each July and September, marking the beginning and the end of the ablation season: one at the drilling site and one at the AWS site. Mass balance measurements were conducted on each snow pit, based on a stratigraphic visual inspection of snow, starting from June 2009. The drilling and the AWS sites are characterized by a slightly different yearly and summer accumulation: the drilling site receives about 80% of the accumulation registered at the AWS site (fig. 3.5-3). The yearly mass balance measurements from 2009 to 2013 are reported below.

RESULTS – MASS BALANCE MEASUREMENTS

	AWS site			Drilling site				
Year	Winter balance (mm w.e.)	Summer balance (mm w.e.)	Annual Net balance (mm w.e.)	Winter balance (mm w.e.)	Summer balance (mm w.e.)	Annual Net balance (mm w.e.)	Net balance ratio (D.S. / AWS)	Mean summer temperature (°C)*
2009	1017	134	1151	-	-	-		-1
2010	872	-433	439	-	-	-		-1.2
2011	1076	209	1285	790	137	927	0.72	-1.7
2012	748	47	795	605	55	660	0.83	-0.2
2013	1674	-454	1220	1075	-74	1001	0.82	-1.3

Fig. 3.5-3 Ortles AWS and drilling site mass balances, credit to Carturan (personal communication)

The annual net balance is always largely positive, and the summer balance is positive too for most of the times; considering this dataset (fig. 3.5-3), only the summers of 2010 and 2013 are characterized by a negative mass balance. Summer accumulation is not always related to the mean summer temperature: 2010 and 2013 summer months were not particularly warm: -1.2 and -1.3°C, respectively, but showed a negative mass balance, while the summer of 2012 was relatively warm (-0.2°C) but the summer balance was still positive (+47 mm w.e.). The winter mass balance is characterize by significant inter-annual variations, ranging from 748 (2012) to 1674 mm w.e. (2013) for the AWS site.

Two 10-m deep shallow cores were retrieved in the area: the first in June 2009, the second in September 2010.

Between September and October 2011, four cores were drilled within 20 m from each other, using a lightweight electromechanical drill, protected by a dome tent and powered by a 1.5 kW diesel generator (Zagorodnov *et al*., 2000). Three ice cores reached the bedrock at final logged depths of 75.5 m (#1), 76.1 m (#2) and 75.1 m (#3); the last drilling was stopped at 61.0 m (#4), approximately 15 m above the bedrock, due to technical problems affecting the drill. The chosen spot is a small col, located at 3859 m a.s.l. (46°30’25” N, 10°32’34” E), where the glacier thickness is approximately 75 m and the stratification close to horizontal.

On average, the cores were wet until a depth of about 30 m, indicating the presence of temperate firn. During the drilling operations the existence of cold ice below 30 m was immediately evident

since the diameter of the borehole began to narrow as meltwater, flowing from the upper firn portion (above 30 m depth) into the lower part of the borehole, refroze.

Fig. 3.5-4 The drilling dome located at 3859 m a.s.l. on the Alto dell'Ortles Glacier

The glacier is currently transitioning from a cold to a temperate state (fig. 3.5-5), and the preservation of the lower strata suggests that the ice had been steadily cold until few decades ago, when most of the temperature increase started to occur. The borehole temperature profile (fig. 3.5-5), obtained in core #1 drilling hole, is characterized by values reaching 0°C in the firn part, but steadily decreasing below the firn/ice transition, eventually reaching -2.8°C at the bottom.

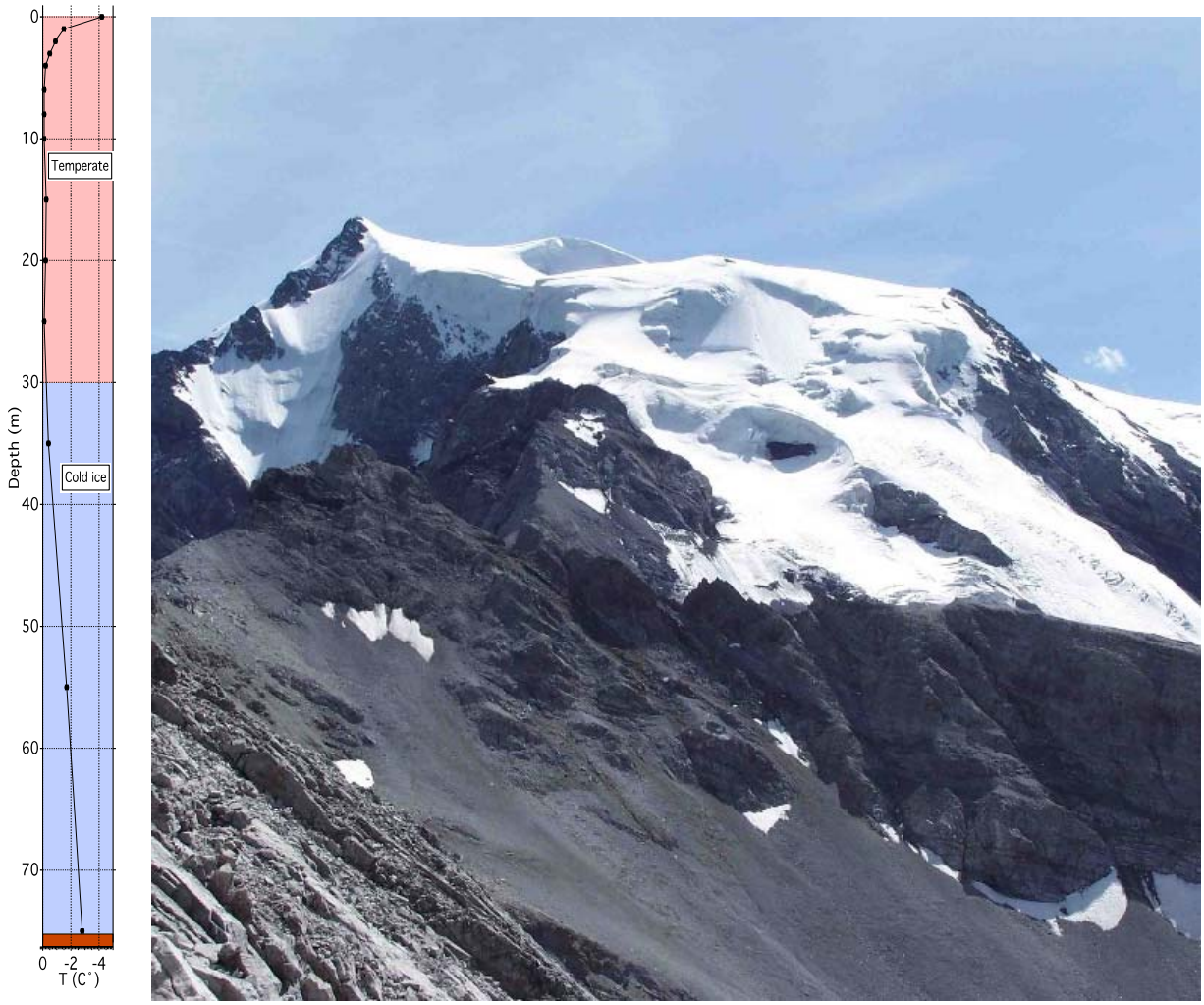

Fig. 3.5-5 Borehole temperature profile, the pink part represents the firn portion, the blue part the ice (left). View of the northern side of Mount Ortles (3905 m a.s.l.) in August 2008, topped by snow (credit to Gabrielli P.). The Alto dell'Ortles glacier is visible on the right of the summit

The reconstructed surface air temperature record (1864-2010) for the upper part of the Ortles (3850 m a.s.l.), obtained via humidity lapse rate from the Careser diga (~15 km southwest, 2605 m a.s.l.), and Säntis meterological station (~120 km southwest, 2502 m a.s.l.) data, shows an increment of ~2°C for the mean summer temperature during the last three-four decades; the yearly average temperature displays a less pronounced positive trend (fig. 3.5-6). The amplitude of inter-annual variations seems also more evident for summer data. The warming, during the first century of the data set, is negligible for both summer and yearly temperatures, but higher temperatures, especially during summer, can be spotted in the late 1940s and the early 1950s. The exceptionally heat wave of 2003 (mean summer temperature: 2°C) is clearly visible in the summer temperature record, but did not remarkably affect the mean annual temperature of that year.

The polythermal state of the glacier is hence in accordance with the temperature behavior for the last part of the 20th and the beginning of the 21th century.

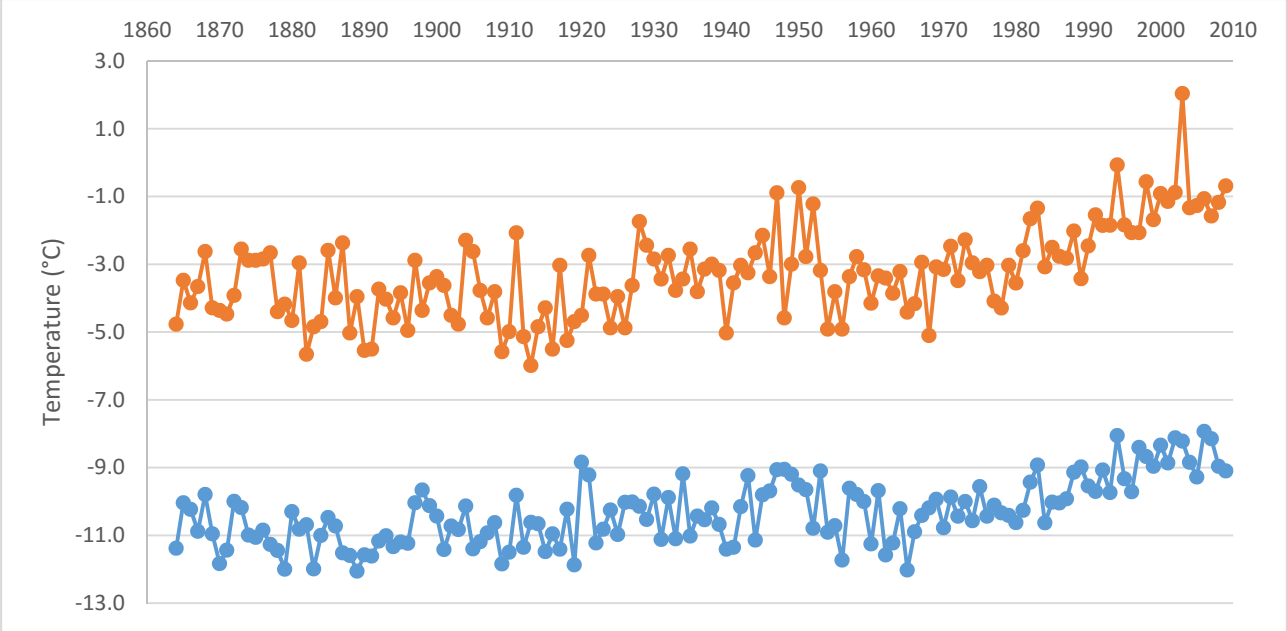

Fig. 3.5-6 Reconstructed mean summer (orange) and mean annual (blue) temperature for the upper part of the Ortles (3850 m a.s.l.)

During June 2010, a first automatic weather station (AWS) was installed 2 m above the surface, to record temperature, precipitation, pressure, elevation, wind intensity and solar radiation, coupled with four thermo sensors to monitor the height of snow. On September 30, 2011, a more advanced AWS has been placed on Alto dell'Ortles (3830 m a.s.l.), in order to measure air temperature, relative humidity, wind speed and direction, snow depth, ingoing and outgoing longwave and shortwave radiation. The AWS was then upgraded by also installing a 20-m temperature string in a new firn borehole. In July 2015 the AWS was removed with the idea of replacing it with a more advanced one within a short time.

3.6 Back-trajectory analysis

The knowledge about the moisture sources and transport patterns has the potential to improve the understanding and interpretation of stable isotopes in precipitation content and in paleo archives (Sodemann and Zubler, 2010).

Using reanalysis data from the ERA-40: European Centre for Medium-Range Weather Forecasts (ECMWF) and a Lagrangian moisture source diagnostic (Sodemann, personal communication), covering a 7-year period from January 1995 to August 2002, monthly moisture source contributions for Mt Ortles grid point on ERA-40 model have been obtained. The results, in terms of precipitation contribution (mm/day), are presented in fig. 3.6-1.

The Alpine moisture sources were inferred using a Lagrangian moisture source transport diagnostic, which identifies changes in specific humidity along the backward trajectories of air parcels precipitating over a target area. The method identifies evaporation sources of moisture based on an air parcel position inside or outside the atmospheric boundary layer during increases of specific humidity (Sodemann *et al*., 2008).

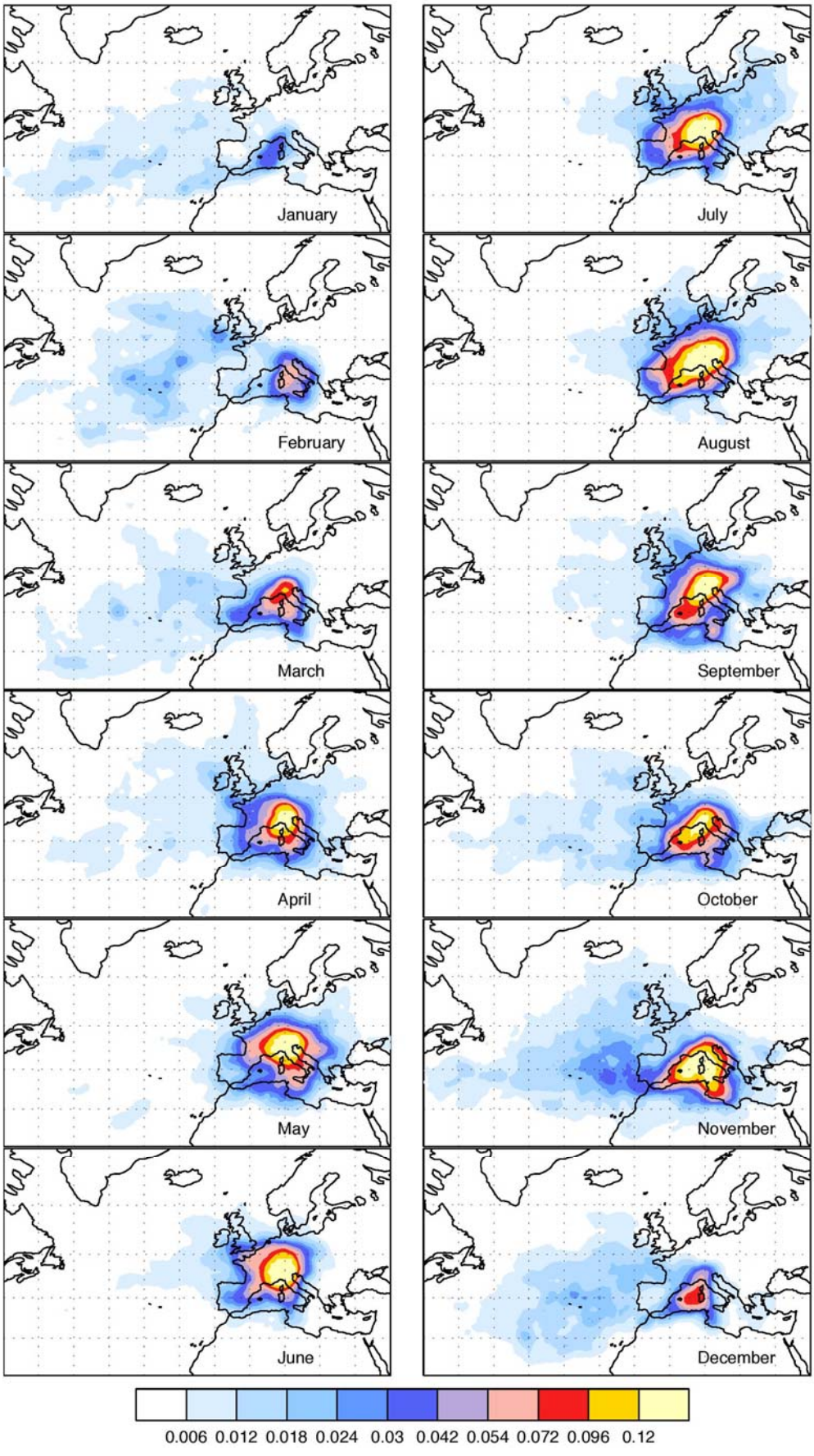

Fig. 3.6-1 1995-2002 reanalysis mean monthly precipitation contribution (mm/day) for Mt Ortles (Sodemann, personal comm.)

In the ERA-40 model, the Mt Ortles grid point is located in the Southern Alps, but close to the border with the Northern Alps; the precipitation contribution is thus somehow in between the two meteorological macro-regions of the Alpine mountain range. The Mediterranean source prevails during autumn and winter (from October to February), while during spring and summer (from March to September), the continental recycled precipitation source seems to be the major contributor to Mt Ortles precipitation. The North Atlantic moisture is never the main source, but its contribution is important during late autumn and winter.

CHAPTER 4: INSTRUMENTAL DATA

4.1 Instrumental temperatures in the Ortles area

The Ortles region has been well-covered in terms of instrumental temperatures for the last 150 years, but no direct temperature measurements from the summit of the Ortles Mountain are available before 2011. The most extensive dataset is the Ortles reconstructed temperature record, characterized by a monthly resolution, going from 1864 to 2009 (Gabrielli *et al*., 2010). The Ortles reconstructed temperature derives from the original instrumental data (1864-1958) from the Säntis meteorological station (~120 km northwest, 2502 m a.s.l., Switzerland), corrected using the linear regression (Careser = 1.1082*Saentis + 0.9098) between the Säntis and the Careser diga station (~15 km southwest, 2605 m a.s.l.), plus the humidity lapse rate measured between the Careser station and Cima Beltovo (3325 m a.s.l.). After 1958, the Careser diga temperature data were used to reconstruct Mt Ortles temperature, using the mean humidity lapse rate between Careser diga and Cima Beltovo (-7.2°C/1000 m).

From 2005 to 2013, a new reconstructed temperature record (Carturan and De Blasi, personal communication) has been developed; based again on the Careser diga instrumental measures, it was corrected using the humidity lapse rate between this station and the Ortles AWS (3835 m a.s.l.), calculated for the period October 2011 - September 2013. Three different methods were used to reconstruct the temperature: i) a fixed mean lapse rate ii) linear regression between Careser diga and Ortles AWS temperature iii) mean monthly lapse rate; the difference between the three is negligible. These series have a daily temporal resolution. The fixed lapse rate found between Careser diga and the Ortles AWS, -7.1°C/1000 m, is very close to the one obtained between Careser diga and Cima Beltovo for the previous temperature reconstruction: -7.2°C/1000 m.

Since October 2011, the instrumental temperature from Mt Ortles has been provided by the AWS placed in proximity of the summit and the drilling site, at 3835 m a.s.l., with hourly resolution.

	Period	Source	Correction
Ortles reconstructed I	1864-2009	Säntis (1864-1958) Careser diga (1959-2009)	• Lapse rate between Careser and Cima Beltovo • Linear regression between Säntis and Careser
Ortles reconstructed II	2005-2013	Careser diga	Lapse rate between Careser and Ortles AWS
Ortles AWS	2011-2014	Ortles AWS	None

Tab. 4.1-1 The different sources of Ortles temperature series are summarized in this table

4.2 The Ortles automatic weather station

The temperature record from the Ortles AWS (Carturan and De Blasi, personal communication), covering the October 2011-December 2014 time period and characterized by a daily and monthly resolution, is showed in fig. 4.2-1. The mean monthly temperature stays below 0°C for the whole period, with the exception of August 2012, the only positive datum (0.23°C). Days of positive temperature occur every summer, with maximum values close or even higher than 5°C during the warmest days. The lowest daily value was recorded on February 11, 2012: -30.72°C, while the highest, +5.23°C, belongs to August 4, 2013. The hourly maximum was measured on May 11, 2012 at 2 PM: +8.47°C while the coldest hour was on February 10, 2012 at 2 AM: -33.88°C. Among the years covered by the Ortles AWS, 2012 shows the highest variation between winter and summer, while 2014 was characterized by a relatively mild winter and cool summer. The average value for the whole period October 2011- December 2014 is -8.74°C; for comparison, the mean temperature from the Ortles reconstructed series 1964-2009 is -10.3°C. The average value from 1864 to 1970 is -10.7°C, while the value from 1971 to 2009 is -9.4°C, implying an increment of 1.3°C for the last four decades mean value. The AWS data (2011-2014) suggest a further increase of 0.7°C and a total rise of 2°C with respect to the period 1864-1970.

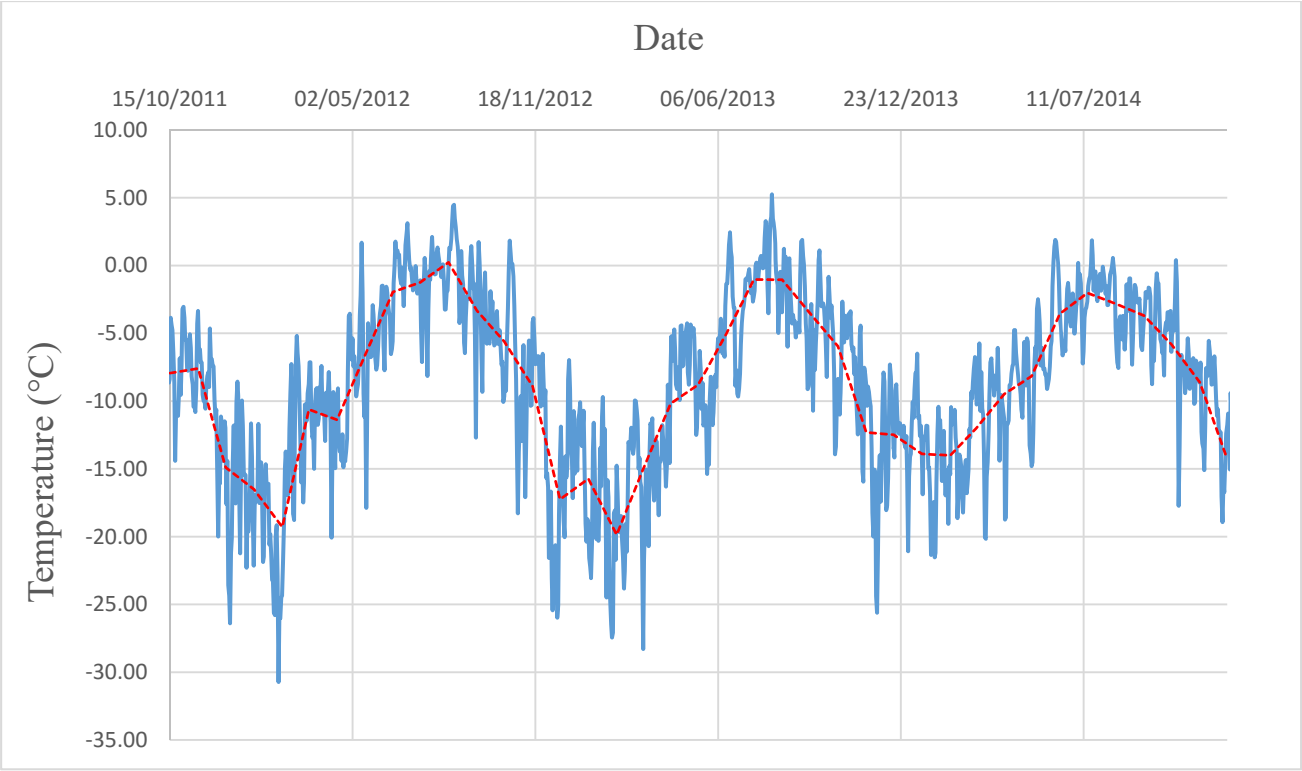

Fig. 4.2-1 Ortles AWS daily (solid blue line) and mean monthly (red dotted line) temperatures Oct 2011- Dec 2014

The snow accumulation was not directly measured, but derives from the snowpack height measurements obtained with a sonic ranger placed on the AWS, with hourly sampling resolution; the value is referred to the distance between the snow surface and the snow gauge. The snow height changes for each month, between October 2011 and December 2014, are showed in fig. 4.2-2, with negative values occurring each year in December and during summer (the month varies from year to year); March shows negative accumulation twice: in 2011 and 2012. July 2013, the worst month of the dataset for accumulation, shows a net balance of -54.2 cm. October is characterized by the highest snow accumulation in three out of four years, with the only exception of 2012. The mean snow height gain for the whole period is 23 cm per month; the yearly snow height increment shows significant variations: 177 cm in 2012, 289 cm in 2013 and 397 cm in 2014. The total snow height gain from October 2011 to December 2014 is largely positive: 899 cm. It has to be taken into account that this is not the actual real accumulation, but the datum derived from sonic ranger measurements, which can be influenced by extremely local conditions.

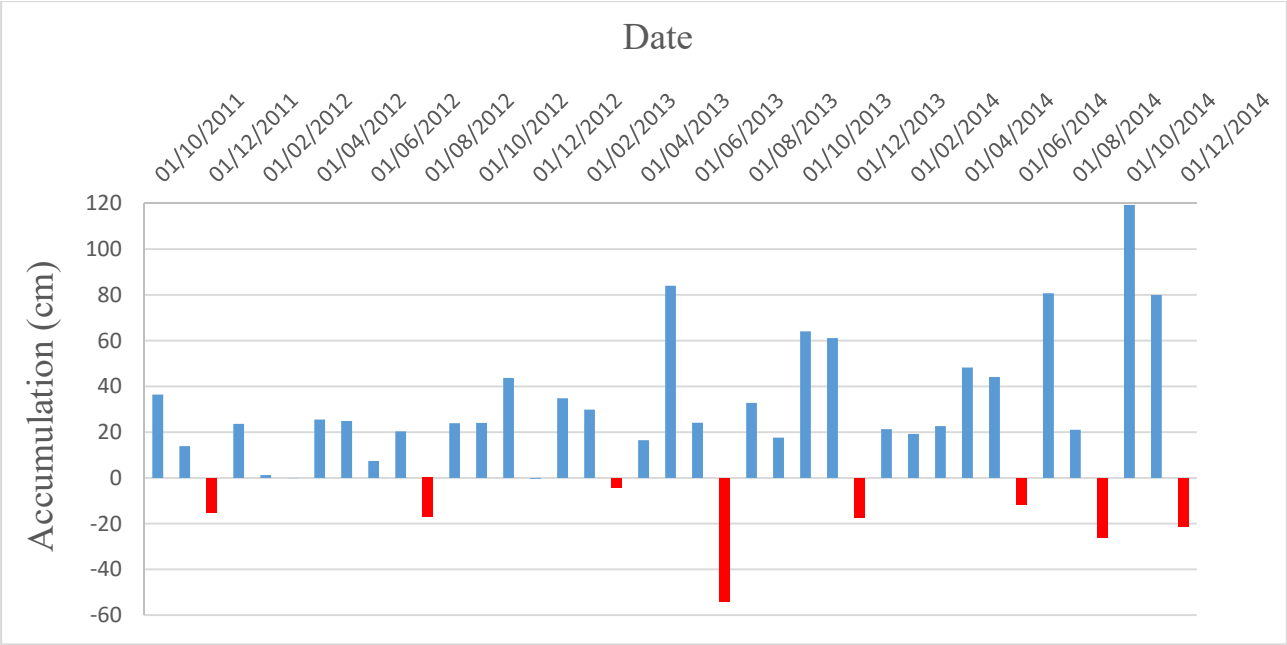

Fig. 4.2-2 Ortles AWS snow accumulation/depletion for each month (October 2011 - December 2014). Blue bars for positive accumulation, red bars for negative accumulation

Wind is believed to play a major role in winter snow depletion and thus in the recorded negative mass balances during each December. Wind speed and direction are reported in fig. 4.2-3 and despite a huge daily variability, and a significant inter and intra-annual variability presented by both speed and direction records, a seasonal trend can be observed for at least the wind speed. The highest mean monthly values, around 8-10 m/s, are recorded during winter, and the lowest, between 3 and 4 m/s, normally occur in summer. The wind direction does not present a clear seasonality.

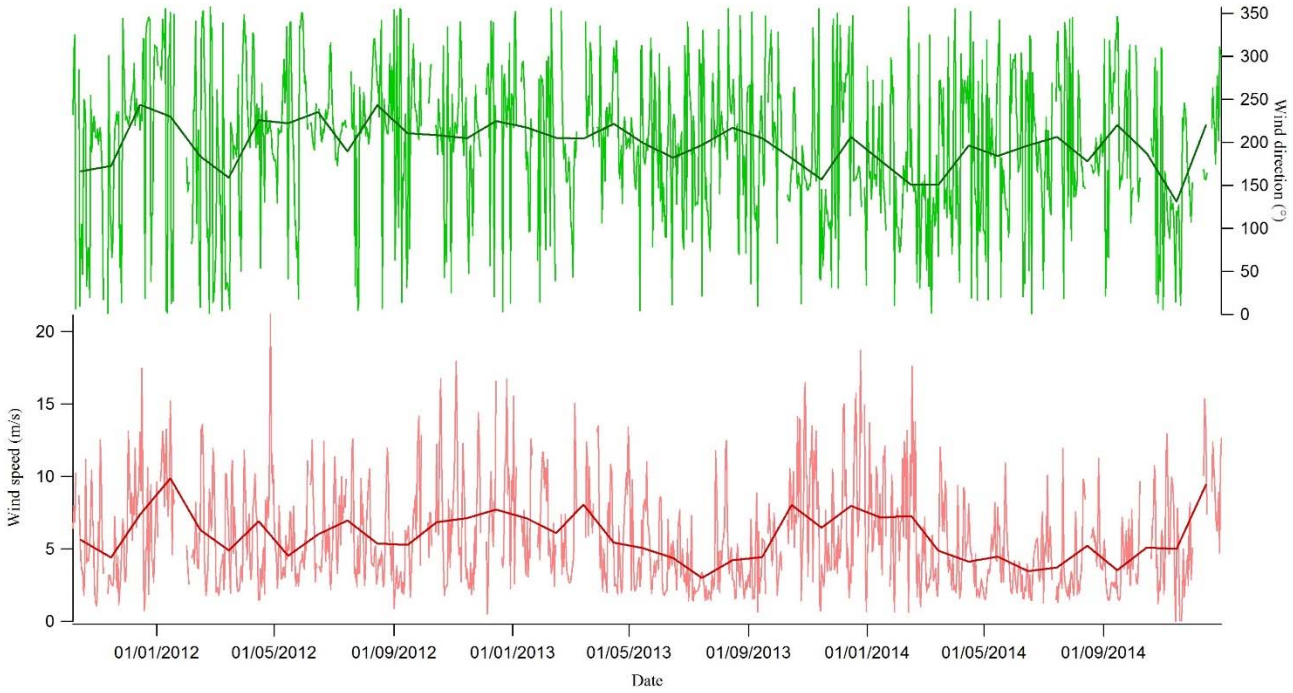

Fig. 4.2-3 Daily (thin red line) and mean monthly (thick red line) wind speed, below; daily (thin green line) and mean monthly (thick green line) wind direction (October 2011 – December 2014)

The incoming and outgoing shortwave radiation have been continuously measured by the Ortles AWS since July 2012. By subtracting the outgoing shortwave radiation from the incoming shortwave radiation we should obtain a measure of the albedo: the higher the difference between incoming and outgoing shortwave radiation, the lower the albedo (it means that a conspicuous part of the incoming shortwave radiation is not reflected). The results are presented in fig. 4.2-4: the higher values (meaning lower albedo) were recorded during summer, the lower (higher albedo) during winter; the glacier surface during summer is characterized by older snow (it is a dry season for the area) and the dust content usually rises in summer, dirtying the snow and lowering the albedo. The data show a significant inter-daily and inter-annual variability: summer 2014 is characterized by lower values (meaning higher albedo) compared to previous summer data, in accordance with the meteorological conditions of that period: low temperatures (with respect to the mean summer values) and frequent precipitation.

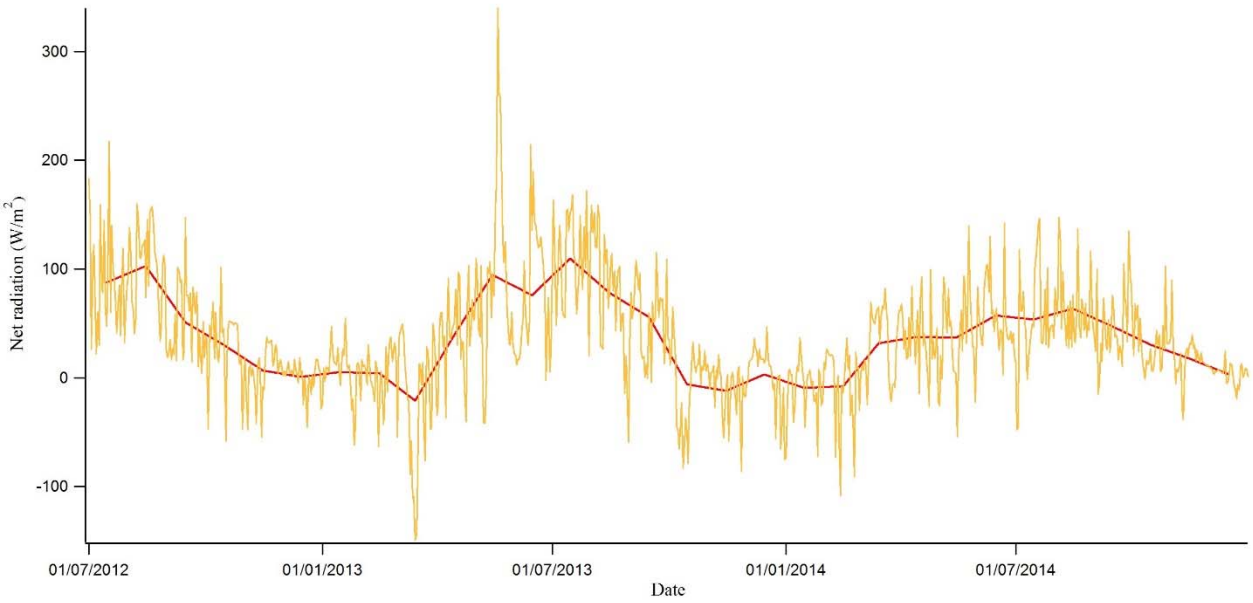

Fig. 4.2-4 Non-reflected radiation from July 2012 to December 2014: daily (yellow line) and mean monthly (red line) data

4.3 Gridded-dataset temperatures

Different gridded temperature datasets are available for the Alpine region; E-OBS and HISTALP (Historical Instrumental Climatological Surface Time Series of the Greater Alpine Region) are among the most used series.

E-OBS is a European land-only gridded dataset for precipitation and minimum, maximum and mean surface temperature, including 2316 stations (Haylock *et al*., 2008). It has a maximum spatial resolution of 0.25x0.25°, so the Ortles cell was chosen to compare the dataset temperature (Palazzi, personal communication) to the Ortles reconstructed temperature (fixed lapse rate between Careser diga and Cima Beltovo: -7.2°C/1000 m). For the period 1950-1958, the Ortles reconstructed temperature was obtained using the Säntis meteorological station data. The DTM (Digital Elevation Model) obviously underestimates the Ortles elevation, averaging the altitude of the entire area included in the cell: the elevation is only 2015.5 m

The predictable consequence is a conspicuous overestimation of the Ortles temperature (fig. 4.3-1), ranging from +7.8 and +14.4°C (average difference: +11.6°C), but the frequency and the magnitude of inter and intra-annual temperature variations is well replicated by the E-OBS record. If only a reconstruction of temperature variations is needed, without needing the absolute temperature values, this gridded dataset temperature record will be suitable for the purpose.

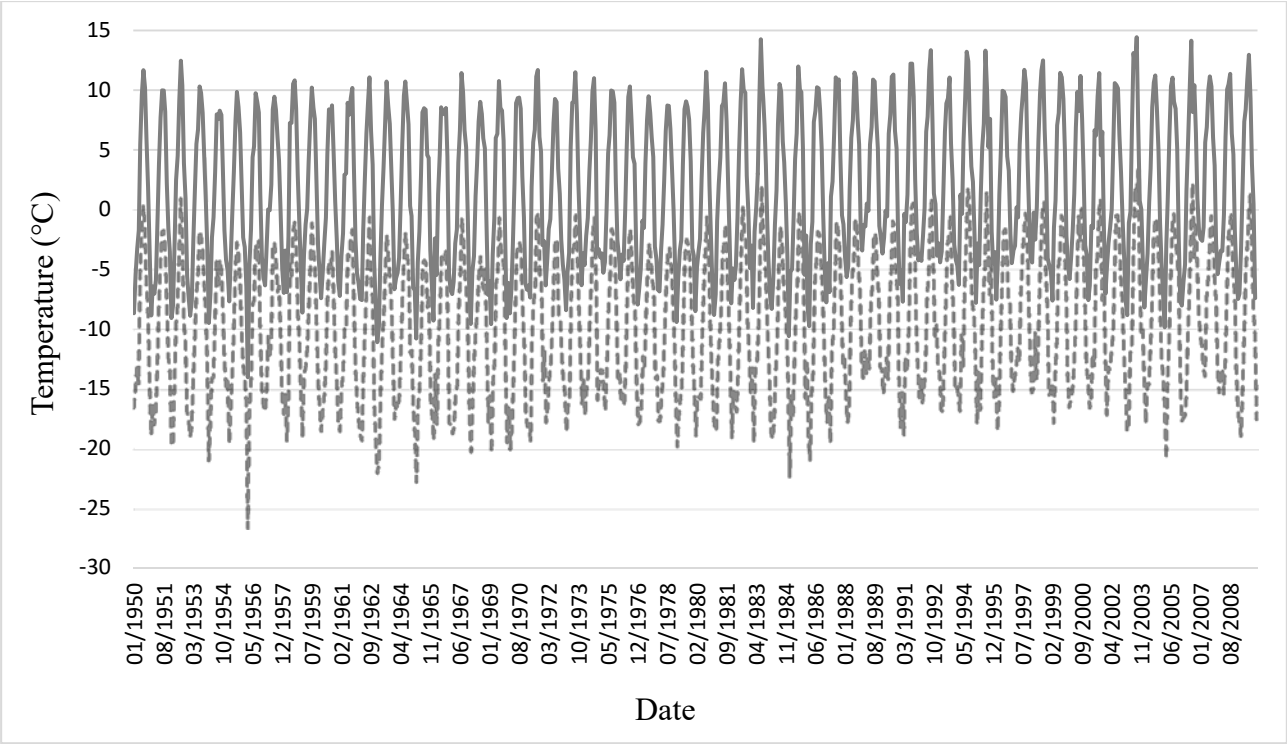

Fig. 4.3-1 Ortles mean monthly temperature (dotted line) and E-OBS mean monthly temperature (solid line) between 1950 and 2009

Knowing the elevation from the E-OBS DTM for the Ortles grid point, it was possible to correct the E-OBS temperature by using the mean monthly humidity lapse rate (measured between Careser diga and Ortles AWS, 2011-2013), considering an elevation difference between the DTM and Ortles of 1820 m and assuming that the lapse rate has remained substantially constant in the last six decades.

The lapse-rate corrected E-OBS temperature for the Ortles grid point is showed in fig. 4.3-2, in this case it is lower than the Ortles reconstructed temperature for the whole record (from -5.2 to -1.26°C, average difference: -2.3°C), but it is closer to the Ortles reconstructed temperature than using the original dataset.

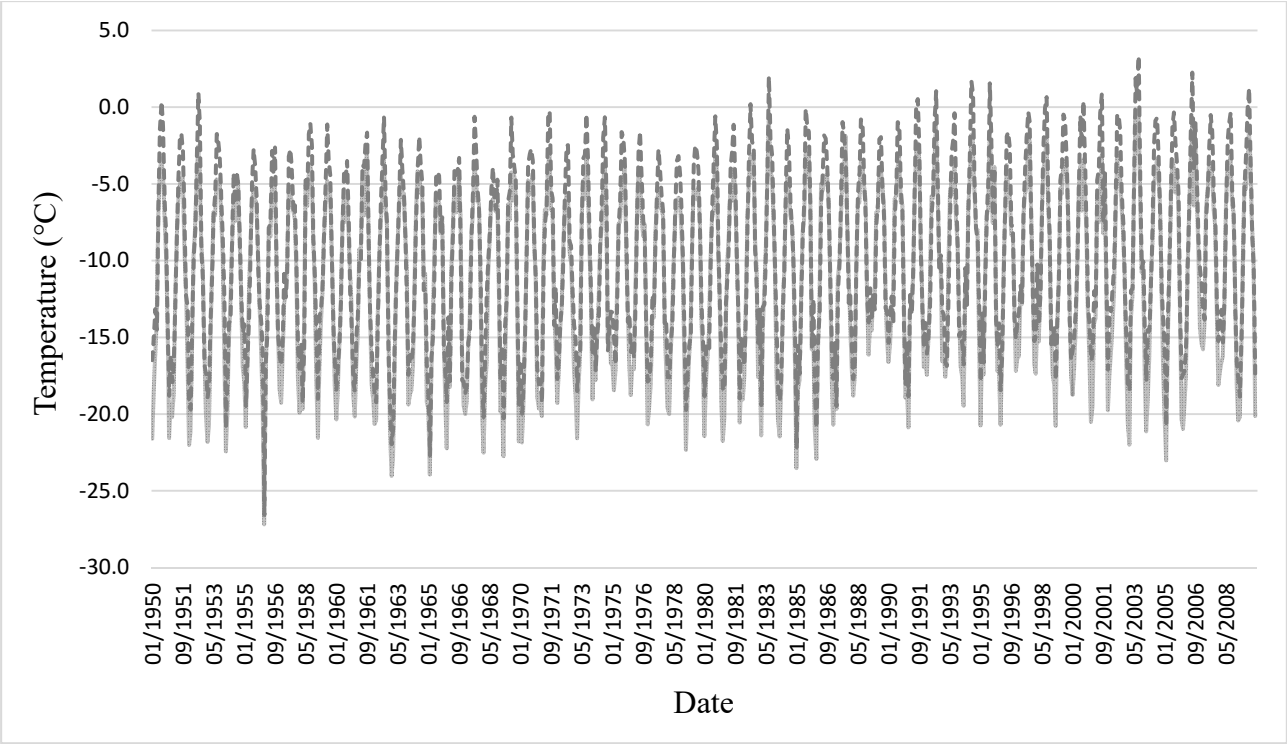

Fig. 4.3-2 Ortles mean monthly temperature (dotted line) and E-OBS mean monthly temperature corrected for altitude (solid line) between 1950 and 2009

HISTALP is a gridded dataset of monthly temperature, air pressure, precipitation and sunshine records for the "Greater Alpine Region" (GAR, 4-19° E, 43-49° N, 0-3500 m a.s.l). The longest temperature series goes back to 1760 (the database includes 131 temperature series, with a mean length of 147.4 years), and has a high spatial resolution: 0.09x0.09°C (Auer *et al*., 2007). Using the temperature from the Ortles grid point (Palazzi, personal communication) it was possible to compare this dataset with the Ortles reconstructed temperature. Unfortunately, no information was available concerning the DTM elevation for the Ortles cell, so it was not possible to adjust the HISTALP temperature via lapse rate. The comparison (1864-2008) is showed if fig. 4.3-3. The Ortles reconstructed temperature was calculated, for the period 1864-1958, using temperatures from the Säntis meteorological station, while from 1959 to 2009 the Careser diga meterological station data were used; Mt Ortles temperature was obtained via humidity lapse rate between the meteorological stations and Cima Beltovo.

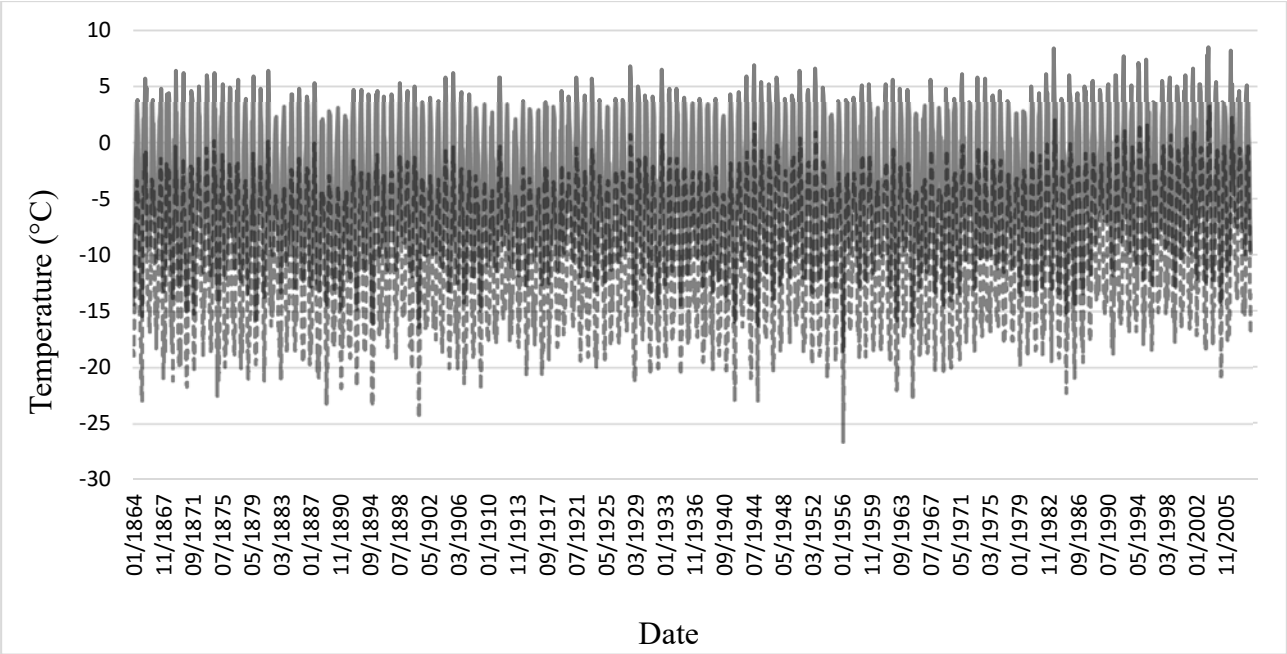

Fig. 4.3-3 Ortles mean monthly temperature (dotted line) and HISTALP mean monthly temperature (solid line) between 1864 and 2008

Like E-OBS, also HISTALP overestimates the Ortles temperature; even in this case it is probably due to the lower elevation of the Ortles grid point with respect to Mt Ortles altitude. The mean difference is +6.5°C, while the maximum (minimum) difference is +9.7 (+3.5) °C. Compared to E-OBS, the temperature overestimation is less pronounced. The HISTALP record replicates very well the magnitude and frequency of temperature variations.

CHAPTER 5: MATERIALS AND METHODS

A total of four deep ice cores were retrieved during the autumn 2011 field campaign at 3859 m a.s.l. on Mt Ortles. From the same spot, several snow pit samples have been obtained since 2008, and two shallow ice cores were drilled, in 2009 and 2010.
In the framework of this PhD project, Core #1 was processed and inspected at the IDPA-CNR cold room at the Ca' Foscari University of Venice. The isotope samples ($\delta^{18}O$, δD, *d*) from core #1 and from the July 2014 and September 2014 snow pits were analyzed at the Isotopic Geochemistry Laboratory of the Department of Mathematics and Geosciences at the University of Trieste, Italy, as well as the tritium samples from the 35-55 m section of core #1. About 250 samples from core #1 were analyzed for water stable isotopes at the BPCRC of the Ohio State University during the period abroad of this PhD, as part of an inter-calibration project between the Italian and American laboratories. All the isotopic data are reported versus VSMOW.

5.1 The mass spectrometer

The mass spectrometer measures the masses and relative concentrations of atoms and molecules. It is based on the utilization of the basic magnetic force on a moving charged particle. The instrument determines the mass of a molecule by means of the mass-to-charge ratio (m/z) of its ion. The ions are obtained from the molecules by inducing either the loss or gain of a charge. Ions are then electrostatically directed into a mass analyzer where they are separated according to m/z and eventually detected. There are several ways to ionize the molecules: protonation, deprotonation, cationization, electron ejection and electron capture. Electron ionization was the most common method until the 1980s and it works fine for small molecules, but it is not suited for most of the bio-organic compounds, characterized by big masses. Many other methods were introduced since then (Scripps).

5.1.1 Isotope Ratio Mass spectrometry (IRMS)

Dole (1935) measured oxygen isotope ratios for the first time in Lake Michigan water.
The IRMS, originally developed by Nier (1937), is a mass spectrometry technique dedicated to the extremely accurate analysis of just few masses and it is performed sequentially on samples and the reference gas.

The instrument is composed by a ion source, a tungsten or thorium filament, which emits an electron beam that ionizes the inserted sample (gas); the ions (usually cations with a single charge) are then accelerated and focalized through electric fields in a vacuum tube. The internal pressure has to be very low (around 10^{-8} Pa) in order to not interferes with the sample. The ions form a thin beam, which flows within the vacuum tube, with the kinetic energy of each particle expressed by the equation

$$1/2mv^2=Ve$$

Where m is the ion mass, v is the velocity, V is the potential difference and e is the ion charge.
The central part of the vacuum tube is curved (angle between 30° and 180°) and exposed to an intense magnetic field (around 7000-8000 Oe), generated by an electromagnet. Once it enters the magnetic field, the ion beam is deflected and each particle is subjected to the following force

$$Hev = mv^2r^{-1}$$

Where Hev is the magnetic force and mv^2r^{-1} is the centrifugal force. From this equation it is possible to obtatin the radius (r)

$$r = (1/H)*(2V*m/e)^{1/2}$$

It is now clear that ions characterized by a different mass-over-charge ratio are deflected in a different way, and given that each ion has the same charge (+1), its deflection only depends on its mass. From the initial single ion beam now different beams are separated, depending on the ion mass, and each beam will impact on a different collector (Faraday cup). Each ion species carries an electric charge and the ion flux generates an electric current, which is registered and amplified. By indicating with A_1 and A_2 two different ion species (isotopes), we have

$$A_1/A_2 = i_1/i_2$$

Where i is the electric current. The IRMS does not precisely measure the A_1/A_2 ratio, but can determine with extreme accuracy the difference between the A_1/A_2 ratio of a reference standard and a sample.
Dual inlet instruments switches many times between the sample and the reference gas, comparing the detected currents from the faraday cups, in order to obtain the isotope ratio of the unknown samples over the reference gas.

Measuring directly the mass of the different H_2O isotopologues is not feasible because of the stickiness of water molecules, not allowing proper vacuum conditions, and because the $HD^{16}O$ molecule can be masked by $H_2{}^{17}O$, having the same mass (19).

In the majority of instruments (and in the one used for this study), oxygen-18 is measured via gas-liquid equilibrium fractionation using gaseous CO_2, where three different masses can be detected: 44 ($^{12}C^{16}O_2$), 46 ($^{12}C^{18}O^{16}O$) and 45, which can be both $^{12}C^{17}O^{16}O$ and $^{13}C^{16}O_2$: this is the reason why oxygen-17 is very difficult to measure. The isotope exchange happens during the following reaction between the liquid (water) and the gas (CO_2): $H_2{}^{18}O+C^{16}O_2 \leftrightarrow H_2{}^{16}O+C^{16}O^{18}O$, through the intermediate formation of H_2CO_3; the different CO_2 isotopologues are then measured with the IRMS, obtaining the $C^{16}O^{18}O/C^{16}O_2$ ratio. The equilibration time is set to 36000 seconds (Epstein and Mayeda, 1953).

Deuterium can be measured by reduction of water over hot (800°C) uranium, nickel, manganese, chromium or zinc, but can also be analyzed via equilibration between H_2O (liquid) and H_2 (gas), using platinum bars as catalyzers to favor the exchange between the two phases (Horita, 1988).

In the IRMS utilized for this study, the deuterium is measured by means of equilibration of the liquid sample (H_2O) with H_2 gas, with the reaction $HDO+H_2 \leftrightarrow HD+H_2O$. The equilibration time is set to 7200 seconds.

When using the equilibration method, is fundamental to maintain a very stable, known temperature, in order to assess the isotope fractionation factor. The ideal thermic conditions can be obtained by using a thermostatic bath or a thermostatic chamber with fixed water/air temperature and by having reduced temperature variations inside the room.

5.2 Cavity Ring-down Spectroscopy (CRDS)

An alternative analytical methodology to the classical IRMS has been recently developed: the laser absorption spectroscopy (LAS). The Lambert-Beer law equation is the physical basis of the laser absorption techniques: a decreasing exponential function describes the intensity decrease of the light traveling through a medium, due to the interaction with the medium. The absorption rate depends on the sample concentration and on the optical path length:

$$I = I_0{}^{-\alpha x}$$

Where I_0 and I are the light intensities before and after crossing the medium, α is the absorption coefficient and x is the path length.

One of the main brand producing high-precision laser absorption spectroscopes is Picarro, which developed its own version of LAS: the Cavity Ring-Down Spectroscopy (CRDS).
The CRDS analytical technique is based on the unique infrared absorption spectrum of gas-phase molecules, used to quantify the concentration of several molecules (H_2O, CO_2, CH_4, N_2O, H_2S, etc.). A specific instrument has been designed to measure the different water isotopologues.
Vibrational modes allow a molecule to absorb photons of corresponding energies; considering the water molecule in the vapor phase, the vibrations include combinations of symmetric stretch (v1), asymmetric stretch (v3) and bending (v2) of the covalent bonds (Chaplin, 2015). The vibrational modes of a molecule are determined by its shape and by the masses of its atoms, so different isotopologues have different vibrational modes, resulting in different optical properties in the infrared range, allowing to discriminate between $^1H_2{}^{16}O$, $^1H_2{}^{18}O$ and $^1H^2H^{16}O$.

A Picarro liquid analyzer for water stable isotopes is composed by the following parts

- The auto-sampler, including the vial tray holder and the syringe holder
- The vaporizer, which receives the liquid water sample from the syringe and vaporizes it at a temperature set at 110°C
- The vaporizer vacuum pump, which cleans off the old sample remains from the vaporizer
- The Data Acquisition Unit (DAS), containing the chamber in which the sample is analyzed, where the temperature and pressure are controlled with high precision
- The Computer Power Vacuum Unity (CPVU), containing the computer hardware and the internal vacuum pump (this pump is external since the 2nd generation of instruments)

Since the 2nd generation of instruments, the DAS and the CPVU units have been merged in one case. A short laser pulse of a specific infrared wavelength is emitted by a diode into the small cavity (35 cc); after reaching a threshold, the laser is turned off and the light bounces back and forth into the cavity using three high-reflectance mirrors (reflectivity: 99.999 %), covering an optical path of more than 10 km. The laser is a 50 mW CW diode laser. A photo detector, placed behind one of the mirrors, measures the beam exponential decay. The absorption time is calculated in presence and absence of the sample, and the difference between the two times is used to calculate the absorbing species concentration. What is really measured is the decay rate, rather than the absolute absorbance (fig. 5.2-1).

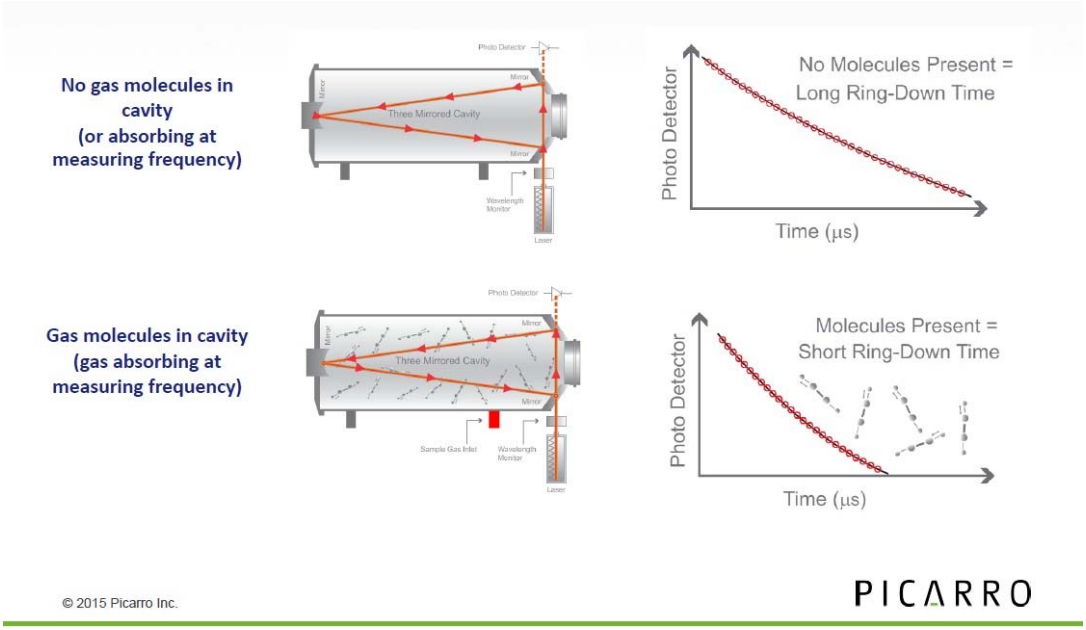

Fig. 5.2-1 Picarro cavity ring-down spectroscopy scheme. Source: www.picarro.com

The temperature inside the cavity is stabilized at 80°C, and the pressure at 35-50 torr, depending on the model.

5.3 Radioactive decay counting (tritium analysis)

There are several analytical methods to measure tritium in water samples, one of the newest and easiest is the Liquid Scintillation Counting (LSC). If the tritium concentration in the sample is very low, its content must be augmented via electrolytic enrichment; this procedure requires a significant water quantity: at least 300 ml. Otherwise, the ^{3}H concentration can be determined by direct counting, mixing the sample (10 ml) with a scintillating liquid (10 ml); the role of this substance is to convert the β^- radiation generated by the radioactive decay of tritium into light energy (photons), which is detected by photomultiplier tubes, converting the light into an electrical signal. Photocells are present within the counter in order to detect external radiation (cosmic rays or spontaneous radioactive decay from the material constituting the instrument) with the purpose of not including them in the counting. The instrument is also protected by radiation coming from the outside by lead plates.

5.4 Visual inspection and sampling of core #1

Core #1 was processed at the IDPA-CNR cold room at the Ca' Foscari University of Venice, at -20°C. A visual inspection, bag length measurement and ice lens counting and measurement was carried out in the cold room as well. This core has been analyzed for oxygen-18, deuterium and tritium at the Isotopic Geochemistry Laboratory of the University of Trieste for this PhD; elemental analyses, dust, black carbon and conductivity analyses are currently carried out in continuum using a newly-developed melting system, at the IDPA-CNR and Ca' Foscari University of Venice; this technique allows a very high resolution. In the cutting scheme for core #1, the external sections of the core were destined to pollen analyses and sent to the Institute of Botany, University of Innsbruck, Innsbruck, Austria. The internal square section was cut for the continuous flow analysis (CFA): an inner part was chosen in order to avoid any contamination caused by the drill on the edge of the core. The isotope section was also obtained from the inner part (some minor melting, and thus isotope fractionation, can occur along the drill cutline), as well as the one destined to organic compound analyses. From 35 to 55 m an additional section was cut for tritium analyses, with a 35-cm resolution, in order to find the 1963 peak due to the maximum in nuclear explosions in the atmosphere. The cutting resolution goes from 9 cm in the upper part to 3 cm in the lower part, except for the tritium section (see above) and the CFA section, which has always the entire bag length since it is destined to the melting system (continuous analysis). The increment of cutting resolution with depth was chosen in order to counterbalance the thinning effect on the ice layers. After the cutting, each sample was sealed into a 100 μm-thick LDPE bag inside the cold room and stored at -20°C.

For the isotope samples, an increased resolution of 2 cm was adopted for the deep part of the core (fig. 5.5-2), in order to maximize the resolution and keep track of seasonal oscillations. The upper firn part of the core was often ruptured, while the ice portion was well preserved for the most part. After being sealed into the plastic bags, the isotope samples were melted at ~20°C and transferred into 15-ml LDPE vials, which were stored frozen at -20°C.

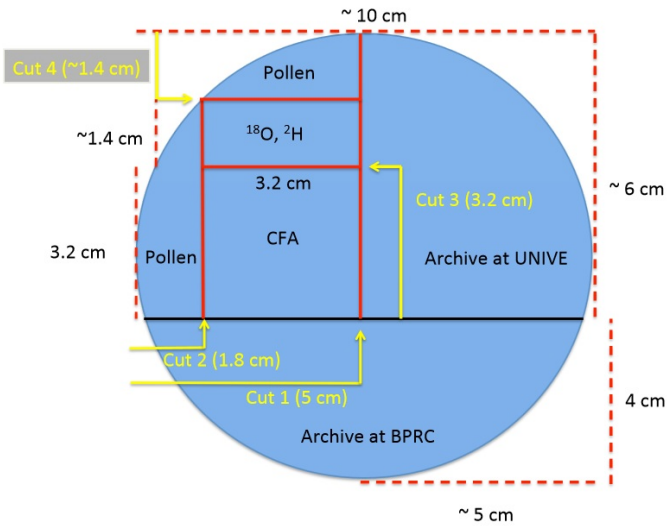

Fig. 5.5-1 The proposal cutting scheme for Ortles cores

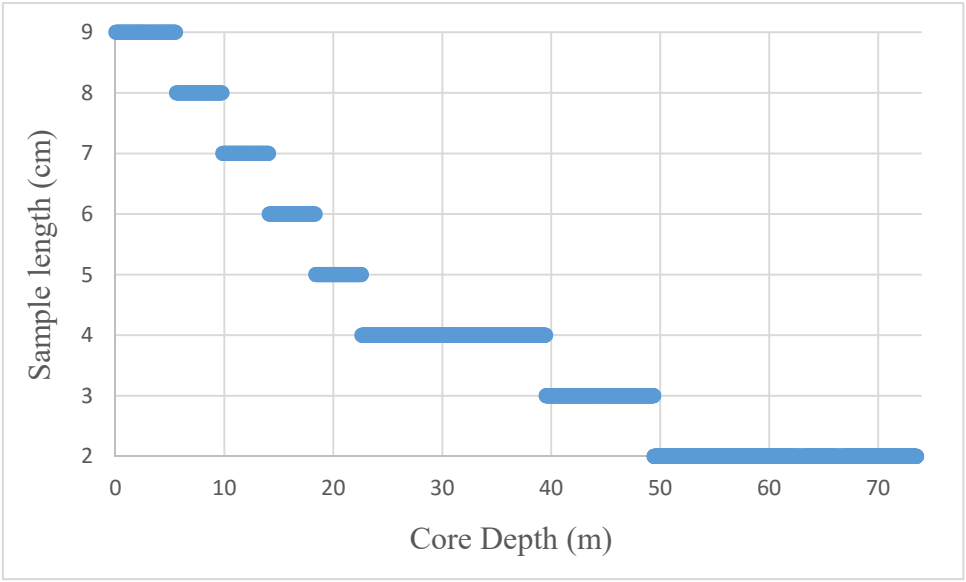

Fig. 5.5-2 Cutting resolution vs core depth for stable isotope samples (core #1)

One semi-rounded section was destined to the archive at the BPCRC, while another section was kept for another archive at the IDPA-CNR and Ca' Foscari University of Venice.

5.5 The isotope measurements

The isotope analyses were performed using a Picarro liquid analyzer L1102-*i* CRDS coupled with a HTC PAL autosampler (Leap Technologies) and a Thermo-Fisher Delta Plus Advantage IRMS coupled with a HDO device (fig. 5.6-1) with a 24-vial capacity. Taking into consideration the impressive number of samples (~2000) and the intermittent availability of the instruments, both the Picarro and the Delta plus were utilized when possible, without discriminating between the two.

Fig. 5.6-1 Picarro L1102-*i* liquid analyzer with HTC PAL autosampler (on the left) and Thermo-Fisher Delta Plus Advantage with the 24-vial HDO device (on the right)

Both guarantee a reasonably high analytical precision, with the hedge in favor of the Delta Plus: <0.1 ‰ (±1σ) for $\delta^{18}O$ and <0.5 ‰ (±1σ) for δD for the Picarro, <0.05 ‰ (± 1σ) for $\delta^{18}O$ and <0.7 ‰ (± 1σ) for δD for the Delta Plus.

The major difference between the two instruments is the amount of sample required for the analysis: the Delta Plus needs 5 ml of water while the Picarro only requires 300 µl when using the reduced-volume vials; otherwise, using the standard 2-ml vials, 1 ml of sample is sufficient. Most of the ice core samples were around 15 ml w.e., but in the upper firn part some sample were just 5 ml w.e.

The time required to complete the measurements is comparable: the Delta Plus needs about 30 hours to analyze 17 unknown samples for both oxygen-18 and deuterium, while the Picarro needs roughly 28 hours when doing 8 repetitions per sample.

A typical sequence for a 17-sample round of analysis for the Picarro and the Delta Plus is showed in fig. 5.6-2. For the Delta Plus this is the highest number of sample that can be analyzed within the same round, while Picarro can analyze up to 128 consecutive samples (including the standards);

such a long sequence is not recommended since it suffers from a drift regarding the isotope measurements. The drift indicated by the Picarro datasheet is <0.3 ‰ for $\delta^{18}O$ and <0.9 ‰ for δD each 24 hours of analysis; considering that, with 8 repetitions per samples, a 128-sample round would last 154 hours, the resulting drift could reach 2.1 ‰ for $\delta^{18}O$ and 6.3 ‰ for δD.

Picarro

DUMMY	SAMPLE	SAMPLE	SAMPLE	SAMPLE	ST-1	ST-2	SAMPLE	SAMPLE
SAMPLE	SAMPLE	SAMPLE	SAMPLE	SAMPLE	SAMPLE	ST-1	ST-2	SAMPLE
SAMPLE	SAMPLE	SAMPLE	SAMPLE	ST-1	ST-2			

Delta Plus

ST-1	ST-1	ST-1	ST-2	SAMPLE	SAMPLE	SAMPLE	SAMPLE
SAMPLE	SAMPLE	SAMPLE	ST-2	SAMPLE	SAMPLE	SAMPLE	ST-1
SAMPLE	SAMPLE	SAMPLE	ST-2	SAMPLE	SAMPLE	SAMPLE	ST-1

Fig. 5.6-2 Typical scheme for a 17-sample analysis for Picarro (above) and Delta Plus (below)

The first position in the Picarro sequence is occupied by the dummy, which is usually filled with the closest internal standard to the isotopic values of the samples; its function is to absorb the eventual memory effect given by the last analytical sequence. The results from the dummy will be discarded. The standard couple (ST-1 and ST-2) is chosen in order to constitute the isotopic boundaries of the round of analysis: all the samples values should fall somewhere between the two standards, which represent the extremes of the isotopic range. In order to minimize the memory effect both standards should not be too far, in terms of isotopic composition, from the samples. The standard duplets are homogeneously distributed among the samples in order to minimize the effect of an eventual drift in isotopic values; if the standards were placed all at the beginning (or the end) of the sequence, they could not keep track of the drift.

For a Delta Plus analysis the two standards are chosen following the same criteria as for Picarro, but since the IRMS cannot measure an absolute isotope ratio, the first one (ST-1) has to be isotopically as close to the samples as possible, since it is used by the instrument for calculating the isotope ratio in each sample. For every sample analysis, the IRMS measures both ST-1 and the unknown sample and then calculate the ratio.

For both Picarro and Delta Plus the standard couple is also used to create the calibration function, which is just a linear function ($y = mx + q$) connecting the two points given by the “true” isotopic value (x-axis) and the mean of measured isotopic values (y-axis) of both standards. Some laboratories prefer to calibrate using a calibration curve based on 3+ standards, but since we

cautiously use a narrow isotopic range within the same round of analysis, two standards are sufficient.

After a long testing series and years of experience on our Picarro, we decided to perform 8 repetitions for each sample and then use an outlier test designed to filter the data: the mean value out of 8 repetitions of the same sample is computed, the standard deviation is calculated and then every datum falling outside the $\pm 1\sigma$ interval is discarded, while the remaining values are averaged and then the obtained mean value is calibrated. This test has been developed in order to get rid of the memory effect, usually affecting the first 3 injections, but also to exclude some outliers produced by bad measurements. An excel sheet containing all the required formulas has been created to speed up the selection and calibration processes.

The IAEA produces worldwide recognized water standards for isotope analyses: VSMOW2, GISP, SLAP2. These international standards are expensive (150-180 € for a 20-ml vial), produced in very limited quantities, and can be purchased every two years, so each laboratory has to develop some internal water standards calibrated against the international IAEA standards in order to perform frequent analyses. The IAEA water standards are listed below.

- VSMOW2 is the substitute of the original VSMOW (Vienna Standard Mean Ocean Water) standard and has a $\delta^{18}O$ and a δD value of 0 ‰ (standard deviation: 0.02 for $\delta^{18}O$ and 0.3 for δD).
- GISP (Greenland Ice Sheet Precipitation) is currently out of stock, has a $\delta^{18}O$ value of -24.76 ‰ and a δD value of -189.5 ‰ (standard deviation: 0.09 for $\delta^{18}O$ and 1.2 for δD).
- SLAP2 is the substitute of the original SLAP (Standard Light Antarctic Precipitation) and has a $\delta^{18}O$ value of -55.50 ‰ and a δD value of -427.5 ‰ (standard deviation: 0.02 for $\delta^{18}O$ and 0.3 for δD).

The internal standards of our laboratory cover the whole isotopic range from 0 to -53 ‰ for $\delta^{18}O$ and have been created using distilled Adriatic sea water (for the most isotopically enriched standard, MSW), deionized tap water (TS), a mixture of tap water and Antarctic snow (NS) and several Antarctic snow samples from different sites: NVL, GVS, ITASE, TD, OC3, with the last and most negative one (OC3) obtained by melting Dome C surface snow.

Core #2 was processed at the Byrd Polar and Climate Research Center (BPCRC) of the Ohio State University in Columbus, Ohio, USA. Oxygen-18, deuterium, major ions and dust were analyzed at BPCRC too. All the snow pits from 2008 to 2013, and the two shallow cores (2009 and 2010), were analyzed at the BPCRC as well.

The isotope analyses were performed using a Picarro liquid analyzer L2120-*i*, the next generation model with respect to the L1102-*i*, but characterized by the same technical specifications.
Core #3 is currently being processed at BPCRC and will soon be analyzed.
Core #4 is stored at the IDPA-CNR cold room at the Ca' Foscari University of Venice.
Tritium analyses were performed at the Isotopic Geochemistry Laboratory at the University of Trieste, Italy, using a multi-canal Wallach L.K.B. Quantulus (LSC), showed in figure 5.6-3. The samples were analyzed by direct counting, with an analytical error of ~20%. The accuracy of this methodology is not very high, but sufficient for the purpose of the analysis: finding the 1963 ^{3}H peak, which should still be reasonably high even if ~50 years have passed (^{3}H half-life: 12.32 years). In order to obtain reliable results each sample is analyzed 8 times, requiring ~40 minutes per cycle. The measurement is provided in Counting Per Minutes (CPM), and has to be converted into Tritium Units (T.U.); 1 T.U. represents the mean natural tritium concentration, corresponding to the ratio $T/H=10^{-18}$. The formula to convert CPMs in TUs is the following, where "dead water" is water with virtually no tritium

TU = [CPM (sample) - CPM (dead water)]*55

Fig. 5.6-3 The Wallach L.K.B. Quantulus liquid scintillation counter

CHAPTER 6: RESULTS AND DISCUSSION

6.1 Snow pit isotopic values

Snow pits were dug at the beginning/end of the ablation season next to the Ortles summit, and are the most recent glacial archives and the most suitable for comparison with precipitation isotopic composition. Since no precipitation has been collected in the nearby area, it is not possible to directly compare the isotope variation in snowfall and in snow pits.

The goal of digging snow pits is to reach the previous summer layer, in order to obtain at least a whole year of snow sampling; not every snow pit, however, reached that objective. Having an entire year of recent snow allows us to observe the amplitude of seasonal isotope variations, while having two snow pits from the same site, one dug at the beginning and one at the end of summer permits to observe how the summer warm conditions modify the snow isotopic content, allowing the evaluation of the magnitude of post-depositional effects on said values. The range of variation for $\delta^{18}O$ can show significant discrepancies between different years.

All the snow pits dug on the Alto dell'Ortles, for which isotope samples were available and analyzed, are listed below (tab. 6.1-1), taking into consideration the samples recovered at the main drilling site and those retrieved at the AWS site.

Year	**Drilling site**		**AWS site**	
	June/July	August/September	June/July	August/September
2008				X
2009			X	
2010				
2011				
2012	X	X	X	X
2013	X	X	X	X
2014	X	X		

Ta. 6.1-1 Scheme of every available isotopic record from the snow pits: those dug in June or July are on the left, those dug in August or September on the right; DS stands for the main drilling site, AWS for the automatic weather station site

The 2008 snow pit, dug on August 11 at 3850 m a.s.l., during the maximum ablation period, reached a depth of 200 cm. It has the narrowest $\delta^{18}O$ range observed so far on this site (fig. 6.1-1): the minimum is -13.52 ‰, while the maximum reaches -7.77 ‰. $\delta^{18}O$ and δD do not show a clear seasonal pattern, suggesting that the glacier probably experienced severe melting during that summer, significantly altering the original snow isotopic signals. It is also possible that the snow pit has not reached the previous summer level, hence not covering an entire year. The deuterium excess signal, surprisingly, looks better preserved (fig. 6.1-4), with a range of variation close to the other snow pits (min: 4.20 ‰, max: 13.58 ‰), despite being characterized, on average, by slightly lower values.

The biggest difference between $\delta^{18}O$ (and δD) winter-summer values is found in the 2009 snow pit (fig. 6.1-1), dug on June 11, when winter conditions were still present at the time of the survey (Gabrielli, personal communication), and reaching a depth (for isotope samples) of 410 cm. The lowest $\delta^{18}O$ value is -24.11 ‰ (-190.32 ‰ for δD), while the highest is -5.84 ‰ (–34.62 ‰ for δD), probably indicating a good preservation of the original isotopic signal of precipitation. The 2009 snow pit is the deepest one, and the snow column inspection suggests the presence of the 2007 summer layer at the bottom (Gabrielli *et al*., 2010, Festi *et al*., 2015); if this is true, this snow pit covers two entire years, but both the highest and the lowest $\delta^{18}O$ and δD values are found within the first 145 cm, thus belonging to the first year without any doubt.

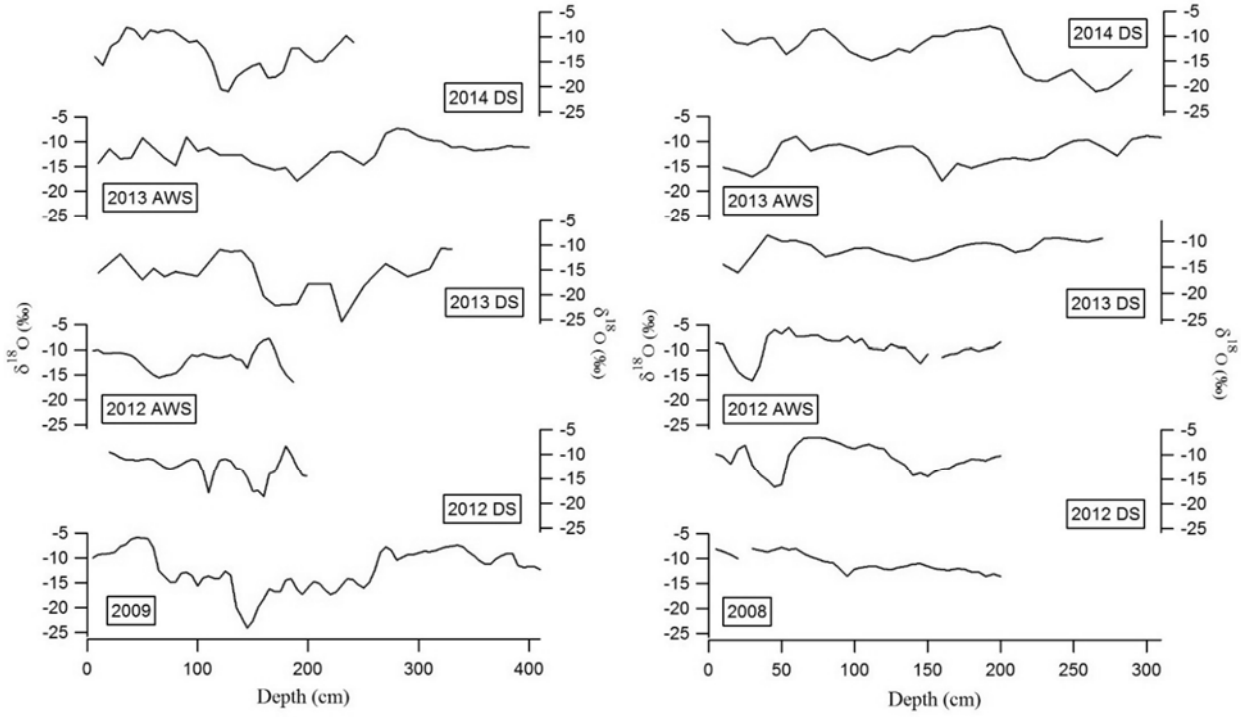

Fig. 6.1-1 $\delta^{18}O$ records from Ortles snow pits: June/July pits on the left, August/September pits on the right

The most negative $\delta^{18}O$ value overall belongs to the 2013 July snow pit, dug at the main drilling site: -25.43 ‰; the highest summer value is -5.84 ‰, from the 2009 snow pit.

The $\delta D/\delta^{18}O$ relation has been calculated for each snow pit, and it is always reasonably close to the global meteoric water line (Craig, 1961), ranging from $\delta D = 8.1*\delta^{18}O + 10.5$ (September 2012 AWS snow pit) to $\delta D = 8.7*\delta^{18}O + 17.2$ (August 2008 DS snow pit). These lines are also similar to the one found for Pontresina precipitation (1994-2013): $\delta D = 8.1*\delta^{18}O + 8.9$ (see section 6.4 for details).

Different summer conditions cause different effects on snow pit isotopic content: the relatively warm summer of 2013 likely altered the pristine $\delta^{18}O$ signal in the September 2013 DS snow pit; compared to the $\delta^{18}O$ record of the snow pit dug in July, the September snow pit $\delta^{18}O$ profile shows a significant increase (fig. 6.1-2). Summer 2013 was characterized by strong ablation, leading to a seasonal mass balance of -454 mm w.e. (Carturan, personal communication). During this summer, the Ortles AWS recorded 29 days with a mean daily temperature equal or greater than 0°C, compared to 41 days in summer 2012 and 12 in summer 2014; the mean temperature of positive temperature days during summer 2013 was 1.56°C, compared to 1.41°C for summer 2012 and 0.86°C for summer 2014. The maximum value (for 2013) changed from -10.88 to -8.84 ‰, while the minimum increased from -25.43 to -16.02 ‰; considering the net ablation, the 2012-

2013 winter minimum could be found closer to the surface, at 140 cm of depth, its magnitude significantly reduced. This two snow pits are an example of how the pristine isotopic signal of precipitation can be altered once the snow has settled, further complicating the climatic interpretation of isotope profiles in ice cores.

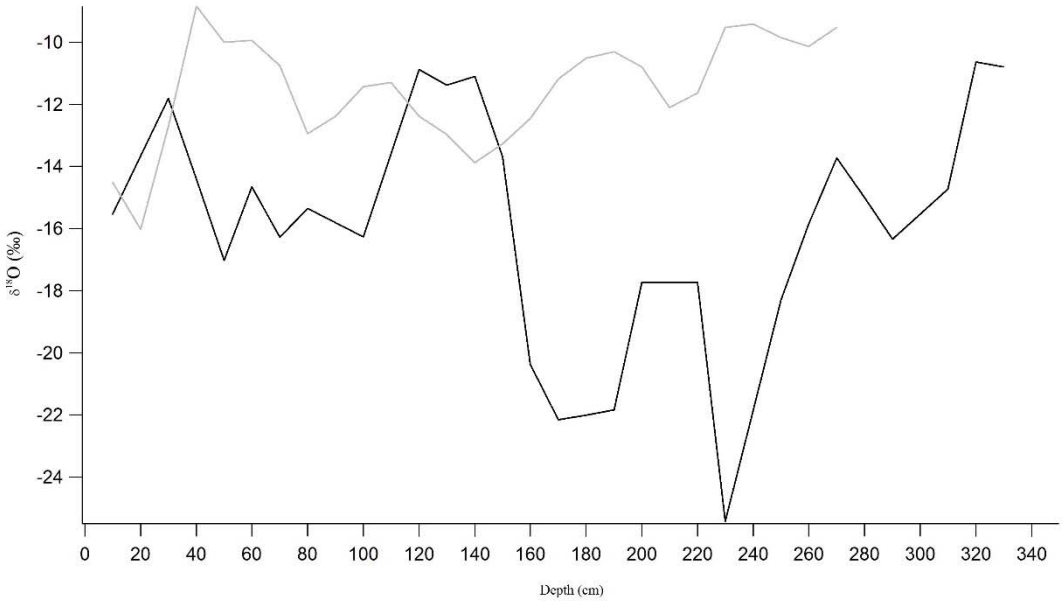

Fig. 6.1-2 $\delta^{18}O$ records from July (black line) and September (grey line) 2013 DS snow pit

It has to be considered, though, that present-day conditions, especially during summer, might be substantially different from those characterizing the formation of the deep part of the glacier (mean summer temperature has increased roughly 2°C during the last four decades; Gabrielli *et al.*, 2010), where the isotope signals look much better preserved.

The comparison between July 2014 and September 2014 DS snow pits gives completely different results (fig. 6.1-3): both the maximum and the minimum have remained roughly the same and the overall signal seems almost unaltered, apart from being shifted downward by the new summer deposition. This is probably due the cold conditions that characterized summer 2014. The summer 2013 layer, found at 240 cm of depth in the July snow pit, was not reached in the September pit.

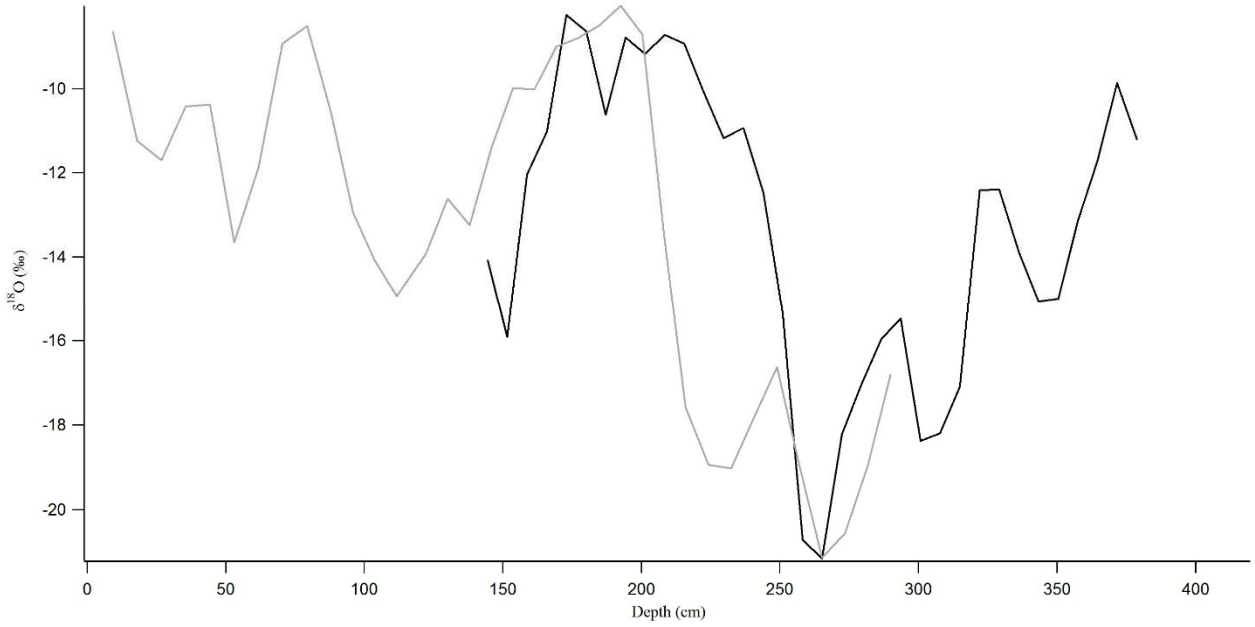

Fig. 6.1-3 $\delta^{18}O$ records from July (black line) and September (grey line) 2014 DS snow pit. The July record has been shifted downward for compensating the summer accumulation

Several processes such as mixing, seasonal scouring and spatial redistribution of snow can alter seasonal and annual records (Fisher *et al*., 1983). In surface snow, wind scouring and firn isotopic diffusion are believed to create a "post-depositional noise" (Steen-Larsen *et al*., 2014); interstitial diffusion, especially through the firn, smoothens the water isotopic signal (Johnsen, 1977; Johnsen *et al*., 2000). Diurnal evaporation is usually counterbalanced by nocturnal condensation; the influence of the effect is limited to the upper few centimeters of the snow cover. A homogenization (smoothing) of the isotope record occurs during firnification, caused by diffusion processes in the vapor phase; vapor moves through the pores following the pressure gradients determined by temperature differences in the snow. The smoothing of the isotope signal basically stops when the critical density of 0.55 g/cm^3 is reached (Stichler and Schotterer, 2000).

Deuterium excess values (fig. 6.1-4) stay between a minimum of 2.56 ‰ (June 2009 snow pit) and 22.75 ‰ (July 2013 AWS snow pit). Within a single year, the maximum variation among *d* values is 12.88 ‰, measured in the July 2013 AWS snow pit, while the smallest variation, 3.27 ‰, belongs to the September 2013 DS snow pit. Deuterium excess shows a visual positive correlation with $\delta^{18}O$ and δD in every snow pit, with higher values during summer and lower values during winter. Even intra-seasonal fluctuations in oxygen-18 and deuterium are usually replicated by *d.*

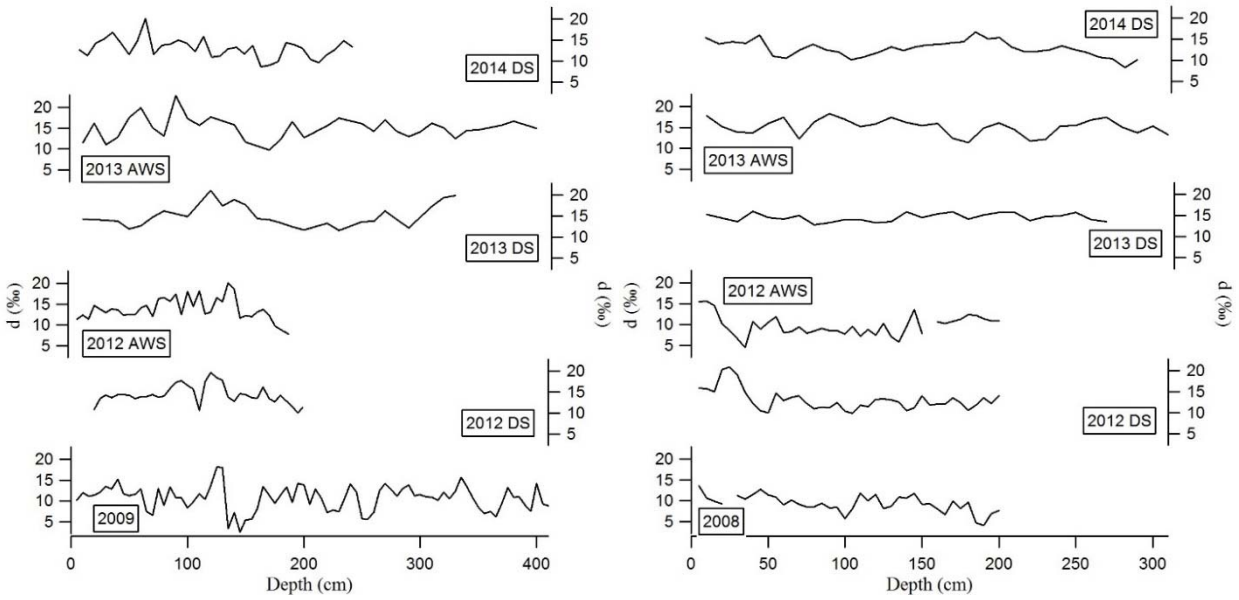

Fig. 6.1-4 Deuterium excess records from Ortles snow pits: June/July pits on the left, August/September pits on the right

Froehlich (1996) indicates a negative correlation between $\delta^{18}O$ and *d* in Alpine precipitation, while a positive correlation is found in Tsast Ula, a Mongolian glacier (Schotterer *et al*., 1997), suggesting a consistent contribution of recycled moisture during summer, leading to higher *d* values. Ortles values from snow pits show a similar *d* trend to the Mongolian glacier, probably indicating a signification contribution of recycled precipitation in summer snow accumulation as well; this hypothesis seems to be confirmed from the back-trajectory analyses (Sodemann, personal communication; see section 3.6). Mountain stations from the Alps show maximum *d* values between June and October, while valley stations are characterized by an opposite behavior (Rank and Papesch, 2005). In most of the Ortles snow pits the *d* signal appears more noisy and characterized by more ample and more frequent oscillations when compared to $\delta^{18}O$ and δD; it is unclear whether they are somehow more significantly affected by post-depositional processes, leading to an overall smoothing of the signals, or they have the same behavior even in precipitation. Despite being widely used to identify the water vapor source region, it turns out that a simple relationship cannot be established between *d* and the moisture source, due to secondary fractionation processes, as snow formation or partial evaporation of raindrops below the cloud base (Rank and Papesch, 2005); the second case, considering the high elevation of the Ortles sampling site and thus the relatively short distance from the cloud base, should be of minor importance.

Despite *d* showing a reasonably good visual correlation with $\delta^{18}O$ and δD most of the times, the linear correlation (positive) between δD and *d* displays significant variations with R^2 ranging from 0.04 (September 2012 AWS snow pit) to 0.58 (July 2013 AWS snow pit).

6.2 Shallow core isotopic records

Two shallow cores were drilled: the first on June 11, 2009, the second on September 2, 2010, both reaching a depth of 10.1 m.; they were then sampled with a 10-cm resolution. The aim of drilling shallow cores is to investigate the seasonal variability and the preservation of the signals within the snow/upper firn, which is usually the most problematic portion of a temperate or polythermal glacier. At first glance, the seasonal chemical-physical signals of the shallow cores seem largely preserved, even if the presence of ice lenses and the crystal morphology provide evidence of significant summer melting: the record might be overprinted to some extent in the lower part of the cores (Gabrielli *et al*., 2010).

The 2009 record shows an isotopic range of variation comparable to those found in well-preserved snow pits: the highest value for $\delta^{18}O$ is -6.25 ‰ (-37.53 ‰ for δD), at 60 cm of depth, while the lowest is located at 231 cm: -22.29 ‰ (-169.07 ‰ for δD). Both these values are found in the upper part of the core, belonging to the 2008/2009 season; from here downward, the amplitude of isotope variations becomes narrower, indicating a possible smoothing of the signal (fig. 6.2-1).

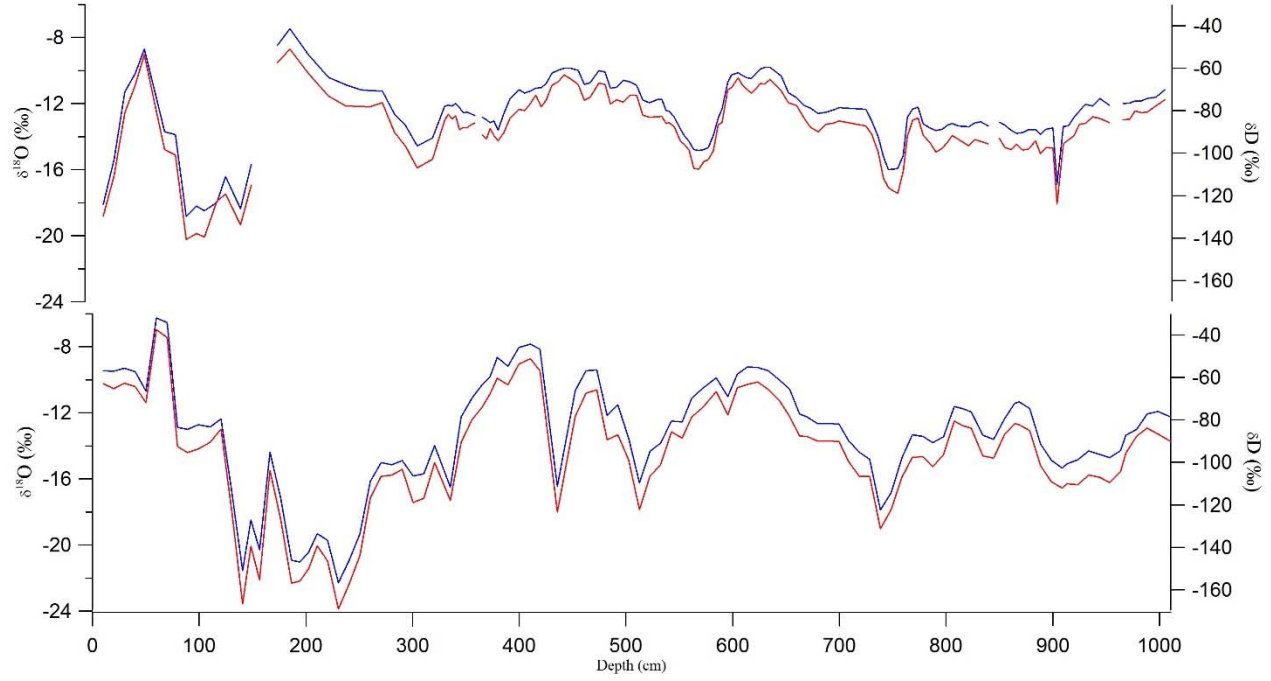

Fig. 6.2-1 Shallow core 2009 (below) and 2010 (above) $\delta^{18}O$ (blue) and δD (red) profiles

For comparison, the summer 2008 maximum (second peak from the surface downward) for $\delta^{18}O$ is -7.85 ‰ (-0.40 ‰ with respect to the previous year), while the winter 2007/2009 minimum is -16.45 (+5.84) ‰; this indicates that post-depositional processes, not only smooth the overall signal, but deteriorate much more low winter isotopic values. Field observations (Stichler *et al*., 1981; Suzuki, 1993), experiments (Arnason, 1969; Nakawo *et al*., 1993) and model calculations (Buason, 1972; Feng *et al*., 2002) have demonstrated that phase change leads to an enrichment in oxygen-18 in the solid phase (snow). It has also to be considered that even the uppermost layer isotopic signal can be biased toward more enriched values, since during summer half year the consolidation of the snow cover is faster and refrozen melt layers can protect from wind erosion (Alean *et al*., 1983; Beck *et al*., 1988; Suter *et al*., 2004). It has to be mentioned that the minimum monthly temperature (Ortles reconstructed temperature) of winter 2008/2009 was -18.9°C, while it was only -15.3°C for winter 2007/2008. Surprisingly, the *d* signal does not show any noticeable smoothing, and the highest values (16.43 ‰) is found at 979 cm of depth, while the lowest is at 493 (5.02 ‰) cm. Unlike in snow pits, the *d* record does not present a good correlation with oxygen-18 and deuterium. The 2009 shallow core covers four entire years. The $\delta D/d$ linear correlation is positive but the correlation index R^2 is low: 0.04, on par with the worst correlation found in snow pits.

The 2010 shallow core does not present such negative values as the 2009 one: the lowest $\delta^{18}O$ (δD) is recorded at 88 cm of depth (winter 2009/2010): -18.83 ‰ (-140.65 ‰), the highest at 185 cm (summer 2009): -7.47 ‰ (-50.88 ‰). Compared to the 2009 core, the isotopic range is narrower, due mainly to the less negative winter values. This core contains also the 2008/2009 isotopic record, making it possible to compare the data with those found in the previous core: the annual accumulation for the 2008/2009 season was 1006 mm w.e., it is thus possible to overlap the two shallow core records by shifting the 2009 profile downward of 1006 mm, while using the depth in water equivalent. The depth w.e. profiles were obtained using the density measures of both cores (fig. 6.2-2).

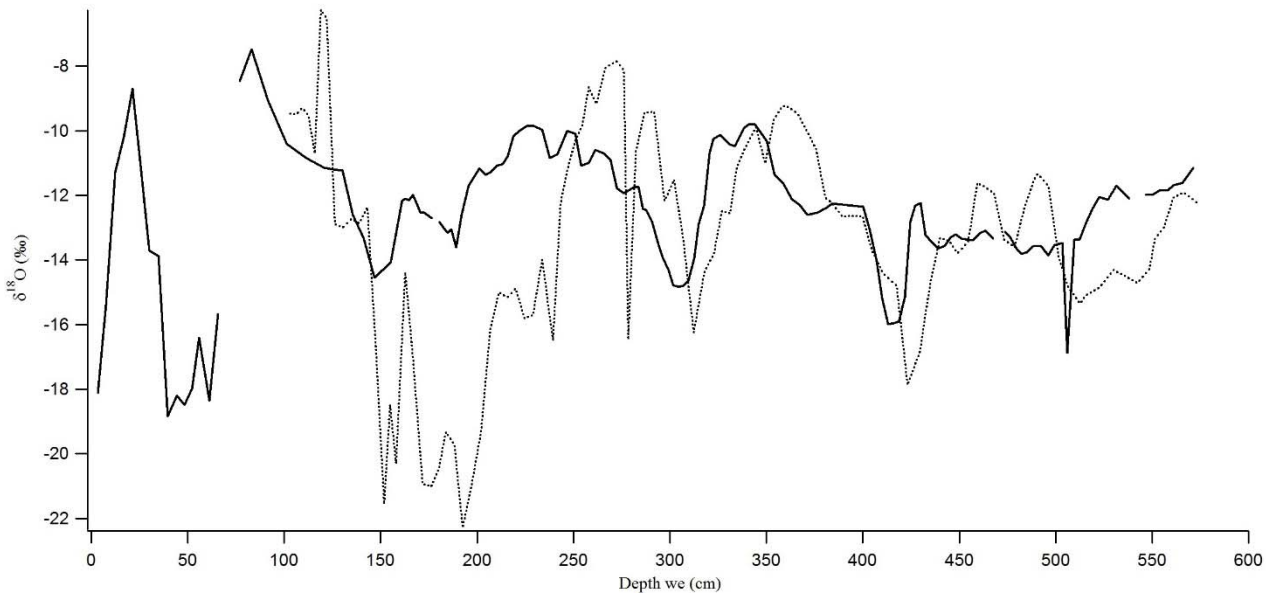

Fig. 6.2-2 Shallow core 2009 (dotted line) and 2010 (continuous line) $\delta^{18}O$ profile. Shallow core 2009 data have been shifted downward by 1006 mm

A good visual agreement is detectable between the two aligned $\delta^{18}O$ profiles (fig. 6.2-2), but the similarity is higher for the deeper part of the cores compared to the upper portion. The 2008/2009 $\delta^{18}O$ winter minimum is just -14.55 ‰, compared to the same period recorded in the 2009 core, reaching -22.29 ‰. This increment (+7.74 ‰) suggests some strong post-depositional effects altering the original winter signal. It can be noticed that the amplitude of $\delta^{18}O$ seasonal variations, excluding the 2008/2009 year, remains virtually identical: this could indicate that the effect of post-depositional processes is confined to the surface and is negligible below few meters of depth. In the Arctic, Koerner *et al*. (1997), considering ice cores from the majority of the sites, have found that at least 50% of the ice column is composed by clear ice (bubble-free), formed by melting and refreezing, while Tarussov (1992) stated that in Austfonna (Svalbard) the effective percolation is comprised between 2 and 5 m. The *d* values ranges from 7.80 (depth: 97 cm) to 21.40 (117 cm); again, it is possibile to compare the 2008/2009 data between the two cores: unlike oxygen-18 and deuterium, the *d* values seem to be better preserved after one year, maintaining a similar range of variability throughout the cores. Even if the two profiles show a good visual agreement, it must be noticed that the 2010 record looks, overall, a little higher (fig. 6.2-3).

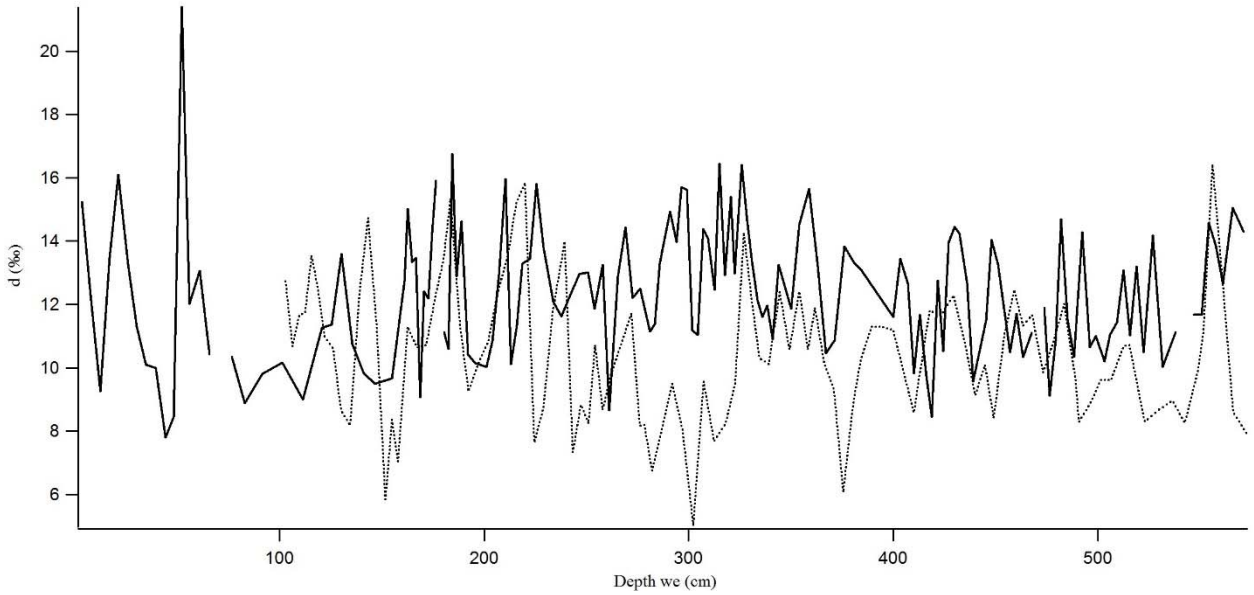

Fig. 6.2-3 2009 (dotted line) and 2010 (solid line) shallow core *d* profiles

Meltwater flow is possibly the main process causing isotopic redistribution in temperate snowpack. On warm days the surface snow may melt, percolating from the surface to layers underneath, where it may refreeze. Like vapor condensation, freezing is also associated with isotopic fractionation, resulting in a depletion of oxygen-18 in the water phase. Therefore, freezing of meltwater as it percolates down through the snow column results in isotopic redistribution in addition to simple mass transfer. In the process described above, vapor may exit from the top of the snowpack, and water may be drained from the bottom: these processes may cause an enrichment of oxygen-18 in the snowpack, with comparison to its original isotopic composition (Stichler, 1987). If there was just a simple mass transfer within the snow/firn column, caused by meltwater percolation and refreezing with no losses (hypothetically assuming that the isotope exchange with vapor is negligible), the long-trend isotopic signal would be unaffected by the process, but its seasonality would be compromised. Melting occurs favorably in summer, where temperature and irradiation are higher, thus affecting primarily the late spring/early summer snow layers on surface, characterized by higher isotopic values; the mass redistribution through refreezing within the snow/firn column mainly affects the more negative layers underneath, canceling out the winter minima. Even during warm periods, meltwater could not percolate downward beyond the firn/ice transition, considering that ice is impermeable, but if the englacial temperature at that depth reaches the pressure melting point, even the ice portion will experience some change.

Since $HD^{16}O$ has a lower diffusion rate than $^{1}H_2{}^{18}O$, δD does not decrease as fast as $\delta^{18}O$, causing less smoothing of the original δD profile compared to $\delta^{18}O$ (Johnsen *et al*., 2000). *d* measurements in different layers of a natural snow cover near Davos, Switzerland, at 2540 m a.s.l. showed a decrease of the parameter from January to June, 1973, in each layer (Martinec *et al*., 1977).

The reason why the *d* record looks negligibly affected by post-depositional processes could be that in the Ortles case those processes occur at equilibrium or in a quasi-equilibrium situation; the minor increase of the overall *d* signal observed in the Ortles shallow cores could be due to the small kinetic part of isotope fractionation between snow/firn and meltwater. The $HD^{16}O$ higher mobility should cause a δD increment in the liquid phase (meltwater) compared to $\delta^{18}O$, leaving the remaining snow enriched in the latter, leading to a decrease of the *d* signal, but during the meltwater refreezing within the firn column, the higher diffusion rate of $^{1}H_2{}^{18}O$ (from water to snow/firn) would cause a relative enrichment of the latter in the snow. In a different case, assuming that no kinetic effects occur during refreezing (equilibrium process), if the meltwater refroze and in certain layers the refrozen part constituted a significative portion of snow/firn, then we would expect higher *d* values.

Precipitation originating from the Mediterranean Sea is characterized by higher *d* values, compared to precipitation coming from the Atlantic Ocean; precipitation receiving a conspicuous contribution from re-evaporated moisture from continental basins is also affected by increased deuterium excess (Gat, 2005). It has to be taken into account, though, that these two effects could cancel each other out, since the Atlantic moisture has a longer travel distance it could receive a larger contribution of recycled moisture, characterized by high *d* values, during its path, while the Mediterranean moisture, despite being originally richer in *d*, could receive a minor contribution from continental evapotranspiration because of its shorter path (Froehlich *et al*., 2008). Those could be the reasons behind high *d* values in the samples, assuming that negligible fraction has occurred after the snow settled.

6.3 Shallow core 2009 dating and temperature comparison

A dating methodology relying on pollen species identification and counting has been applied to the shallow firn core of 2009, with the intent of detecting annual and inter-annual variations in the pollen spectra, hence enabling the development of an accurate pollen-based timescale (Festi *et al*., 2015). The use of pollen as a chronological constraint presents some evident advantages: i) plants have distinct flowering periods, from spring to late summer/fall, allowing to link the snow/ice layers containing the pollen with the corresponding flowering season, while layers containing less

than 5 grains/cl are assigned to winter (Haeberli *at al*., 1983); ii) pollen can reach the snow via dry or wet deposition (it is not precipitation-dependent); iii) since alpine glaciers are normally close to the pollen sources, small samples (~10 ml) contain enough pollen to perform the analyses (Nakazawa *et al*., 2005, 2011). For this core, the sampling resolution for pollen counting was the same as for isotope measurements: 10 cm. to In order to create a pollen calendar for the Ortles mountain region, daily airborne pollen data collected at Solda (BZ, Italy) from 2008 to 2010 were used. Pollen identification was performed using an optical microscope at 400 x and 600 x magnification (Festi *et al*., 2015).

Having a temporal scale allows us to match temperature and isotope data; the $\delta^{18}O$ record is compared with the Ortles reconstructed temperature from July 16, 2005 to June 12, 2009 (fig. 6.3-1). The visual correlation seems quite good overall, but it is a lot better for the two most recent years (and especially good for the most recent one), while it gets worse with depth, going back in time. The oldest year of the dataset (2005-2006) shows a weak correspondence between temperature and $\delta^{18}O$; in this section the isotope signal is heavily smoothed, and the matching with temperature could be worsened by the age scale uncertainties affecting the bottom part of the core.

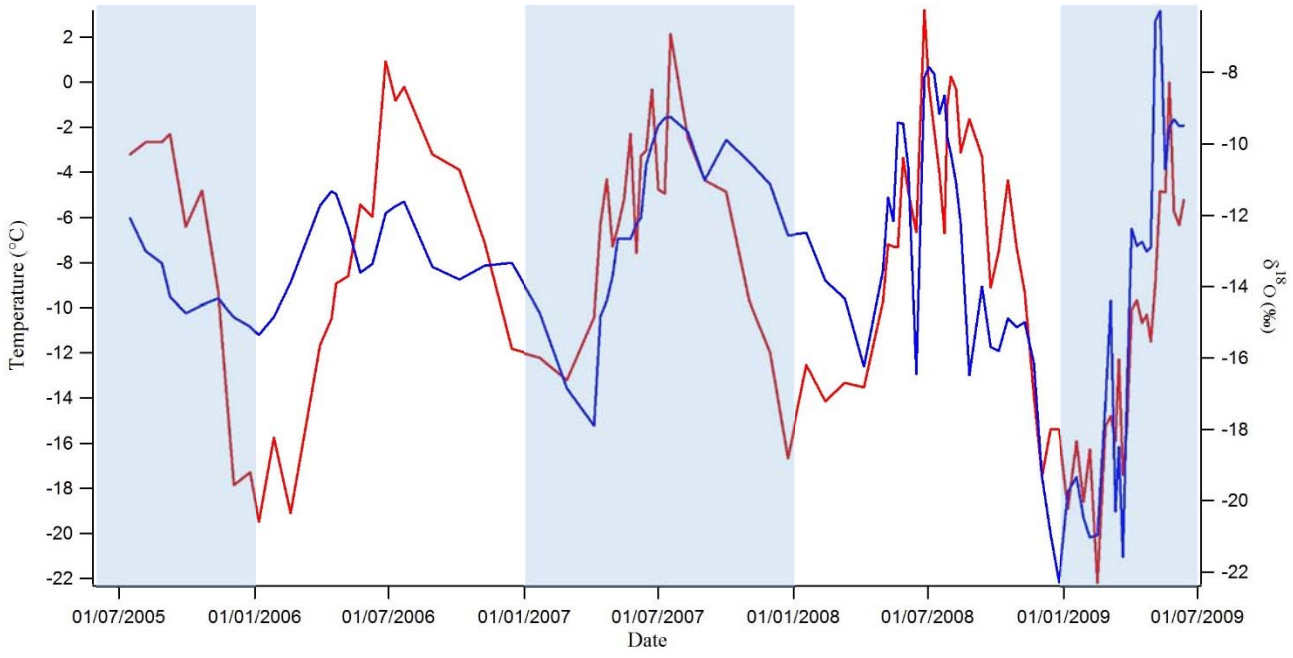

Fig. 6.3-1 Shallow core 2009 $\delta^{18}O$ profile (blue line) and temperature (red line). The different years are separated by different background colors

In order to establish the $\delta^{18}O$-temperature relation for this shallow core, the linear regression was calculated for three different sections of the 10-m profile: for the first 30 values, for the last 23 values and for the whole core length. This choice was made after the visual inspection of the apparent correlation between temperature and isotope data as seen on the graph (fig. 6.3-1), which appears not homogeneous throughout the core: the first 30 values are characterized by a very high visual correlation, the last 23 by the worst visual correlation of the dataset. The results are presented in table 6.3-1.

SH 2009	**$\delta^{18}O$/T**	**R^2**	**δD/T**	**R^2**
First 30 values	0.75	0.71	6.12	0.72
Last 23 values	0.10	0.25	0.94	0.28
Entire core	0.41	0.46	3.29	0.46

Tab. 6.3-1 $\delta^{18}O$/T and δD/T relationship for different sections of Ortles shallow core 2009

Both the slope and the R^2 show significant variations when considering different parts of the core. The upper portion, where the isotopic seasonal oscillations are ampler, is characterized by a high slope for both $\delta^{18}O$ and δD: 0.75 and 6.12, respectively. The R^2 coefficient for this part indicates a very good correlation between isotopes and temperature (0.71 and 0.72). Below the first year of the record, though, the isotopic record starts to get smoothed, and at the bottom part both slope and R^2 decrease a lot: 0.10 for $\delta^{18}O$ and 0.72 for δD, while the R^2 drops down to 0.25 and 0.28. The entire core displays slope and R^2 values in the middle: 0.41 for $\delta^{18}O$ and 3.29 for δD (slope), 0.46 for both (R^2).

6.4 Water stable isotopes in precipitation

No precipitation was ever collected for isotope analysis on the Ortles-Cevedale group and in the surroundings, but the Global Network of Isotopes in Precipitation (GNIP) is available for free (mandatory registration) on the International Atomic Energy Agency (IAEA) website, and can provide some useful isotopic data to compare with the Ortles glacial archive measurements.

Stations collecting monthly precipitation are normally located below 2500 m a.s.l.; for technical reasons, at higher elevations, the sampling of precipitation becomes problematic (Stichler and Schotterer, 2000).

No high-elevation stations are available in proximity of Mount Ortles, but rain and snow have been collected and measured at 1724 m a.s.l. in Pontresina, Switzerland, from 1994 to 2013. The small Alpine village is located in the canton of Graubünden, about 50 km away from Mount Ortles. By looking at the two decade long precipitation record, we can notice that despite a clear seasonality of the isotope signal ($\delta^{18}O$ and δD), with lower values occurring during summer and higher during winter, the lightest (and heaviest) precipitation does not occur in the same month every year: the lowest monthly values of the year might occur from November to March, while the highest from June to September. The mean isotopic values are -13.71 ‰ for $\delta^{18}O$, -101.75 ‰ for δD and 7.9 ‰ for *d*; the mean amplitude of yearly variation for $\delta^{18}O$ is 16.12 ‰, but the intra-annual gap between the lightest and the heaviest precipitation ranges from 10.86 to 21.56 ‰. The lightest monthly precipitation was recorded in February 2012 ($\delta^{18}O$ ‰ = -26.85, δD ‰ = -214.18), while the heaviest was in July of the same year ($\delta^{18}O$ ‰ = -4.53, δD ‰ = -27.33). For comparison, the mean isotopic values from all 2008-2014 Ortles snow pits are -12.09 ‰ for $\delta^{18}O$ and -84.09 ‰ for δD. The Ortles survey site sits over 2000 m above the Pontresina station, and hence should display much more negative isotopic values, while, on average, Ortles data are even less negative than Pontresina precipitation. Snow pit data though, are different from precipitation data: despite being recent snow/firn it might have already undergone significant post-depositional processes altering the original isotopic composition. It has to be considered that snow pits usually contains two summer layers: the one from the year in which they were dug and the one belonging to the previous one, so the values might be biased toward less negative summer values.

Despite being slightly more negative than snow pit data, mean isotopic values from the two Ortles shallow cores (2009 and 2010), -13.32 ‰ for $\delta^{18}O$, -96.11 ‰ for δD (2009) and -12.55 ‰ for $\delta^{18}O$, -88.06 for δD (2010), are still higher than those measured in Pontresina precipitation.

The deuterium excess of Pontresina precipitation ranges from -1.3 ‰ (February 2000) to 27.9 ‰ (September 1995), while the mean *d* value, 7.9 ‰, is lower than the one from Ortles snow pits (all data): 12.7 ‰. The average *d* values for the Ortles shallow cores are also higher that the Pontresina one: 10.42 and 12.33 ‰ for the shallow core 2009 and 2010, respectively. The high-elevation site (Mt Ortles) shows, on average, higher *d* values than the valley station (Pontresina), in accordance with Froehlich *et al*. (2008). The $\delta D/\delta^{18}O$ relation is very similar: $\delta D = 8.1*\delta^{18}O + 8.9$ (Pontresina) versus $\delta D = 8.1*\delta^{18}O + 14.4$ (Mt Ortles); they share the same slope and both are very close to the Global Meteoric Water Line (Craig, 1961): $\delta D = 8*\delta^{18}O + 10$.

The seasonality of $\delta^{18}O$ and δD is clear, with lower values during winter and higher during summer, while the deuterium excess data do not show any persistent seasonal trend and are characterized by a high inter-annual variability.

No monthly temperature record is available for Pontresina between 1994 and 2013, but data have been collected by an automatic weather station placed in Samedan, about 5 km away from Pontresina, standing at 1709 m a.s.l. (MeteoSwiss), Pontresina mean temperature (1961-1990, fig. 6.4-1) is significantly higher than the one measured for Mt Ortles: considering the monthly and yearly average it is roughly 10°C higher (Fig. 6.4-1); this should imply much less negative isotopic values. The intra-annual temperature trend looks quite similar: the magnitude and the timing of seasonal oscillations is comparable.

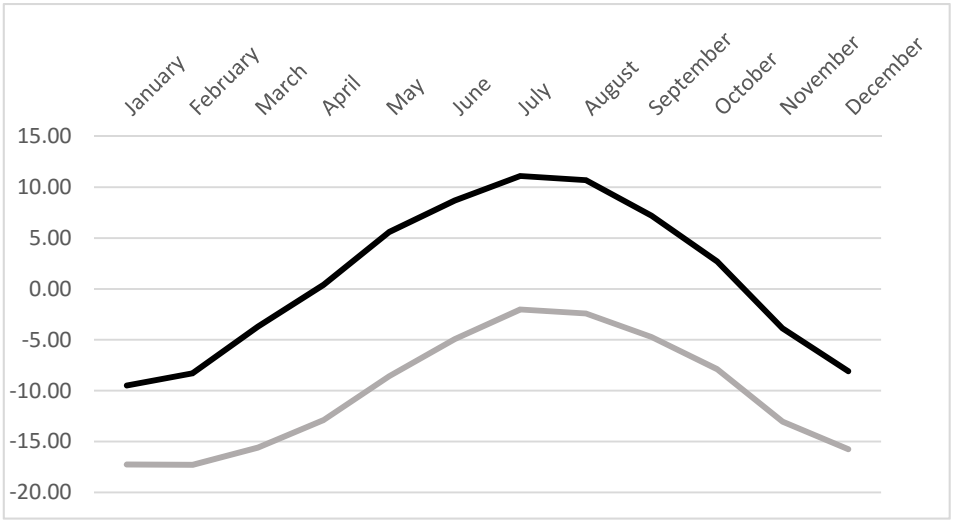

Fig. 6.4-1 Mt Ortles reconstructed (grey line) and Samedan (black line) mean monthly temperature (1961-1990). From MeteoSwiss

A good visual correlation between temperature and $\delta^{18}O$ is noticeable (see fig. 6.4-2), even if during certain years the oxygen-18 does not seem to clearly follow temperature variations, especially in winter.

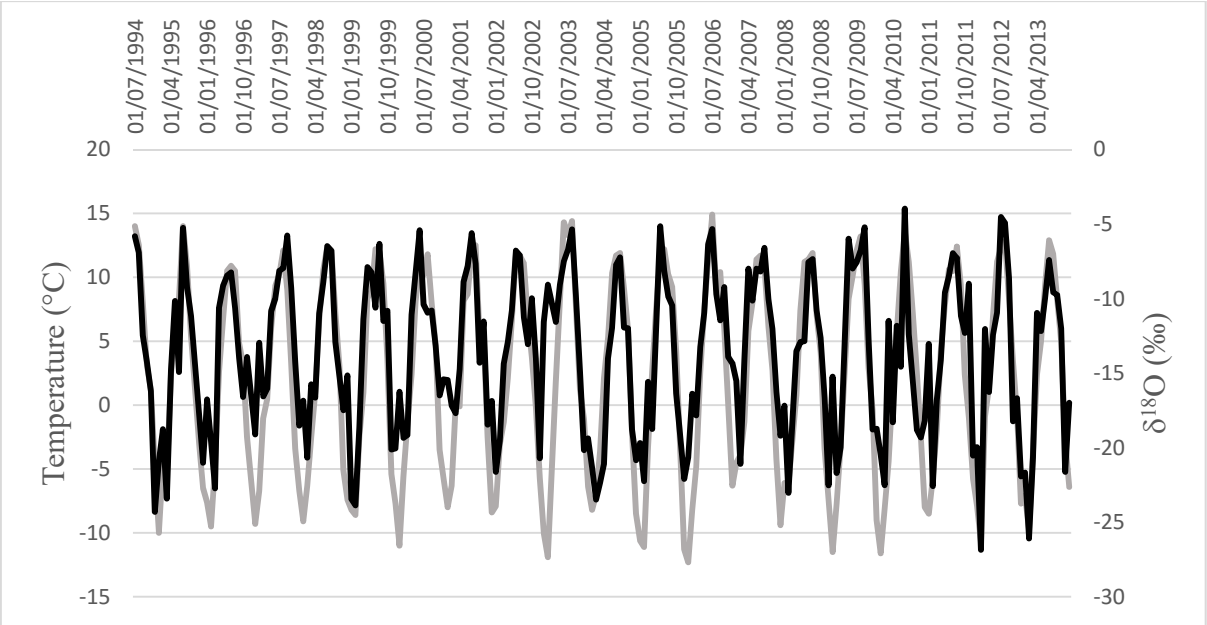

Fig. 6.4-2 Samedan AWS monthly temperature (grey line) and Pontresina $\delta^{18}O$ in monthly precipitation (black line) between July 1994 and December 2013

The $\delta^{18}O/T$ relationship, considering the whole dataset (1994-2013) with monthly resolution, returns a slope equals to 0.58 and a R^2 of 0.71. Using monthly data for the single years, the seasonal $\delta^{18}O/T$ linear correlation R^2 coefficient ranges from 0.52 (2010) to 0.88 (1999), while the slope goes from 0.44 (2010) to 0.76 (2012); the sensitivity of the isotope thermometer is very variable and a single value could not be suitable to reconstruct temperature oscillations using $\delta^{18}O$ (or δD) monthly data. Considering the single years, a remarkable positive correlation is present between all the R^2 data and all the slopes: the more significant the $\delta^{18}O/T$ correlation, the higher the slope. In fact, by looking at fig. 6.4-2, we can notice how the years characterized by a low $\delta^{18}O/T$ correlation are usually those in which the $\delta^{18}O$ oscillations are small compared to temperature variations (2000, 2010, 2011), and vice-versa (1999, 2012, 2013).

By using mean annual temperature and isotope data to calculate the linear regression between $\delta^{18}O$ and T, the inter-annual slope and R^2 have been obtained: 1.51 and 0.36, respectively.

6.5 The deep Ortles ice cores

6.5.1 Ice lenses

When temperature reaches the snow and ice melting point (0°C) during warm summer days, melting takes place and the newly formed liquid water percolates downward within the snow and firn layers. If the whole vertical snow temperature profile is not sufficiently cold, meltwater continues to percolate until an ice layer is reached. The ice strata can be approximately considered impermeable, and once the water encounters the ice, it can either drift or refreeze. In cold glaciers, during warm summer days a small amount of meltwater usually penetrates only few centimeters of snow before it refreezes, but in a polythermal glacier such as the Alto dell'Ortles, a bigger amount of melted snow can percolate downward for several decimeters if not meters before refreezing. During core #1 drilling operation, in early autumn, meltwater partially filled the ice portion of the borehole and started to refreeze overnight when the drilling procedure was paused. The ice forming the lenses contains a small amount of air bubbles, and they usually appear elongated. Sometime melt layer ice is referred to as "bubble free", but in the Ortles cores there was always a presence of air bubbles. All the visible ice lenses of core #1 were counted and measured in the cold room during the cutting process, placing the core bags on a transparent plastic board containing a neon lamp. By using just the naked eye and a visible-spectrum lamp, it was possible to spot only well-formed ice lenses; the identification was easier in the upper part of the core, where the firn density was still low and the melt layers formed a clear discontinuity in the firn matrix. In the bottom of the core, consisting of ice strata (density≥0.83 g/cm^3), melt layers were difficult to recognize with an adequate precision and so the inspection was stopped with bag N°95, at 66 m of depth.

Ice lenses in a glacier are related to the frequency and intensity of summer warm events; considering the impressive temperature increase over the last four decades in this area, especially regarding summer temperature (~+2°C), we expected to find an increment in lens number and size in the upper part of the core.

Ice lens thickness is very variable, ranging from 0.5 cm to 28 cm; thin lenses are the most common in core #1, especially in the lower part, with a thickness between 0.5 and 1 cm (fig. 6.5-1). The lens distribution (vs depth) and single lens thickness is showed in fig. 6.5-1; the biggest lens (28 cm) is found at 11 m, while a 27-cm thick ice lens is located at 27 m of depth, marking the water table.

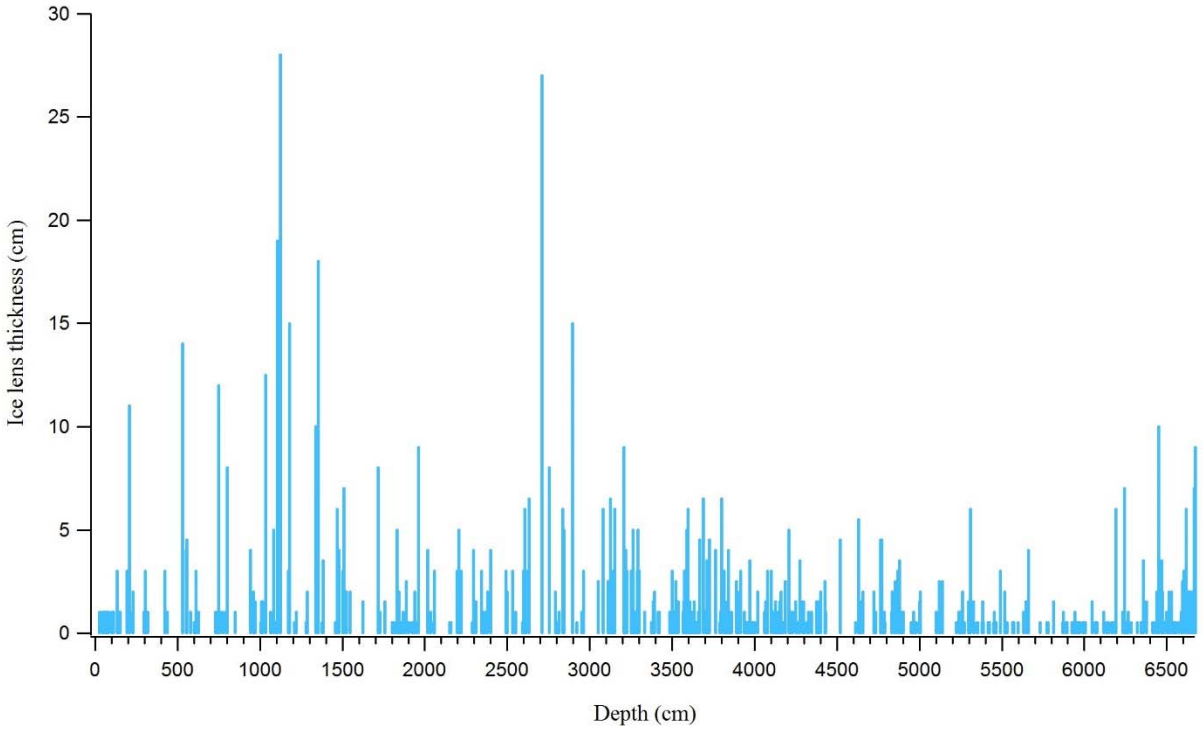

Fig. 6.5-1 Ice lens thickness vs depth (core #1)

The following graph (fig. 6.5-2) shows both the frequency and the thickness per tube of ice lenses versus depth; the frequency per tube is the number of lenses for each bag (~70 cm), while the thickness per tube is given by the sum of each lens thickness within the same bag (tube).

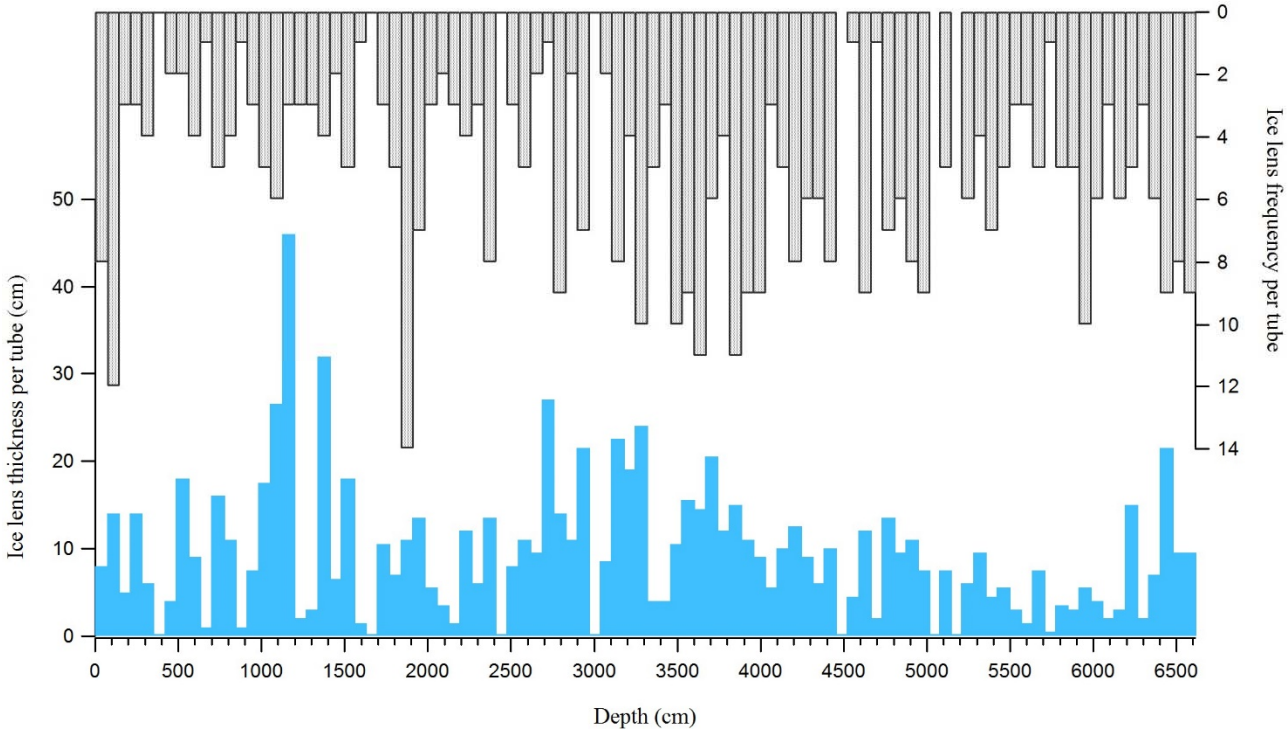

Fig. 6.5-2 Ice lens frequency (grey bars) and total thickness (blue bars) for each bag of Ortles core #1 vs depth

No clear trend is detectable for both frequency and thickness; ice lenses have been detected in the whole core, indicating that summer melting (and refreezing) was already occurring centuries ago, probably limited to a small portion right below the snow surface.

6.5.2 Core #1 isotope profiles and comparison with core #2

The whole core #1 $\delta^{18}O$, δD and *d* profiles versus depth are shown in fig. 6.5-3. A first look at the isotope records confirms that the glacier is divided into two decoupled parts (above and below the firn/ice transition), and that the lower portion (below 30 m of depth) is likely not influenced by the processes occurring in the firn portion.

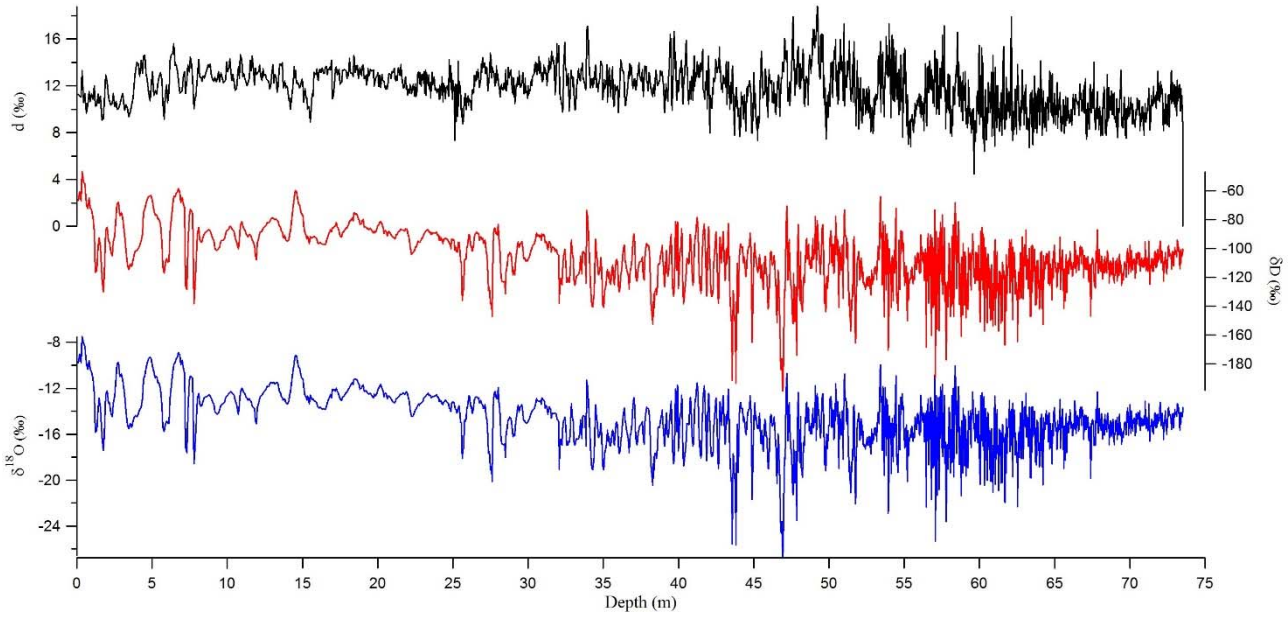

Fig. 6.5-3 Core #1 $\delta^{18}O$ (blue), δD (red) and *d* (black) record (raw data) vs depth (this study)

The $\delta^{18}O$ and δD profiles are characterized by a significant increment in the upper part (0-25 m of depth), possibly indicating the recent warming; the central portion shows the amplest isotope seasonal variations while the bottom part displays a significant shrink in seasonal oscillations and higher isotopic values. The latter is in contrast with a depletion observed in proximity of the bedrock (starting 4-5 m above) in several low-accumulation cores (Wagenbach *et al*., 2012). The deuterium excess record is difficult to interpret, but considering the overall trend, it seems to follow the $\delta^{18}O$ and δD behavior, with the exception of the very upper portion (first ~4 m). The entire

core is characterized by the following mean isotopic values: -15.07 ‰ for $\delta^{18}O$, -108.98 ‰ for δD and 11.57 ‰ for *d*. Core #2 mean isotopic values are: -15.40 ‰ for $\delta^{18}O$, -110.29 ‰ for δD, 12.90 ‰ for *d*. For comparison, other mean $\delta^{18}O$ values from ice cores and station collectors of precipitation in the Alps are reported in fig. 6.5-4, from Stichler and Schotterer (2000). Station collector data were used to calculate the expected $\delta^{18}O$ values, by using an altitude effect of -0.2 ‰/100 m (Siegenthaler and Oeschger, 1980; Schürch *et al*., 2003). Most of the measured values are higher than expected, and higher than the mean value found in Ortles core #1.

Location	Altitude (m a.s.l.)	$\delta^{18}O_{mean}$ (‰)	$\delta^{18}O_{expected}$ (‰)	Comment
Grimsel	2000	−13·8	–	Monthly composite of precipitation, rain + snow
Jungfraujoch (Research Station)	3500	−15·9	–	Monthly composite of precipitation, rain + snow
Plaine Morte	2800	−13·3	−15·1	Rain + snow, superimposed ice, flat, little drift, nearly total melting
Jungfraujoch (Glacier site)	3500	−12·5	−16·4	Exposed, strong erosion, partial summer melting
Fiescherhorn	4000	−17·5	−17·1	Flat, little erosion, net accumulation close to potential precipitation
Colle Gnifetti	4500	−14·5	−18·0	Exposed, strong erosion preferential loss of winter snow

Fig. 6.5-4 Mean $\delta^{18}O$ and expected $\delta^{18}O$ values from precipitation and ice cores in some Alpine sites (from Stichler and Schotterer, 2000).

The density profile has been obtained from core #2 bag measurements (fig. 6.5-5), with a resolution of ~70 cm throughout the core (Gabrielli, personal communication). The ice density is reached at ~30 m of depth. Some outliers might be due to small measurement errors.

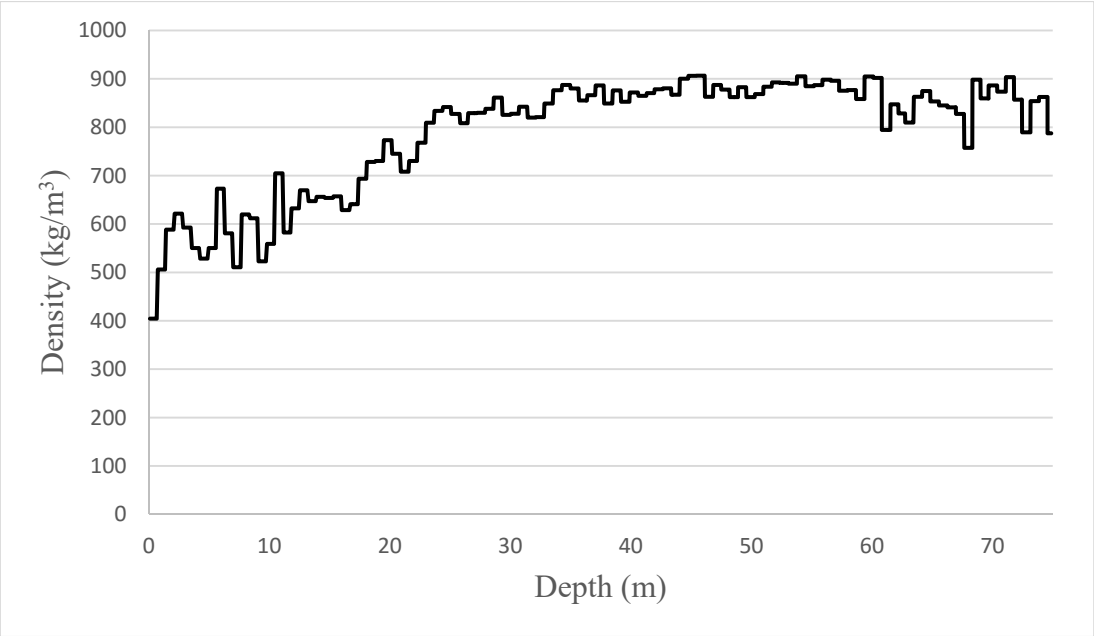

Fig. 6.5-5 Density profile from core #2 (Gabrielli, personal comm.)

In order to better understand the isotopic variations in core #1 and #2, we will consider different sections of the core with increasing depth.

The first 7-8 meters (fig.6.5-6) of core #1 are characterized by ample $\delta^{18}O$ and δD seasonal oscillations, between ~6 and ~10 ‰ (for $\delta^{18}O$) amid the maximum and the minimum value of the year; below this depth the magnitude of seasonal variations is significantly reduced, but it is still possible to detect annual layers by visually inspecting the water isotope profiles. Despite a significant smoothing of the $\delta^{18}O$ and δD signal in the surroundings, the 2003 summer peak clearly towers over the previous and following years, recording the exceptional warm temperature of that summer. The maximum $\delta^{18}O$ value of 2003, tough, is -9.12 ‰, lower than the 2008 and 2011 summer peaks: -9.10 and -7.49 ‰, respectively, implying a smoothing of that year signal. For the entire first 20 m of the core, it is still possible to recognize the annual layers and properly date this portion, going back to 2001, which means that a decade is contained in 20 m of the upper firn part of the core. The average $\delta^{18}O$ value is -12.54 ‰, which is quite high considering the latitude and the elevation of this drilling site. Two close minima are clearly visible between the supposed 2007 and 2008 summer peaks, spaced out by a peak in between, but it is unlikely that an entire year is comprised between the two. The visual dating (fig. 6.5-6) has been confirmed by the comparison with the first 20 meters of the core #2 isotope profiles (fig. 6.5-7); in this record the ambiguous interpretation between 2007 and 2008 summer peaks was clarified by the absence of one of the two minima. These two cores were drilled just 5-6 m apart from each other, but also other

differences are noticeable between the two $\delta^{18}O$ profiles in the first 20 meters: the 2004-2005 winter minimum is much more pronounced in core #2 than in core #1, and the 2003 summer peak is considerably wider. Both records have apparently kept track of all the seasonal oscillations at this depth, both covering a time span of roughly ten years, but the seasonal variations for this depth interval are slightly ampler in core #2. The mean $\delta^{18}O$ value for core #2, considering the 0-20 m interval, is -12.51 ‰, just 0.03 ‰ higher than the one found for core #1.

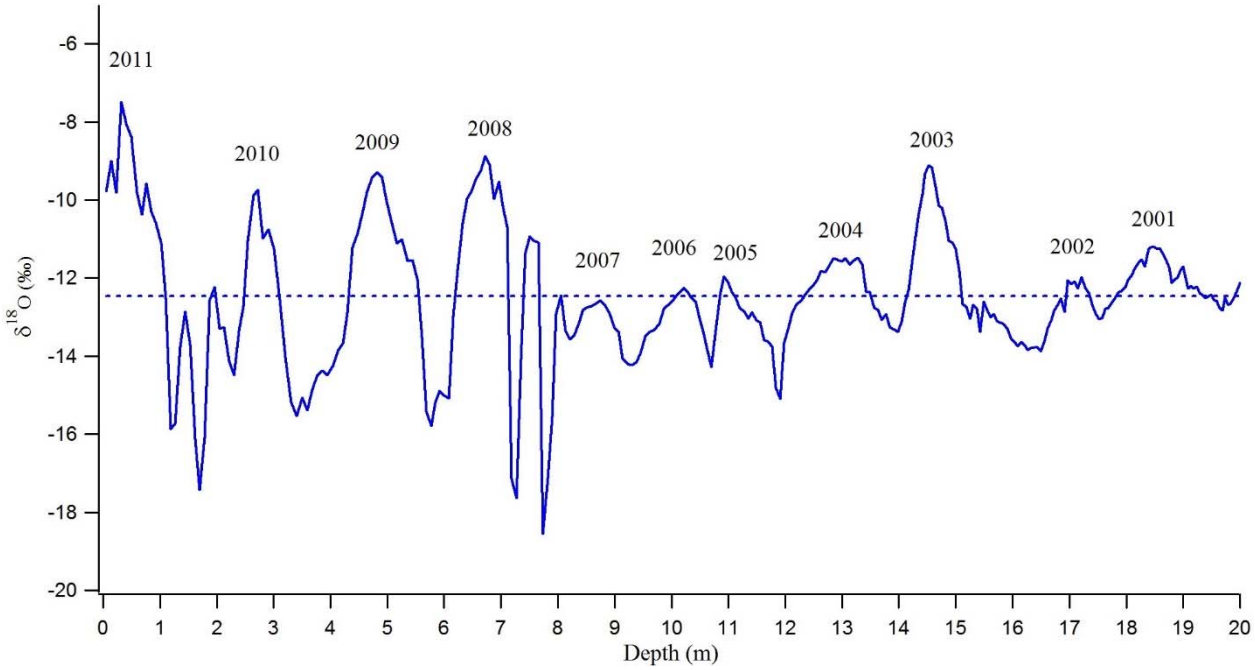

Fig. 6.5-6 $\delta^{18}O$ record (solid blue line) for the first 20 m of core #1, the dotted line is the average value of this section (this thesis)

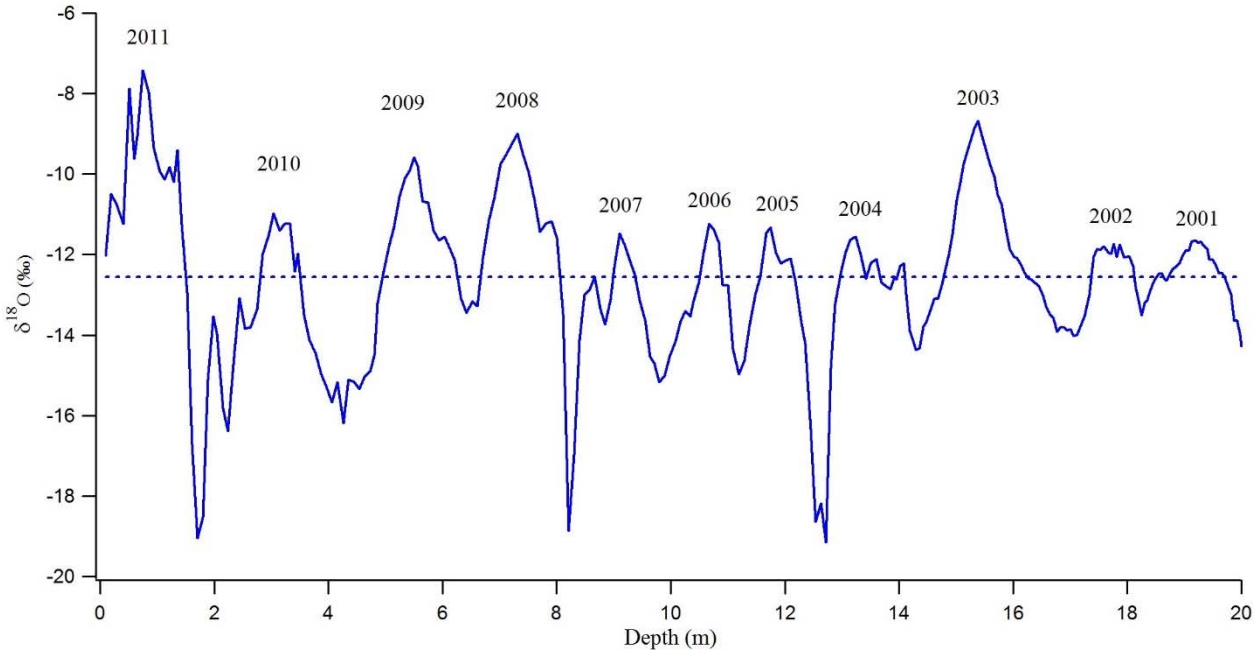

Fig. 6.5-7 $\delta^{18}O$ record (solid blue line) for the first 20 m of core #2, the dotted line is the average value of this section (Gabrielli personal commun.)

Between 20 and 40 m (fig. 6.5-8) the annual oscillations are not clearly detectable anymore, at least above 32 m of depth; this is the section in which core #1 and #2 differ the most. The last eight meters of this portion (from 32 to 40 m), in core #1, show a restoring of isotope seasonality and it is possible to count the annual layer again. The mean $\delta^{18}O$ value of this part for core #1 is -14.64 ‰, while for core #2 is -15.22 ‰; both cores show a marked decrease of the mean value with respect to the upper section (0-20 m), more pronounced in core #2. This remarkable difference can be only partially explained by the recent temperature increment, which has probably been amplified, in the isotopic signal, by meltwater percolation and refreezing, causing a further isotopic increment for this part of the record.

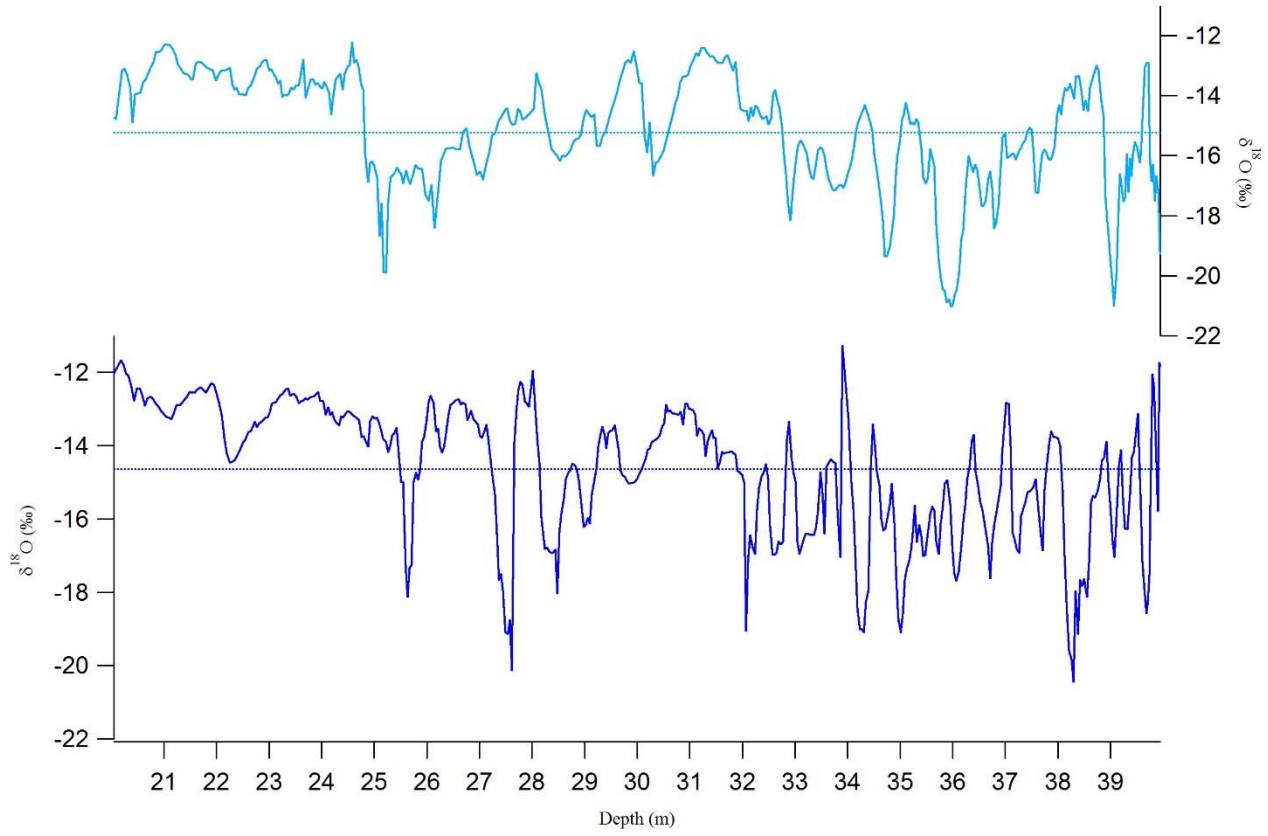

Fig. 6.5-8 Core #1: dark blue, core #2: light blue; $\delta^{18}O$ records (20-40 m of depth), the dotted line is the average value of this section

The ice portion from 40 to 50 m (fig.6.5-9) appears to be well preserved, and should span between 1918 (K^+ peak, see section 6.6.2; Gabrielli, personal communication) and 1963 (tritium peak, see 6.5.3), covering roughly 45 years: for comparison, about 5 years were represented in the upper 10 meters of core #1; this means that annual layers are nine times thinner in this part of the core compared to the surface (0-10 m). With respect to that shallow part, the cutting resolution of this section is more than five times higher. Between 43.5 and 44 m, and again around 47 m of depth, there are the deepest $\delta^{18}O$ minima of the entire core #1 isotope profile: -25.58, -25.64 and -26.64 ‰, the last being the most negative value of all the Ortles glacial archive analyzed for water stable isotopes so far and even more negative that every $\delta^{18}O$ measured in snow pits. Surprisingly the first two minima cannot be found in core #2 record, while the one at 47 m is present, even if less pronounced, around 0.7 m below in core #2 profile; considering the magnitude and the amplitude of this winter minimum, and the usual smoothing affecting the core and normally causing a slight increment of the isotope signal (compared to the snow pit winter minima), this extremely low value must have recorded a particularly harsh winter period, but for some reason it is less negative

in core #2. The average core #1 $\delta^{18}O$ value between 40 and 50 m of depth is -16.07 ‰, while for core #2 is -16.21 ‰; both are the lowest average values with respect to all the other sections.

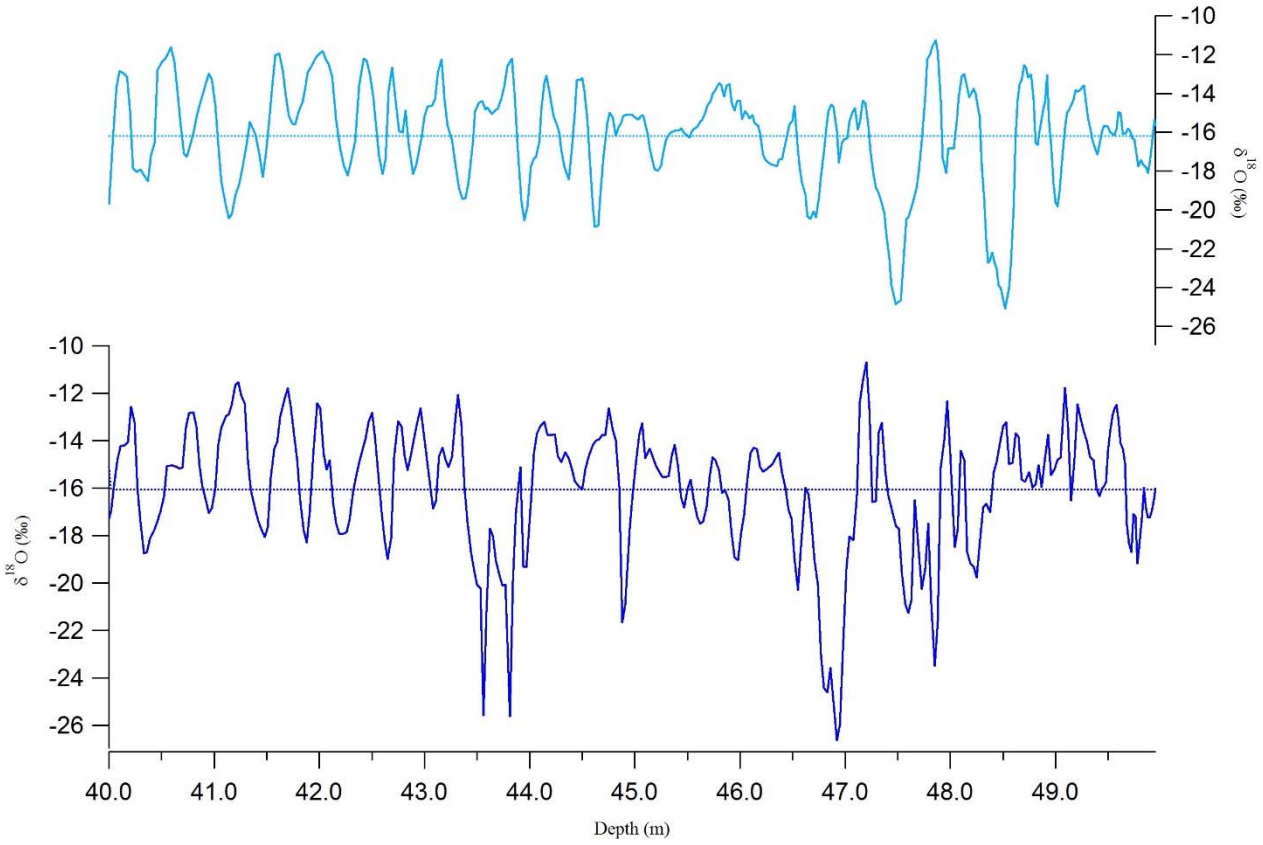

Fig. 6.5-9 Core #1: dark blue, core #2: light blue; $\delta^{18}O$ records (40-50 m of depth), the dotted line is the average value of this section

The core sections between 50 and 60 m of depth (fig. 6.5-10) have similar average $\delta^{18}O$ values compared to the upper one (40-50 m): -15.68 and -15.87 ‰ for core #1 and #2, respectively. A further thinning of the ice layers is clearly noticeable, especially below 53 m of depth. Despite a reasonably good preservation of the seasonality, in some portion (52-53 m and 55-56 m for core #1, slightly below for core #2) the $\delta^{18}O$ signal is characterized by limited variations, appearing to be smoothed. The amplest fluctuations are recorded around 57 m of depth, more marked in core #1: a variation of 14.48 ‰ for $\delta^{18}O$ takes place in only 5 cm of ice; it is one of the largest seasonal variations recorded in this core.

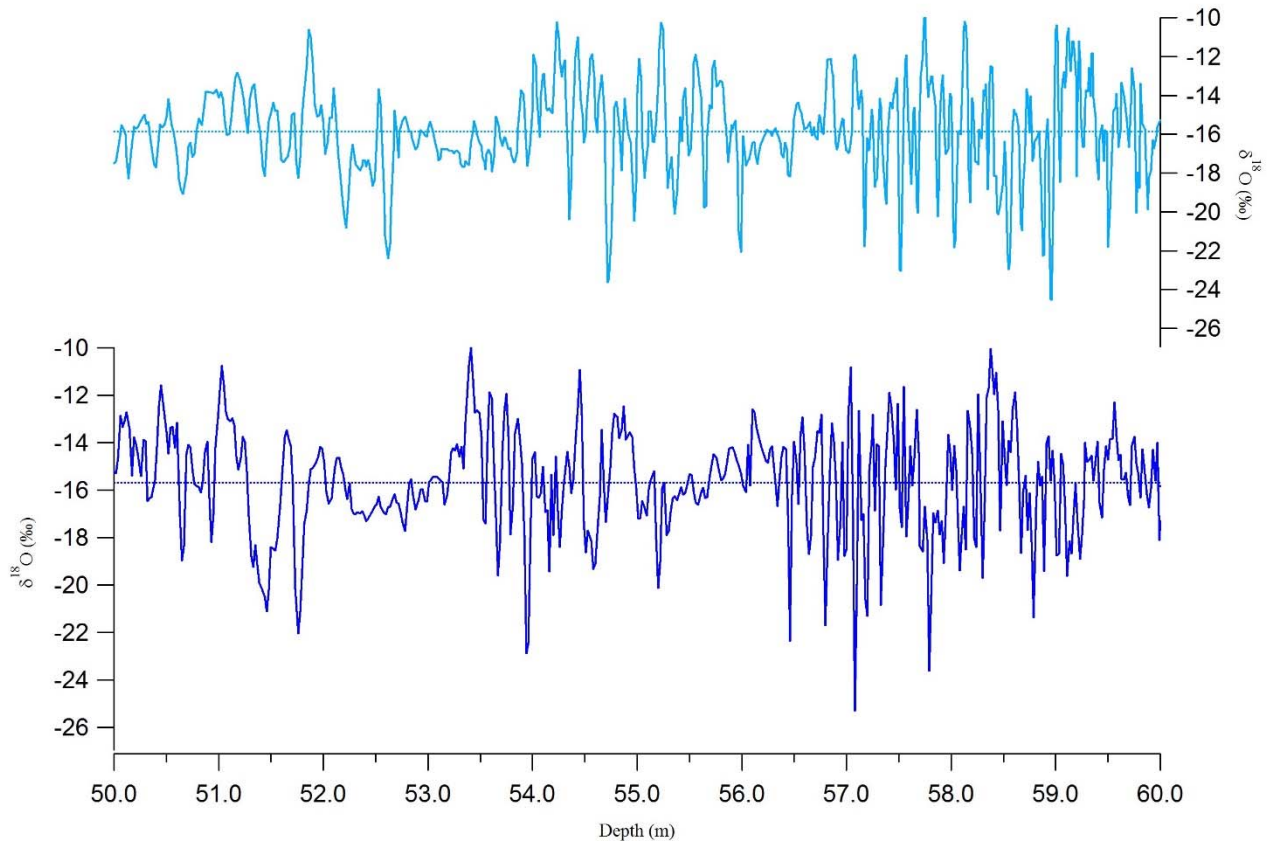

Fig. 6.5-10 Core #1: dark blue, core #2: light blue; $\delta^{18}O$ records (50-60 m of depth), the dotted line is the average value of this section

The core sections between 60 and 67 m (fig. 6.5-11) have mean $\delta^{18}O$ values of -16.03 ‰ and -16.13 for core #1 and #2, respectively; slightly lower than the previous one (50-60 m). Thanks to high cutting resolution (2 cm for core #1, 1 cm for core #2), the seasonal oscillations are still detectable, but their amplitude shows a significant reduction from 64-65 m to the end of this section, and the mean $\delta^{18}O$ is higher in the deepest part of this portion, showing a positive trend going back in time. No further thinning of the annual layers seems to take place in this deep part.

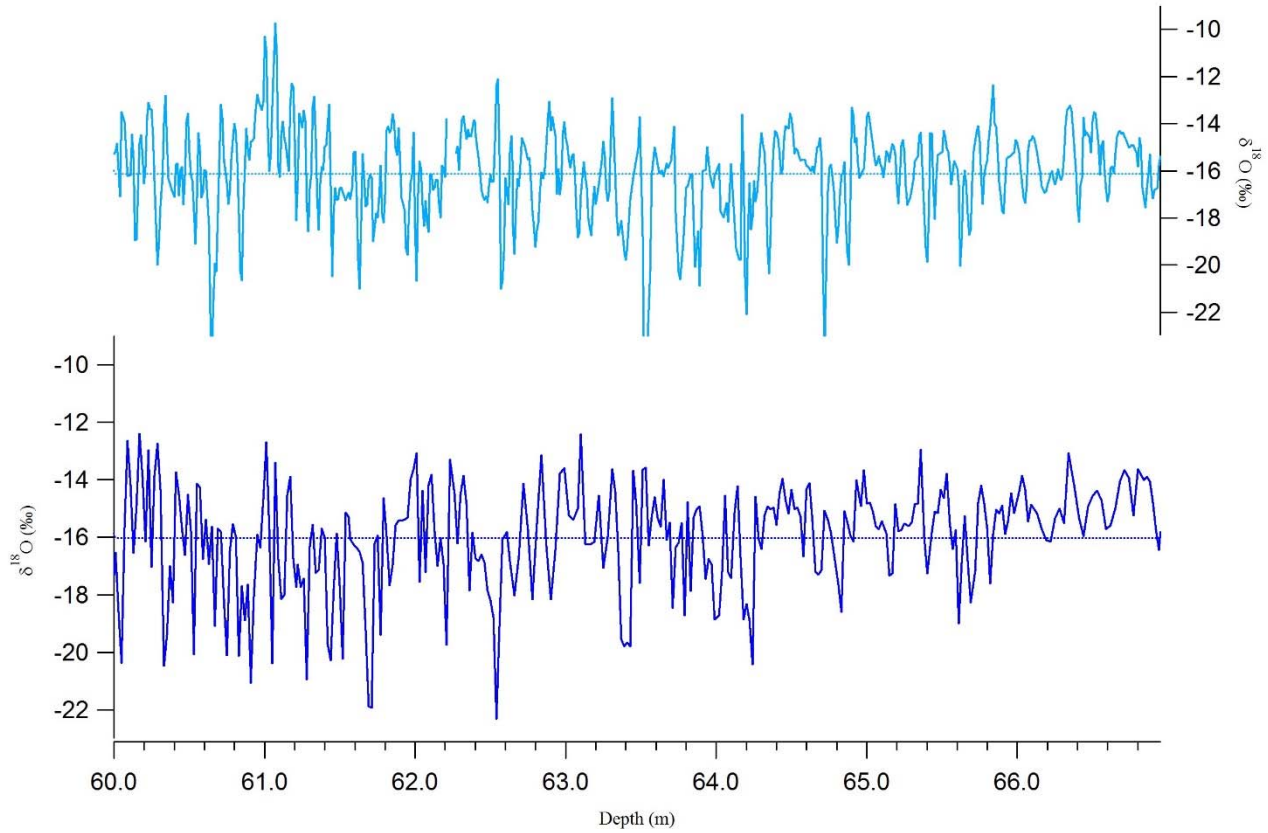

Fig. 6.5-11 Core #1: dark blue, core #2: light blue; $\delta^{18}O$ records (60-67 m of depth), the dotted line is the average value of this section

The deepest part of both cores (67-75 m) displays an evident reduction of the seasonal variability, and an increase of the average $\delta^{18}O$ values: -15.04 and -14.99 ‰ for core #1 and #2, respectively, confirming the incremental trend along with depth for the bottom part of the glacier. These values, despite being higher than those found in the close upper sections, are still significantly lower than the mean values for the 0-10 m section (-12.54 ‰ for core #1 and -12.51 ‰ for core #2), and very close to the mean values for the entire core (core #1: -15.07 ‰, core #2: -15.40 ‰). Seasonal oscillations appear to be equally detectable until the end in both cores, despite the different cutting resolution for the bottom part (2 cm for core #1 and 1 cm for core #2), but their amplitude is further reduced: the $\delta^{18}O$ range of variation between 68 and 74 m (core #1) is less than 4 ‰. In core #1 a very low minimum is present at 67.4 m of depth (-19.84 δ ‰), followed by a clear summer peak (-12.31 δ ‰) just 0.4 m below; this feature is not observable in core #2. There is a minor difference regarding core lengths: core #1 measures 73.52 m, while core #2 reaches 74.88 m.

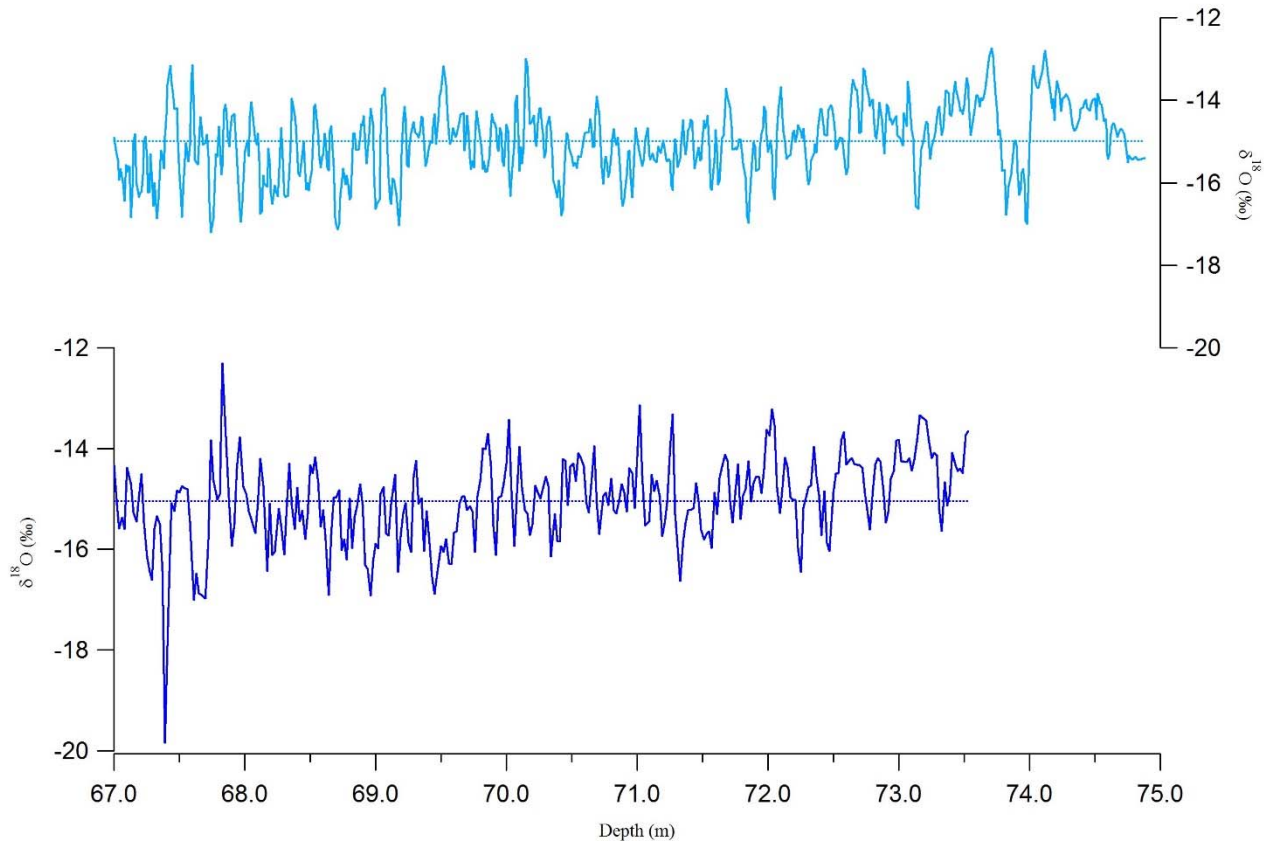

Fig. 6.5-12 Core #1: dark blue, core #2: light blue; $\delta^{18}O$ records (67-75 m of depth), the dotted line is the average value of this section

6.5.3 The tritium measurements

Core #1 was analyzed for ^{3}H content between 35 and 55 m of depth (sampling resolution: 35 cm), knowing that the 1963 tritium peak was found in core #2 at 41 m. During the maximum of nuclear tests in the atmosphere, the tritium concentration in precipitation increased by several order or magnitude; in Alpine ice cores we expect to find a clear peak in ^{3}H concentration even if ~50 years have passed since that time. The ^{3}H half-life is 12.32 years, meaning that, with respect to the original 1963 concentration, the original content has been halved four times. A clearly visible peak was found in core #1 at ~40 m of depth, characterized by a concentration of 196 TU (fig. 6.5-13); considering the low concentration in the surrounding ice layers, it is safe to say that it unequivocally identifies the 1963 nuclear tests maximum.

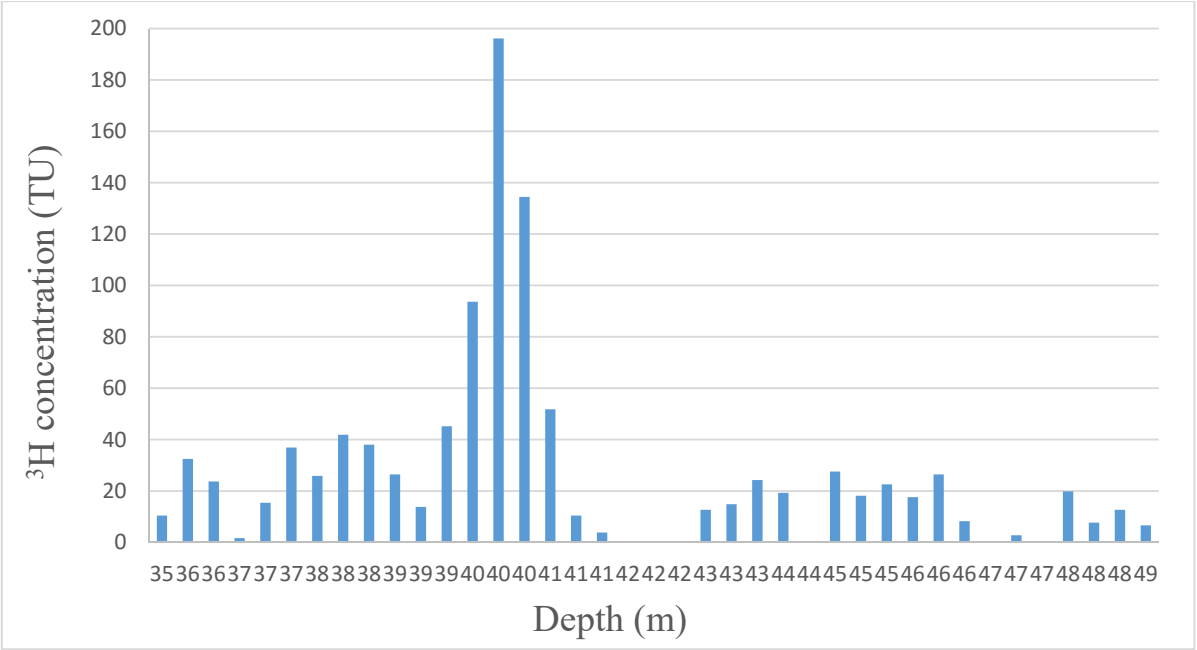

Fig. 6.5-13 ^{3}H concentration in Ortles core #1; the 1963 peak is clearly visible at 40 m of depth

Considering that in core #2 the ^{3}H peak was found at 41 m of depth and comparing the $\delta^{18}O$ and δD records from both cores (#1 and #2); the whole core #2 isotope profiles appear to be shifted downward of about 0.8 m, with respect to core #1.

6.6 Isotope and temperature comparison from deep cores

6.6.1 The simplest line

In order to calibrate the isotope thermometer, isotope data ($\delta^{18}O$ and δD) and temperature data from corresponding periods are needed. When a reliable and with sufficiently high resolution age scale is not available, it is hard to match temperatures and isotopes. The dating of the Ortles core #1 and #2 was originally based on core #2 sampling, and it covers the entire 75 meters, but with non-sufficient accuracy for this purpose. This core is characterized by the highest resolution for isotope samples, reaching 1 cm in the deepest part. Few are the absolute stratigraphic layers that serve as absolute age markers present in this ice archive: the tritium peak of 1963 AD at 41 m of depth, the potassium peak of 1918 AD (see 6.6-2) at 51 m and the larix leaf of 652 BC (±166 a) at 74 m. The annual layer counting is feasible at least back to the beginning of 2001 from the surface (autumn 2011) downward, so it is possible to assign a reliable chronology to the first 10 years of

the record and compare the mean isotope values of this portion to those found between the two absolute age markers of potassium (1918, see 6.6.2) and tritium (1963).
Using the Ortles reconstructed temperature datasets, it is possible to compare the mean temperature values between 1919 and 1962 and between 2001 and 2010 with isotopic data from the same periods (Tab. 6.6-1). The most recent interval is the hottest decade since 1864, while the period from 1919 to 1962 should not be affected by climate change yet.

Time interval	Mean Temperature (°C)	Mean $\delta^{18}O$ (‰)	Mean δD (‰)
1919-1962	-10.28	-16.29	-118.26
2001-2010	-8.77	-12.64	-86.45

Tab. 6.6-1 Mean Ortles temperatures and mean isotope data for the period 1919-1962 and 2001-2010

By connecting the two dots given by temperature (x-axis) and $\delta^{18}O$ (y-axis), the resulting linear equation is $\delta^{18}O = 2.42*T + 8.56$; the slope (2.42) is much higher than those normally obtained in $\delta^{18}O/T$ linear regressions around the globe (Rozansky *et al*. 1993). The linear equation for deuterium is $\delta D = 20.94*T + 97.01$; also in this case the slope is much higher than expected.
This was just an experiment, a linear correlation (which is, in fact, just a line) between two points does not have any statistical meaning, but the important information given by these data is that the water stables isotopes have registered the significant temperature increase of the last decades with a high sensitivity.
Several temperature records are available for the Ortles region, the longest extending back in time to 1864; the Ortles AWS temperature is the only dataset actually recorded on Mt Ortles summit, while all the other data are derived from other meteorological stations but have been corrected using the humidity lapse rate between the stations and Mt Ortles (see section 4.1). Nonetheless, each record has been proved to be sufficiently reliable by comparison with Ortles AWS measured temperatures.
In order to visually compare temperatures with isotope profiles, a depth scale in water equivalent (w.e.) of all isotope data is needed. The entire density profile, measured on each bag, is characterized by a resolution of ~70 cm throughout the core (fig. 6.5-7).
The second must-have is a reliable dating of the core, for assigning a chronological scale to the isotope data in order to make the comparison with temperature possible.

The first 20 m of both core #1 and #2 display clear seasonal oscillations, permitting the identification of the annual layers and hence a proper annual dating.

In the graph (fig. 6.6-1), the $\delta^{18}O$ record is compared to the Ortles reconstructed temperature data, based on Careser diga record. Despite adopting a w.e. depth, the yearly correspondence between isotopes and temperatures is not always good, but the black lines provide a help in the visual correlation. This is due to the variable accumulation rate from one year to another, considering that in this upper firn portion the density is significantly lower than ice and therefore the thinning of the layer, beyond the density increase, does not have to be taken into account.

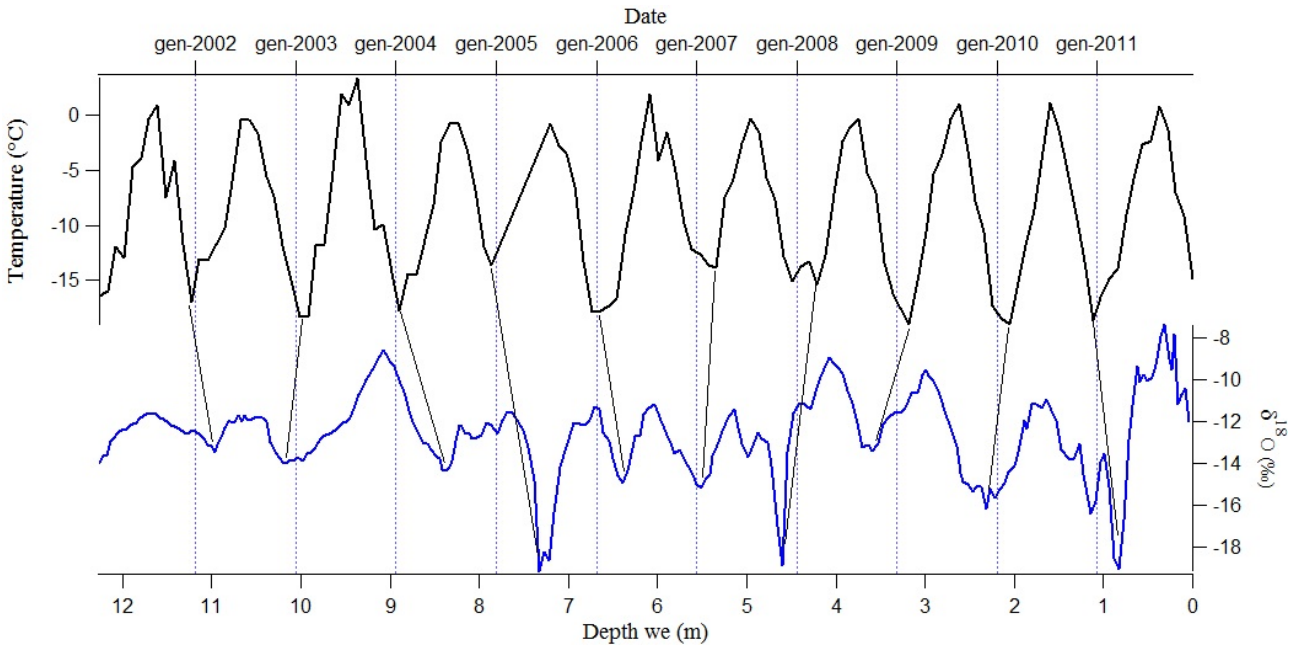

Fig. 6.6-1 $\delta^{18}O$ record (blue line, below) from core #2 (first 12 m of depth, we) and Ortles temperature (black line) between 2001 and 2011

The $\delta^{18}O$ has recorded reasonably well the seasonal temperature oscillations, but the isotope profile appears smoothed from the surface downward, with the amplitude of seasonal variability clearly reduced along with depth. The less pronounced intra-annual variations does not correspond to less ample fluctuations in the temperature record, and while the 2003 summer $\delta^{18}O$ clearly corresponds to the high temperature of that period, for other years the correspondence is weak: the 2004-2005 winter was mild, but the corresponding $\delta^{18}O$ minimum is the lowest of this portion, suggesting low winter temperatures. The same can be observed for the 2007-2008 winter. The amplitude of seasonal variations for $\delta^{18}O$ for 2001 and 2002 is very narrow, but the range of

temperature oscillations for this period is comparable to those observed for other years of the record.

According to the traditional approach, the isotope profiles do not record the air temperature variations in dry conditions, but the air temperature during precipitation events, and thus the record is biased toward the periods in which more snow fell; more recently it has become clear that at least the superficial snow layer isotopic composition is also influenced by the overlying water vapor (Steen-Larsen *et al*., 2014), but to my knowledge no experiment has been conducted at this latitude and elevation in order to quantify the magnitude of these isotope exchange. Considering the high variability of precipitation distribution (see fig. 4.2-2), one year might be characterized by more winter precipitation, biasing the isotope signal toward more negative values, while another could present higher isotopic values because more precipitation occurs during warm months. The wind speed and direction can also play a major role in eroding more or less accumulation, especially during winter (when the instrumental record shows stronger winds), removing the most negative values from the isotope record.

6.6.2 A tentative age scale for Ortles deep cores

Few stratigraphic features, useful for dating the ice, were identified in the Ortles deep cores so far. While for core #1, up to now, only oxygen-18, deuterium, tritium and melt layer data are available, core #2 was analyzed also for dust and major ions. In both cores the ^{3}H peak, caused by the maximum of nuclear experiments in the atmosphere (1963), is clearly visible (around 200 TU) at 40 (core #1) and 41 (core #2) meters of depth. The annual layer identification is usually achieved by means of $\delta^{18}O$, δD and sometimes *d* seasonal oscillations, as well as by inspecting the seasonality of the dust record (normally more dust is associated to summer periods) or NH_4^+, which again usually shows higher values during warm months. Neither in core #1 nor in core #2 was possible to precisely count the annual layers below a depth of about 20 m; even if the seasonality was restored below the firn/ice transition, in many portions of the cores it is not possible to properly discriminate one year from another. No Saharan dust events were identified in core #2, neither by visual inspection nor by major ions analysis. In core #1 no thick dust layer was identified during the visual inspection at the neon lamp.

A potassium peak, found in core #2 at 51 m of depth, is believed to be caused by world war I wood combustion from the Austrian soldier camp located in proximity of the Ortles summit; it has been assigned to the year 1918 AD (Gabrielli, personal communication).

A larix leaf was found within the deepest ice layers, close to bedrock, at 74 m of depth. It has been dated using the radiocarbon (^{14}C) dating methodology, and it belongs to the year 652 BC (±166

years). This discovery is quite surprising since before the larix leaf dating, the core was believed to cover only three or four centuries.

The remaining age markers are given by the annual layer counting using water stable isotopes and dust, where possible, from 2007 to 2011, and by the identification of the layer of the exceptionally warm summer of 2003 and of the summer of 1947 AD, which was warmer than the surrounding years.

A simple best polynomial fit between the previously mentioned dating points have been computed in order to provide a preliminary chronology based on core #2 (fig. 6.6-2).

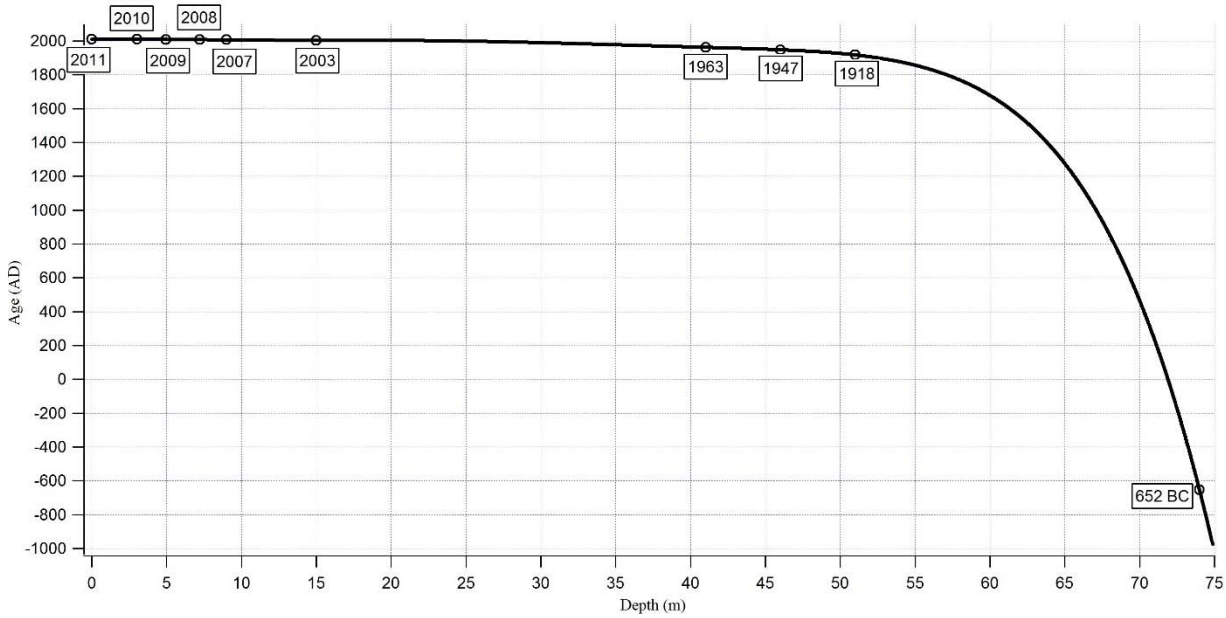

Fig. 6.6-2 The preliminary age scale for Ortles core #2 (Gabrielli, personal comm.); the circles represent the age markers used to create the best polynomial fit

The age curve is characterized by a low slope for roughly two third of the record and then suddenly drops down to cover more than 2600 years in 24 meters. Such a drastic turn can be explained only by the exceptional thinning of the ice layers in the bottom part of the glacier; by looking at the $\delta^{18}O$ seasonal oscillations between 50 and 60 m of depth (see fig. 6.5-10), a significant thinning is observed after 53 m, which is right below the age makers given by the K^+ peak (depth: 51 m): this could partially explain the behavior of the age curve. For this reason, plus many others previously described, this dating is assumed to be reliable only for the last century.

The chronological scale described above was designed for core #2, but can be applied to core #1 as well. In order to fit the scale in the other deep core we need to take into consideration the minor differences affecting the two $\delta^{18}O$ profiles (other species profiles could be used as well), which

show similar features but one appears slightly shifted with respect to the other. For this reason, core #1 $\delta^{18}O$ profile has been shifted downward by about 0.7 m, which is the distance between the same peaks identified in both cores. Another possible method for applying the age scale to core #1 would be to independently identify each age marker found in core #2 and then compute the best polynomial fit between those points, but it is not feasible since the potassium record is not available for core #1.

Once core #1 was dated, it was possible to compare the two deep cores isotope profiles and create one stacked record out of two. In order to do that, the two cores must have the same dating resolution, so all the isotopic data were resampled to a 1-year resolution. Other scales have been created, with a 3-year, 5-year and 10-year resolution.

After adapting the age-scale model to core #1 and resampling the data to a 1-year resolution, it was possible to compare the $\delta^{18}O$ record with the Ortles reconstructed temperature record for the last century using the same age scale. The result is shown in fig. 6.6-3. The visual correlation between the two parameters appears to be quite good, even if some relevant discrepancies are present, the overall warming of the last four decades is captured by the $\delta^{18}O$ trend. Other features, such as the cold year 2010 (Ortles reconstructed mean annual temperature: -10.3°C; 2006-2013 average value: -8.8°C), or the cold year 1941 (Ortles reconstructed mean annual temperature: -11.4°C; 1864-2009 average value: -10.3°C), are detectable in both records; in other cases, such as the cold year 1956 (-11.7°C), the temperature anomalies are not recorded in $\delta^{18}O$ data. It has to be considered that the uncertainty related to the chronology (>1 year) could lead to a mismatch between isotopes and temperatures for some years.

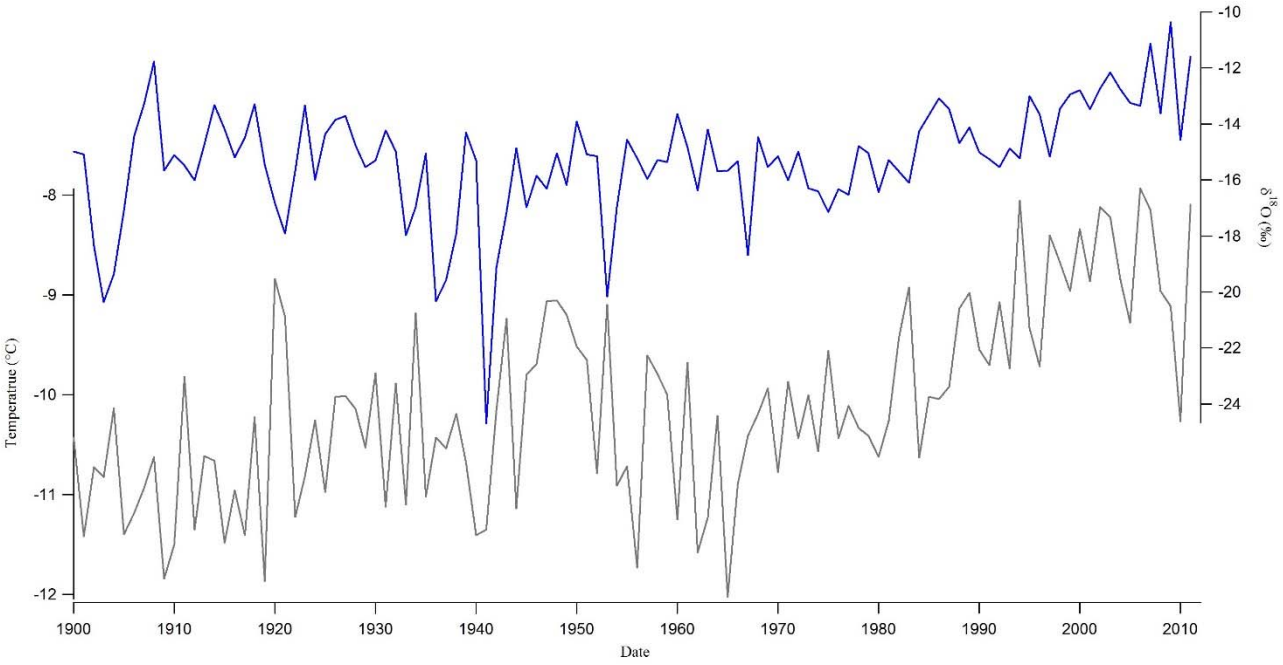

Fig. 6.6-3 Core #1 $\delta^{18}O$ (blue line) and temperature (grey line) vs age (resolution: 1 year)

A $\delta^{18}O$ composite record has been created, averaging core #1 and core #2 isotope data, with a 1-year resolution (fig.6.6-4), in order to increase the signal-to-noise ratio, minimizing the particular features characterizing just one of the two ice cores, which are not representative of the climate fluctuations of the area but are instead the consequence of the extremely high spatial variability in mountain glaciers, related to accumulation, meltwater seepage and stratigraphic features.

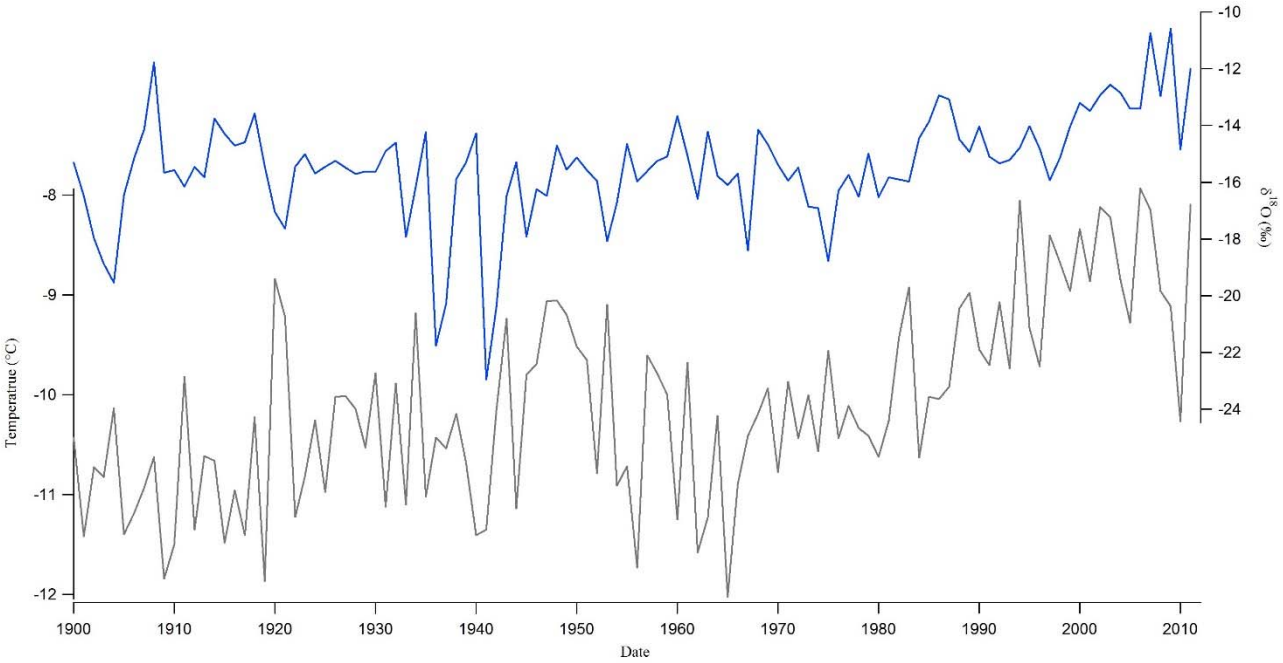

Fig. 6.6-4 Core #1 (this study) and #2 stacked record $\delta^{18}O$ (blue line) and temperature (grey line) vs age (resolution: 1 year)

The stacked record of $\delta^{18}O$ looks very close to core #1 $\delta^{18}O$ profile, confirming the similarities between the two cores; the isotope record oscillations are almost equal, but some minima have been reduced by the averaging of the two core values. In the table 6.6-2 the linear regression values (slope and R^2) between temperature and $\delta^{18}O$ (and δD) are reported.

Res: 1 year	**$\delta^{18}O/T$**	**R^2**	**$\delta D/T$**	**R^2**
Core #1	0.53	0.06	4.28	0.06
Core #2	0.56	0.07	4.80	0.07
Composite	0.59	0.09	4.54	0.08

Tab. 6.6-2 $\delta^{18}O/T$ and $\delta D/T$ relationship for the last century in core #1, #2 and in the stacked record (1-year resolution)

The obtained linear regressions indicate a weak correlation, slope increases when using the composite record isotopic values, for both $\delta^{18}O$ and δD; in the single records, core #2 performs a little better than core #1. The significance of the deuterium-temperature correlation is comparable to the one obtained using oxygen-18, but in any case the R^2 values are surprisingly low. At this temporal resolution, the isotope-temperature correlation does not seem to be very robust. This

might be due to the uncertainties affecting the chronological scale, for which a year could correspond to another and so it might end up to be associated with the wrong temperature datum. The inter-annual variability for this site is usually higher than long-term variations.

For the aforementioned reasons, isotope and temperature data have been resampled to a 3-year resolution, and another stacked record between core #1 and #2 has been created. The linear correlation with temperature is reported in table 6.6-3.

Res: 3 year	**$\delta^{18}O/T$**	**R^2**	**$\delta D/T$**	**R^2**
Core #1	1.08	0.28	8.15	0.24
Core #2	0.96	0.25	7.75	0.23
Composite	1.02	0.29	7.95	0.26

Tab. 6.6-3 $\delta^{18}O/T$ and $\delta D/T$ relationship for the last century in core #1, #2 and in the stacked record (3-year resolution)

When using the 3-year average values, slopes and R^2 data present a significant increment for both $\delta^{18}O$ and δD; a higher R^2 means that the robustness of the correlation has increased. Even in this case the R^2 coefficient is slightly higher for $\delta^{18}O$, and for both isotopes is higher when using the composite record. However, despite the increment of the correlation significance, the isotope data still does not correlate with temperature very well.

In attempt to further increase the correlation between temperatures and isotopes for the Ortles cores, the values have been rescaled to a 5-year average; the reconstructed Ortles temperature and the $\delta^{18}O$ 5-year resampling for the stacked record are reported in fig. 6.6-5. The major temperature increase of the last four decades is well replicated by the isotope, as well as some other fluctuations between the late 1930s and the late 1950s, but the two profiles show also some remarkable differences. The $\delta^{18}O$ peak around 1910 does not find any correspondence in the temperature record.

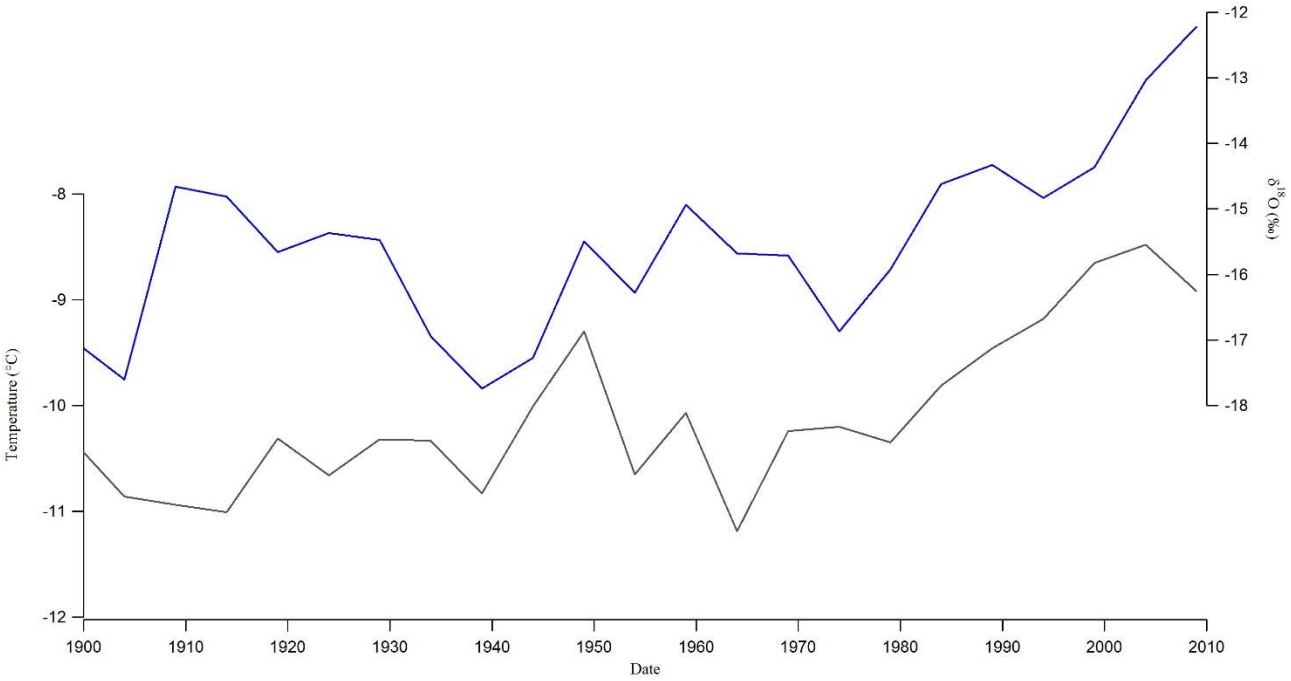

Fig. 6.6-5 Core #1 (this study) and #2 stacked record $\delta^{18}O$ (blue line) and temperature (grey line) vs age (resolution: 5 year)

The correlation results are presented in table 6.6-4; this time the *p*-values are included.

Res: 5 year	**$\delta^{18}O/T$**	**R^2**	***p*-value**	**$\delta D/T$**	**R^2**	***p*-value**
Core #1	1.19	0.39	<0.01	9.01	0.34	<0.01
Core #2	1.00	0.34	<0.01	8.26	0.31	<0.01
Composite	1.10	0.39	<0.01	8.64	0.36	<0.01

Tab. 6.6-4 $\delta^{18}O/T$ and $\delta D/T$ relationship for the last century in core #1, #2 and in the stacked record (5-year resolution)

As expected, the correlation has increased for both $\delta^{18}O$ and δD and temperature, for each record; the slope has raised too in every case, and the composite record shows again the best correlation. The *p*-value indicates if the correlation between two series of data is statistically significant: when lower or equal to 0.05, the correlation is considered significant (Buchan, 2015). In each case the *p*-value is lower than 0.01, meaning a high significance of the correlations.

It is not recommended to further reduce the temporal resolution, given that even using the 5-year average the dataset has been reduced to only 23 data, starting from 1904. Considering the reliability of the age scale and the narrowness of the dataset when using a low temporal resolution, presenting

here the 10-year average appears to be pointless, even if in that case the R^2 coefficient for the linear regression between isotopes and temperatures rose up to about 0.5. The dataset, using a 10-year average, is reduced to 12 data.

The slope of the linear regression represents the sensitivity of the isotope thermometer to temperature variations: the higher the slope, the higher the sensitivity. When the temporal resolution of the dataset is lowered, an increase of the slope is observed, as well as an increase in the R^2 coefficient, meaning that the isotope signals are more representative of the temperature oscillations. By getting rid of seasonal isotopic oscillations (the highest resolution was 1 year), most of the $\delta^{18}O$ and δD variability is excluded, since the intra-annual variations in the Alpine cores are always much larger than long-term variations (Wagenbach, 2003). The representativeness of temperature is thus reduced, and the climate reconstruction appears less feasible.

The use of a composite record averaging 2+ core data seems to be the right approach to minimize the noise of the isotope signal and to improve the correlation with temperature; however, the correlation increase is limited.

6.6.3 The seasonal δ/T relation

The portion of the glacier below 30 m of depth is still in a cold state (Gabrielli *et al*., 2012), and appears to not be affected by meltwater percolation from the surface. The firn/ice transition, during the drilling procedures, was observed at a depth of approximately 30 m; the ice layers are not permeable to water, and thanks to the cold temperature (below the pressure melting point at this depth), the preservation of seasonal oscillations is still possible. The strata surrounding the tritium peak, located at 41 m of depth in core #2 (40 m of depth in core #1), display a clear seasonality and thus can be dated by means of annual layer counting, starting from the age marker of 1963. Around 40 m of depth, the thinning of the layers is still limited, so the visual observation of intra-annual variations is still feasible (see fig. 6.6-7).

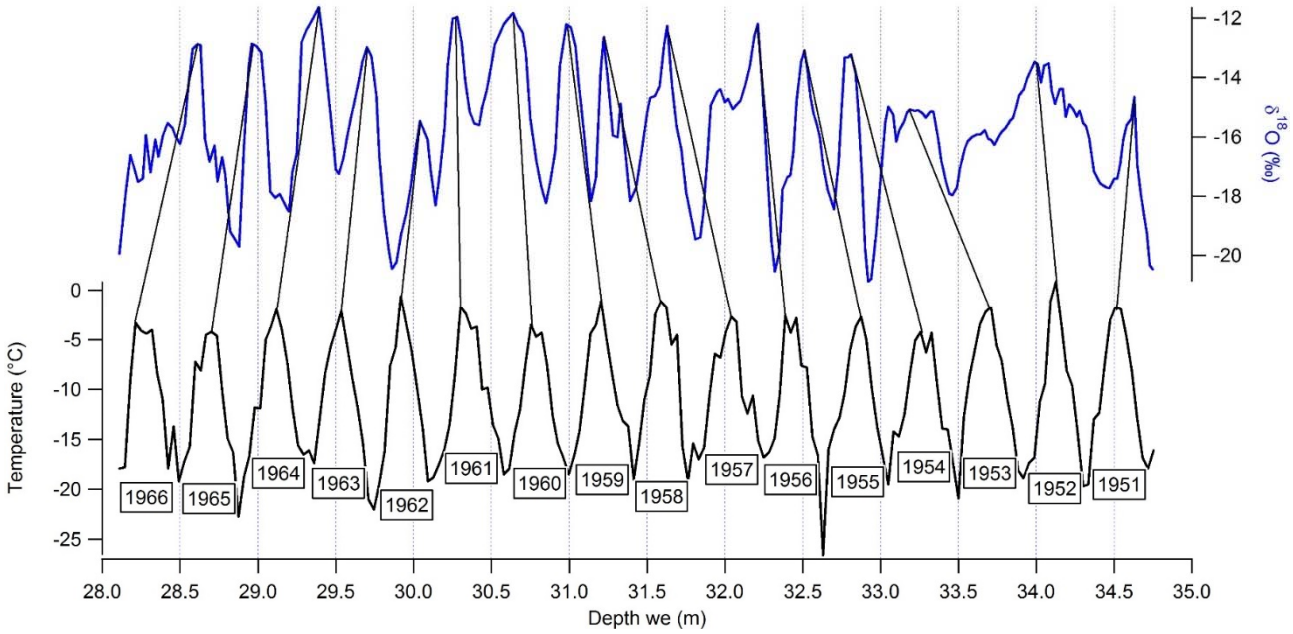

Fig. 6.6-7 $\delta^{18}O$ annual layers (blue line, Gabrielli personal comm.) matched with temperature oscillations (black line) between 1951 and 1966 (core #2)

In order to assign a high-resolution dating to this portion, the $\delta^{18}O$ summer maxima were matched with mean monthly temperature summer peaks, as well as winter minima with the lowest temperatures (Ortles reconstructed temperature series, 1864-2009) between 1951 and 1963. The year 1963 is identified by the presence of the tritium peak. Uncertainties affected the identification of the years 1951, 1952 and the year 1966, so the comparison was carried out between 1953 and 1965. After the identification of summer maxima and winter minima for each year on the $\delta^{18}O$ profile, and the consequent matching with maximum and minimum mean monthly temperature for the same year, a $\delta^{18}O$ value was manually assigned to each monthly temperature datum.

The seasonal linear regression was calculated between $\delta^{18}O$ and temperature data, obtaining the following results (tab. 6.6-5).

Interval: 1953-1965 (monthly res.)	**$\delta^{18}O/T$**	**R^2**
Core #2 (depth: 40-45 m)	0.29	0.56

Tab. 6.6-5 $\delta^{18}O/T$ relationship for the 1953-1965 interval of core #2 (monthly resolution data)

By using temperature and isotope mean annual values, the inter-annual linear correlation between $\delta^{18}O$ and temperature data was also calculated, with the results showed in table 6.6-7.

Interval: 1953-1965 (annual res.)	**$\delta^{18}O/T$**	**R^2**
Core #2 (depth: 40-45 m)	0.26	0.06

Tab. 6.6-7 $\delta^{18}O/T$ relationship for the 1953-1965 interval of core #2 (monthly resolution data)

The extremely low R^2 indicates a very poor correlation between these data, and the calculated slope is hence not reliable.

6.6.4 Considerations

It seems evident that lowering the temporal resolution of the dataset causes a slope increment, augmenting the assessed sensitivity of the isotope thermometer, permitting to avoid overestimating temperature variations (it happens when using a seasonal, lower, slope). The $\delta^{18}O$ gap (+3.64 ‰) between the 1919-1962 and 2001-2011 mean values, would translate in a temperature increase of +12°C if a 0.29 seasonal slope was used. If a 2.42 slope was utilized instead, it would be translated in a ~1.5°C temperature increase, close to the observed temperature raise in instrumental data.

When using monthly data, the correlation coefficient (R^2) displays a high value (0.56), implying a strong correlation between $\delta^{18}O$ and temperature; the R^2 is higher than those found for core #1, #2 and composite record for the last century (with annual or sub-annual resolution). This time the temporal resolution was sufficiently high to maintain the seasonal variability of the signal, even if just for a small portion of the core (~5 m w.e.). The slope (0.29) is quite low compared to the values found for core #1, #2 and composite record for the last century (inter-annual slopes), and still low when compared to the slopes found in literatures (seasonal slopes) for other mountain ice cores (see tab. 6.6-8). The R^2 tough, is comparable to the values found on Fiescherhorn and Mt Rosa (Grenzgletscher), in Switzerland.

Seasonal scale	$\delta^{18}O/T$	R^2
Fiescherhorn (Mariani *et al.*, 2014)	0.47	0.55
Grenzgletscher, Unweighted (Mariani *et al.*, 2014)	0.53	0.56
Grenzgletscher, Precipitation weighted (Mariani *et al.*, 2014)	0.55	0.58
Colle Gnifetti (Kech, 2001)	1.7	--
Jungfraujoch (Schotter, 1997)	0.68	0.83
Fiescherhorn (Schotterer, 1997)	1.1	0.74
Tsast Ula (Schotterer, 1997)	1.9	0.46
Ortles Shallow Core 2009 (this thesis)	0.41	0.46
Ortles core #2 (this thesis)	0.29	0.56

Tab. 6.6-8 Seasonal $\delta^{18}O/T$ relationship for some alpine ice cores

It has to be considered that all but one (Tsast Ula, Mongolia) of these drilling sites are located in the Western Alps, in an area characterized by high accumulation and where the glaciers are still in a cold state. Not only the higher accumulation enhance the temporal resolution, but the continuously formed newly snow strata protect the underlying layers, diminishing the influence of post-depositional processes; the cold state of the glaciers implies that their englacial temperature is lower, minimizing melting and meltwater percolation.

CHAPTER 7: OTHER ALPINE CORES

7.1 The Vernagtferner glacier ice cores

The Vernagtferner glacier (fig. 7.1-1) is located at the end of the Ötztal valley, in Western Austria (46° 52' N, 10° 49' E), between 3400 and 2800 m a.s.l. (fig. 7.1-1): it is one of the few drilling sites of the Eastern Alps, hence the importance of a comparison with Mt Ortles; the Vernagtferner was already temperate more than three decades ago and will probably represent the evolution of the Alto dell'Ortles glacier if the temperature keep increasing. The glacier is part of the Danube river basin, and is hence very important in regulating the water supply for one of the main European rivers. The Vernagtferner has been retreating since the beginning of the 20th century (fig. 7.1-2), after a short period of advance occurred from 1893 to 1901 (www.glaziologie.de).

Fig. 7.1-1 The Vernagtferner location (left) and the Vernagtferner glacier from Google Earth (right)

During March 1979, three deep cores have been drilled at an approximate elevation of 3150 m a.s.l. The month of March was chosen in order to minimize the firn meltwater content: in the late seventies the glacier was already considered temperate. During summer the water table reached a height of 17-23 m below the surface (Oerter *et al.*, 1982).

The first ice core was meant to reach the bedrock, located between 90 and 100 m of depth (Oerter, 1977; Miller, 1972), but the drilling had to be stopped at 83.45 m due to the presence of a conspicuous amount of water in the borehole that was impossible to drain. Other two cores were retrieved in the same month: the second reached a depth of 45.10 m (the purpose was to drill enough to find tritium-free ice), while the third was stopped at 34.45 m in order to study the firn-ice transition, located at 20-25 m from the surface (Oerter *et al.*, 1982).

Another drilling operation was carried out four years later, in March 1983, when three more cores (core IV, core V and core VI) were obtained from the same site. Five out of six cores were retrieved in the accumulation area of the glacier, while core VI was located near the mean equilibrium line (Oerter *et al*., 1985). After only four years since 1979 the glacier had already lost more than 10^{10} kg (fig. 7.1-2), while in 2010 the mass loss (since 1979) was equal to $17.3*10^{10}$ kg (www.glaziologie.de).

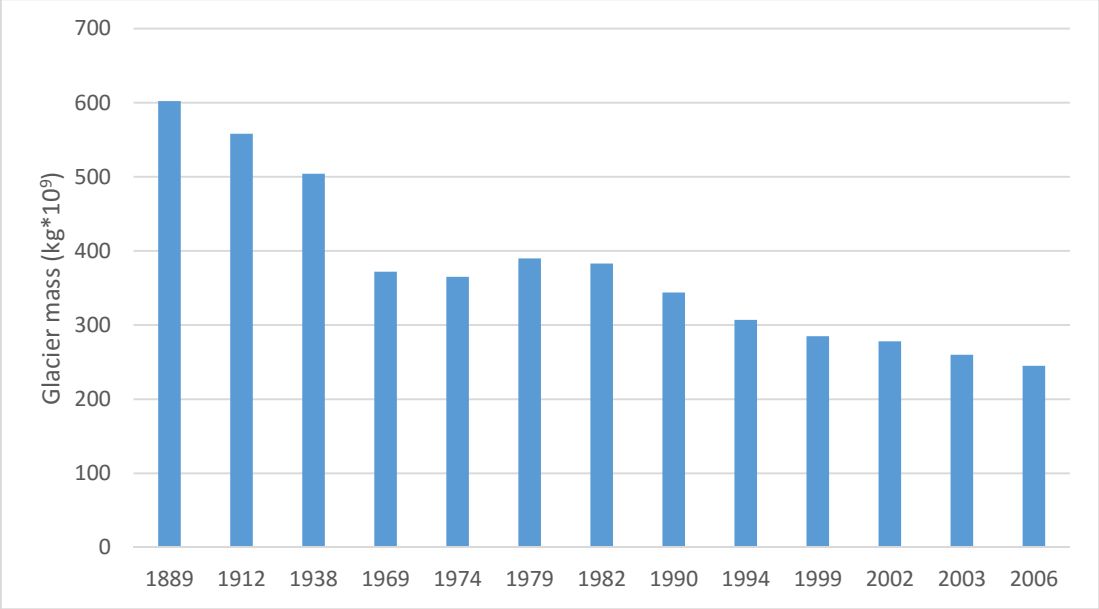

Fig. 7.1-2 The Vernagtferner glacier mass balance (1889-2009), from www.glaziologie.de

In temperate glaciers the annual precipitation is usually not made up entirely of snow, and post-depositional processes such as melting and evaporation are relevant (Stichler *et al*., 1982).
Core I is the most significant of the group, being the longest and probably the best preserved. Even if the core was wet in many parts, it has retained most of its information, permitting an accurate dating: the estimated age is comprised between 77 and 83 years, extending the record back to the transition between the 19th and the 20th century. The dating is primarily based on annual layer counting relying on deuterium excess (*d*) seasonal variations: the parameter shows maxima during winter and minima during summer for this site, when melting and evaporation are strong: the opposite behavior of oxygen and hydrogen stable isotopes. Deuterium excess seasonal variations have been chosen because they appeared more regular than oxygen-18 or deuterium oscillations (Stichler *et al*., 1982). The dating has been implemented by the measure of the 1963 tritium peak (Oerter and Rauert, 1982), following the highest number of nuclear experiments conducted in the atmosphere. Given the dilution effect caused by meltwater seepage, the radioactivity fall-out

dating method, based on total beta and cesium-137, has not provided useful results for dating the ice core. On the other hand, the lead-210 measurement has proved to be suitable even for temperate glaciers, offering a tool to estimate the ice age: the result was in accordance with the annual layer counting. Lead-210 can be displaced by meltwater seepage, but despite that process, the specific activity of ^{210}Pb decreases with depth, and so it can be used for dating the ice core (von Gunten *et al*., 1982).

The estimated accumulation rate (Stichler *et al*., 1982), obtained from the annual layer counting, ranges from 0.77 to 0.85 m w.e./a, depending on the different age estimations of core I (77-83 years). The value is roughly 20% inferior to the recent Ortles accumulation rate estimation: 1007 mm w.e. (Festi *et al*., 2015).

δ^{18}O and δD profiles of core I were obtained utilizing a high-resolution cutting of 2.5 cm per sample, but since the signal showed many irregular variations, weighted mean values (10-point centered average of 10-point averages of raw data) have been used in order to reduce the noise. δ^{18}O values range from -20.49 to -8.31 ‰ (mean value: -14.56 ‰), while δD varies from -154.6 to -73.3 ‰ (mean value: -108.4 ‰). The deuterium excess goes from -9.3 to +20 ‰ (mean value: +8.1 ‰) (Stichler *et al*., 1982). For comparison, the Ortles core #1 mean isotope values are -15.07 ‰ for δ^{18}O (max: -7.49 ‰; min -26.64 ‰), -108.98 ‰ for δD (max: -46.62 ‰: min: -199.12 ‰) and 11.57 ‰ for *d* (max: 0.00 ‰; min: 18.80 ‰). The mean δ^{18}O value for the Vernagtferner (core I) is only +0.51 ‰ higher than the Ortles mean; considering a supposed altitude effect of -0.2 ‰/100 m (Siegenthaler and Oeschger, 1980; Schürch *et al*., 2003) and an elevation difference of ~800 m, the expected mean δ^{18}O for the Ortles should be -16.16 ‰. It has to be considered though that the complex Alpine topography has a big influence on moisture paths and precipitation, and despite being just 50 km apart from each other, the two drilling sites could be characterized by different moisture sources and precipitation regimes. The isotope range of variation is wider for the Ortles cores; this could be due to less severe post-depositional processes smoothing the original precipitation signal. It has to be considered that the Vernagtferner core, retrieved in 1979, does not contain the warming-influenced, most recent part, characterized by higher isotopic values, and does not go back in time as much as the Ortles core.

The isotope variations were visually compared with temperatures (5-year running annual mean). Thermometer data were provided by the meteorological station located at Vent (1893 m a.s.l. until 1971, then 1906 m a.s.l.), approximately 8 km away from the drilling site (Stichler *et al*., 1982). The correlation between temperature and isotopic profiles is not very good, but the late 1940s temperature peak coincides with the maximum of δ^{18}O, δD and the minimum of *d*, even if the datum is shifted back to 1944 in the isotopic profiles, indicating some errors in the age scale. Both

isotope and Vent temperature records show a slight warming trend, more clear for the $\delta^{18}O$ profile, for the recent period (fig.7.1-3).

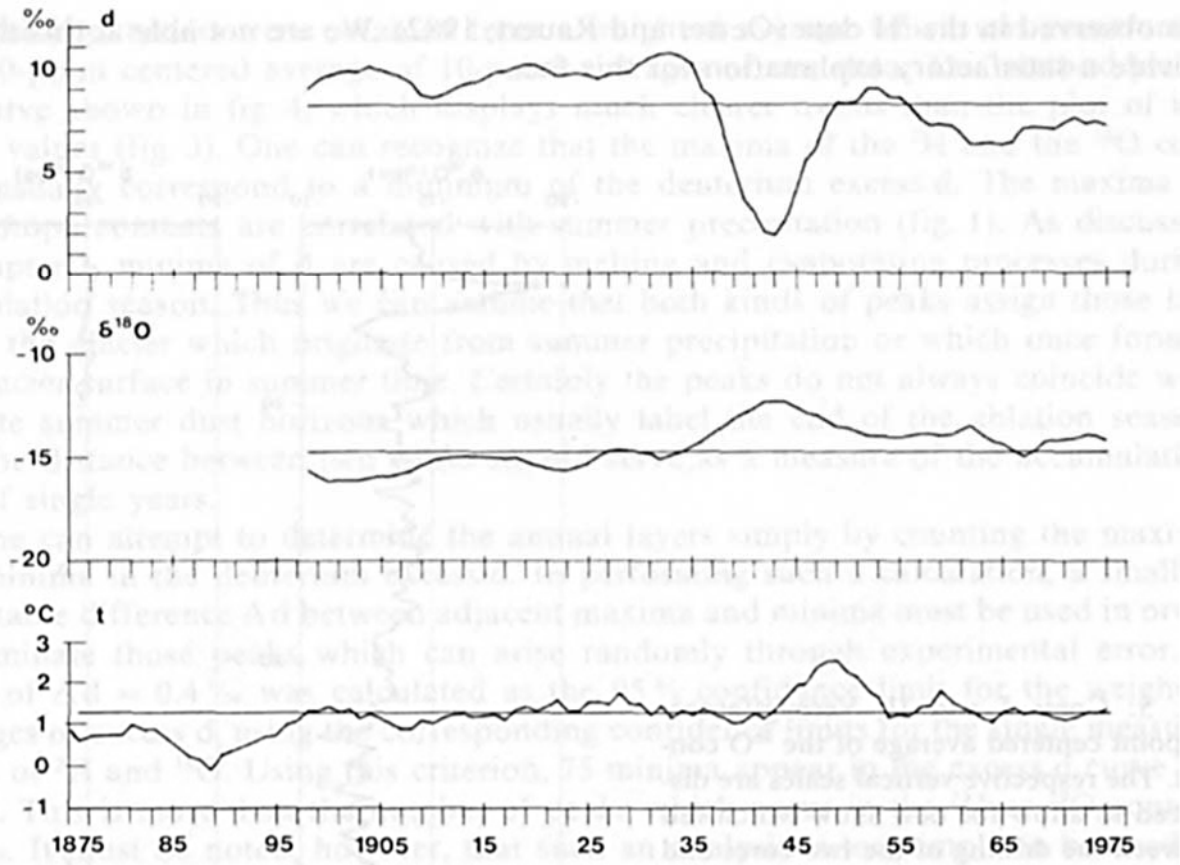

Fig. 7.1-3 temperature (at the bottom) and *d* (on top), $\delta^{18}O$ (in the middle) profiles for core I. From Stichler *et al*., 1982

The isotope profiles of core IV (length: 40 m; 1983) reveals a relevant damping when compared to core I (1979), resulting in a smoothing of the signals for $\delta^{18}O$ and *d* (fig. 7.1-4); tritium values are also lower (fig. 7.1-5), even when multiplied by 0.8 in order to compensate the decaying factor (^{3}H half-life: 12.32 years): this is probably due to the dilution effect caused by meltwater seepage (Oerter *et al*., 1985).

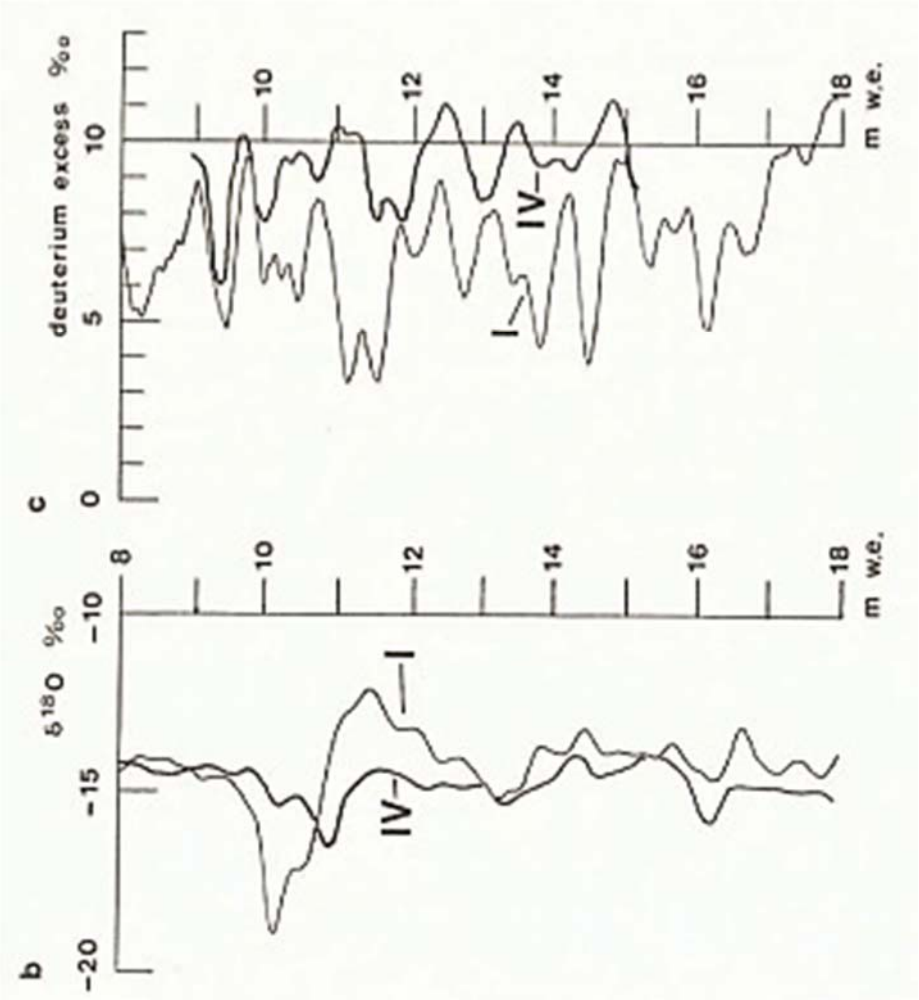

Fig. 7.1-4 *d* (above) and $\delta^{18}O$ (below) profiles from core I and core IV. From Oerter *et al*., 1985

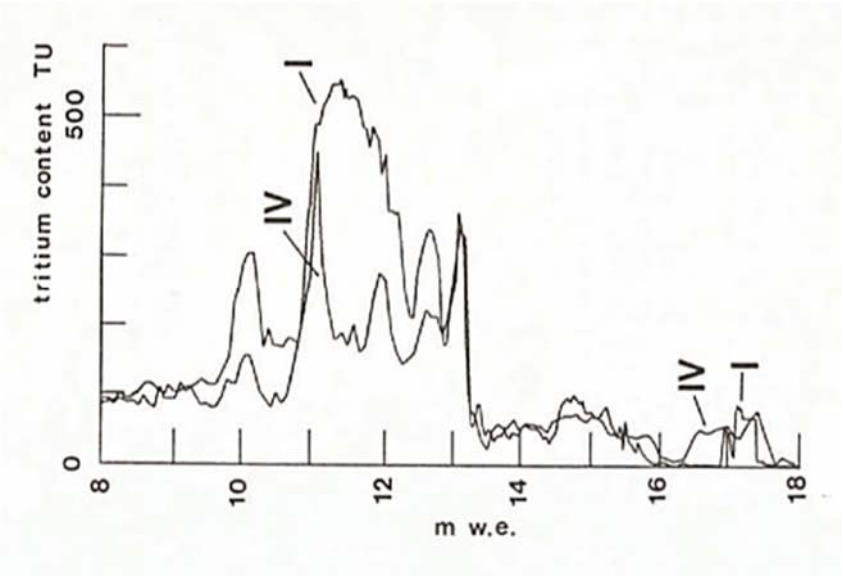

Fig. 7.1-5 ^{3}H profile from core I and core IV; the core IV profile has been corrected for the decay factor. From Oerter *et al*., 1985

7.1.1 Recent data

The 1975-2010 summer temperature (from May to September) at the Vernagtbach gauging station (2640 m a.s.l.) shows a remarkable positive trend (fig. 7.1-6), with a total increment of about 1°C (Escher-Vetter *et al*., 2014).

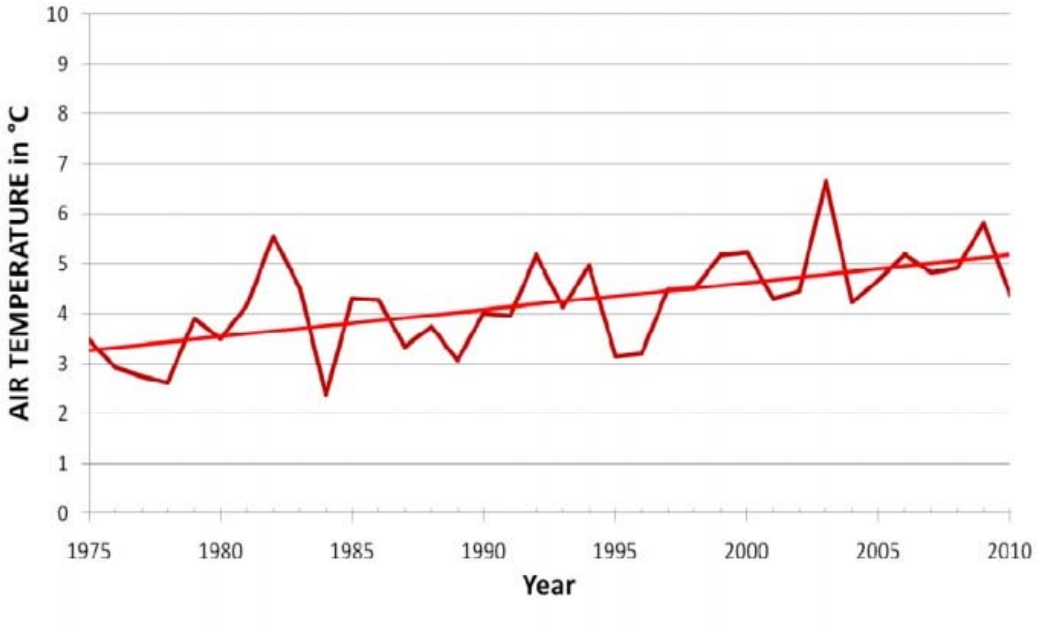

Fig. 7.1-6 Mean annual temperature and temperature trend (1975-2010) from the Vernagtbach gauging station (2640 m a.s.l.). From Escher-Vetter *et al*., 2014

The Vernagtferner glacier melting discharge rate has incremented during the last decades: its value, measured at the Vernagtbach gauging station (fig. 7.1-7), has roughly doubled in less than forty years (Escher-Vetter *et al*., 2014).

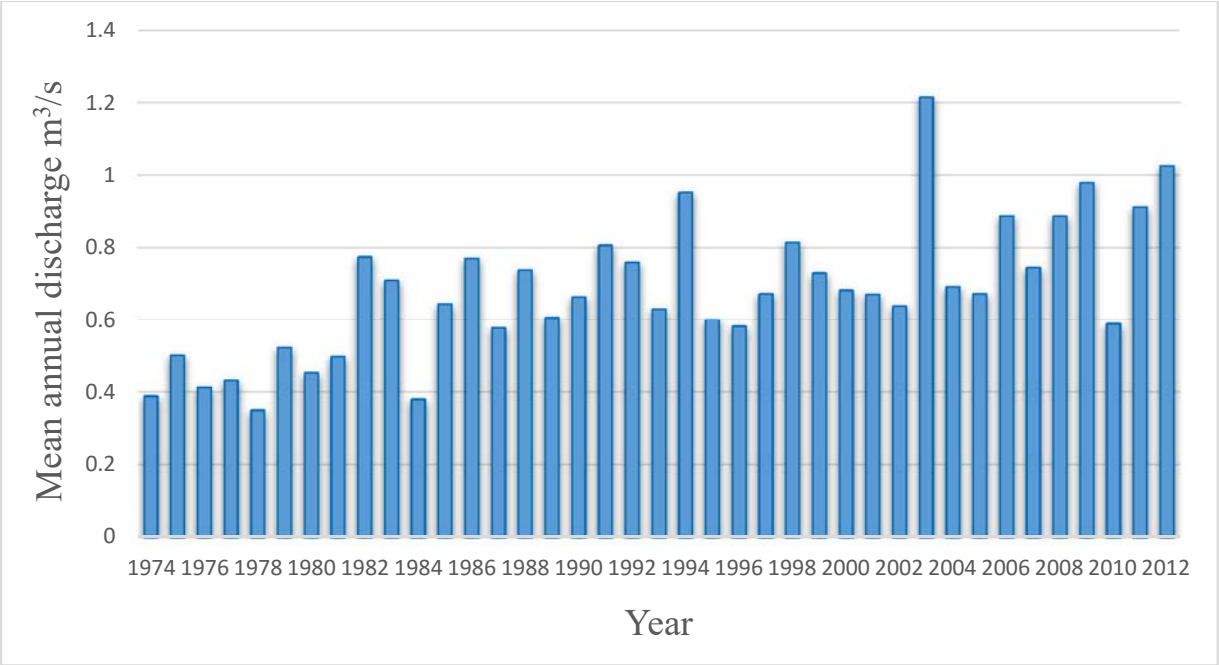

Fig. 7.1-7 Vernagtferner mean annual discharge, in m^3/s (1974-2012) measured at the Vernagtbach gauging station (2640 m a.s.l.). From Escher-Vetter *et al*., 2014

Up to now, the Vernagtferner drilling project remains the only extensive isotope study based on deep ice cores from the Eastern Alps. Considering the pace at which the Vernagtferner has been retreating in the last decades, the possibility of obtaining good climate archives from the glacier is now close to zero.

7.2 The Fiescherhorn ice cores

The Fiescherhorn (46°33’ N, 8°04’ E), in the Bernese Alps (fig. 7.2-1), is the closest drilling site to Mt Ortles in terms of elevation (3900 m a.s.l.) and latitude, but is located in the Northern Alps, 190 km away from the Ortles.

Fig. 7.2-1 The Fiescherhorn location (left) and the Fiescherhorn massif (right) from Google Earth

The surface snow accumulation is estimated to be 1.7 m w.e./year (Jenk *et al*, 2006), significantly higher than the estimated accumulation for the Ortles drilling site (1007 mm w.e./a). The first FH ice core, 77-m long, was drilled in 1989 (Schotterer, 1997) and the second, just 100 m apart from the first one, in 2002, reached the bedrock at 151 m of depth (Mariani, 2013). The $\delta^{18}O$ record of FH 1989 (Schwikowski *et al*., 1999) is compared with the Ortles core #2 record (fig. 7.2-2). The FH 1989 mean $\delta^{18}O$ is -15.40 ‰, very close to the Ortles core #1 (-15.07 ‰) and equal to the core #2 (-15.40 ‰) mean values. While the Ortles profile shows a steep increment in the upper part, the Fiescherhorn profile does not appear to have recorded any warming, but 22 years separate the two drillings. The seasonality of FH 1989 is clearly preserved throughout the core, and the amplitude of seasonal variation is on average higher than the one characterizing the Ortles record. Despite being converted to water equivalent, the Ortles $\delta^{18}O$ record still displays an evident thinning in the lower portion, absent in FH 1989. Overall, this Fiescherhorn record looks substantially homogeneous from top to bottom.

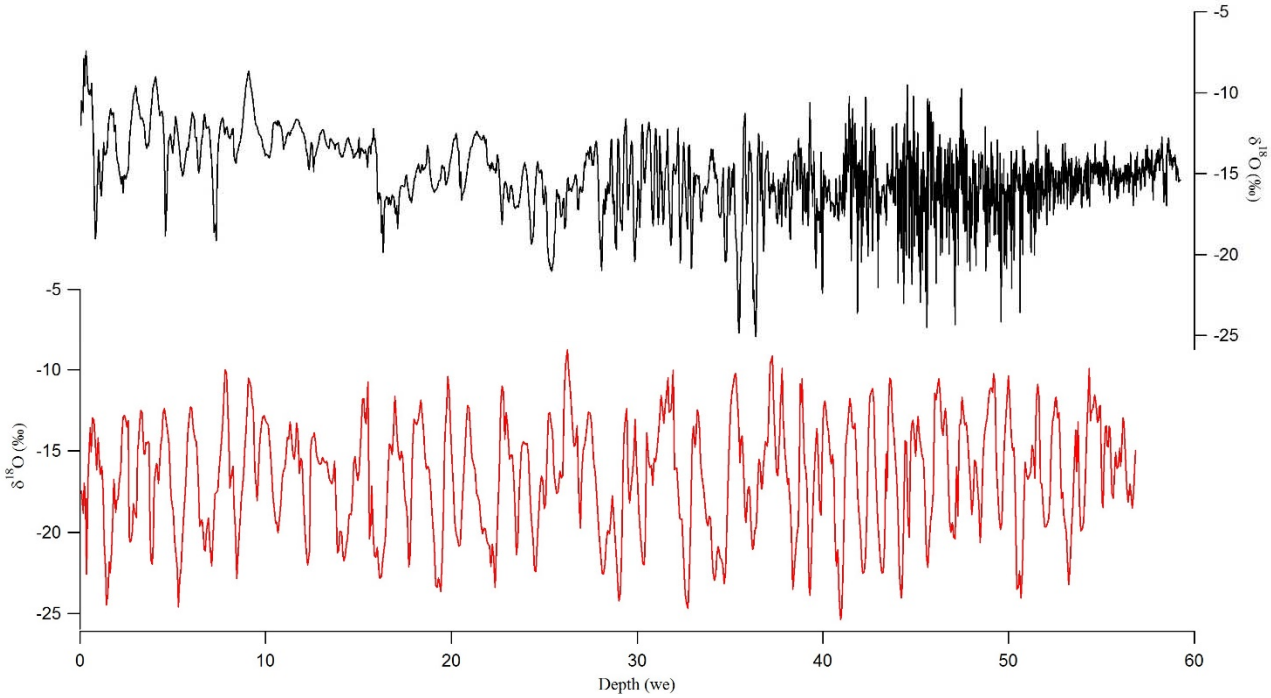

Fig. 7.2-2 FH 1989 (red; Schwikowski *et al*., 1999) and Ortles core #2 (black) $\delta^{18}O$ profile

The FH 2002 core covers the period ~1680-2002, having a dating uncertainty of ±2 years (1899-2002) rising to ±5 years for the period 1818-1899; for the bottom part, the dating uncertainty reaches ±30 years (Jenk *et al*., 2006). As in the FH 1989 core, The conservation of the $\delta^{18}O$ signal is impressive (see fig. 7.2-3), characterized by a good preservation of seasonal oscillations, and the isotopic data correlate well with instrumental temperature from the Jungfraujoch meteorological station (3466 m a.s.l.): the $\delta^{18}O/T$ slope is 0.47, while the R^2 is 0.55 (Mariani *et al*., 2014).

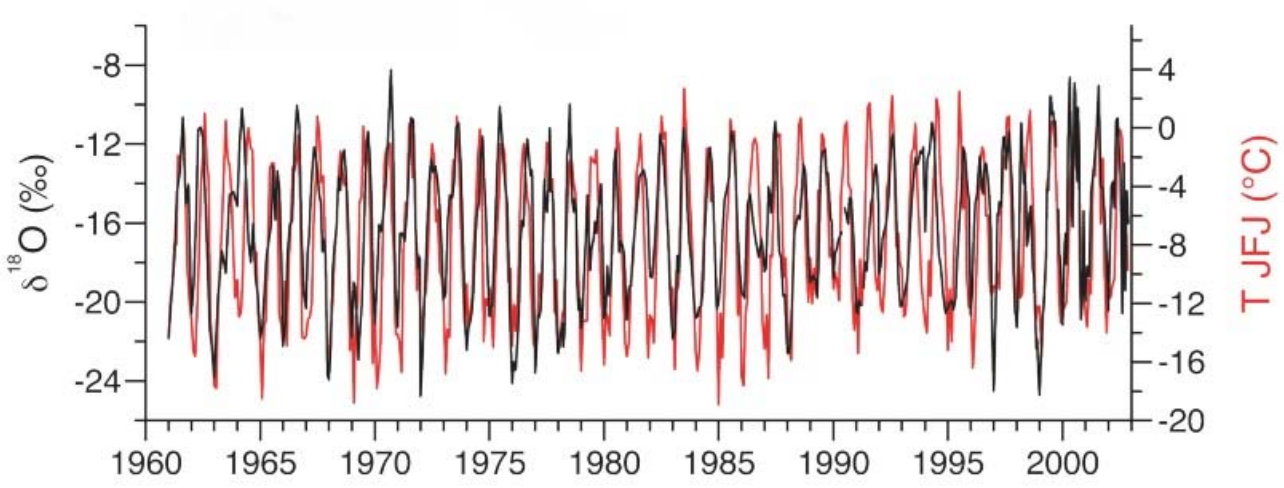

Fig. 7.2-3 FH 2002 $\delta^{18}O$ profile (black) compared with instrumental temperature (red, 1960-2002). From Schwikowski *et al*., 2014

7.3 Two Mt Rosa drillings: Colle Gnifetti and Colle del Lys

Mount Rosa (fig. 7.3-1) is a large massif in the Western Alps, located on the watershed between Northern and Southern Europe. Its main summit (Dufourspitze) culminates at 4634 m a.s.l. Mt Rosa is the highest mountain of Switzerland and the second-highest mountain of the Alps. Colle Gnifetti and Colle del Lys, both located on Mt Rosa massifs (fig. 7.3-1), are among the most utilized coring sites in the Alpine region.

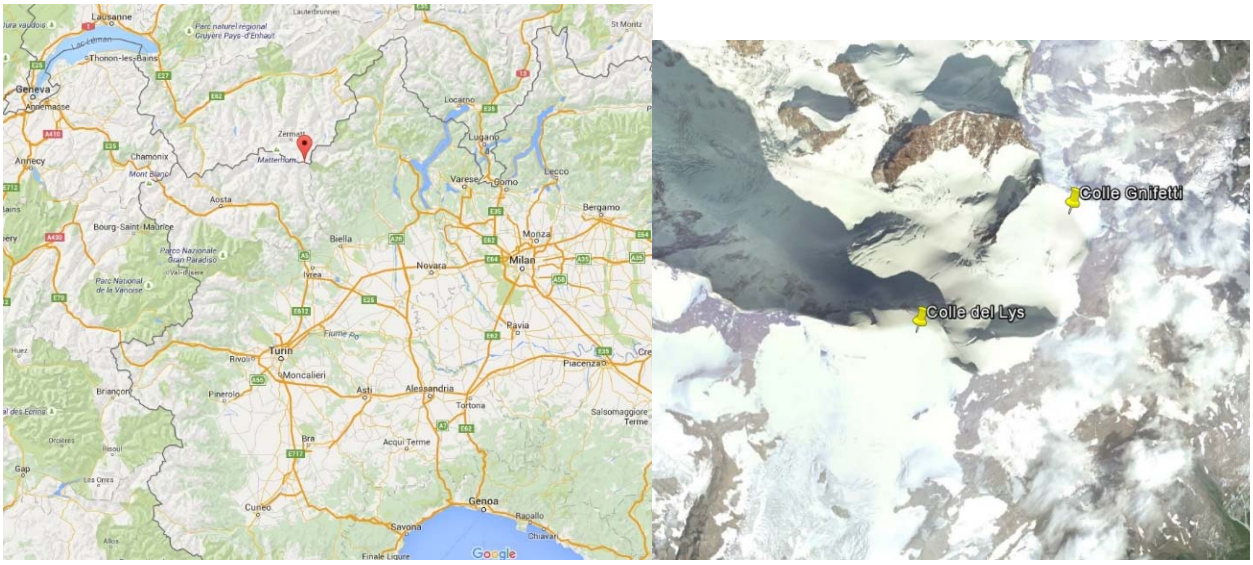

Fig. 7.3-1 Mt Rosa location (left) and Colle Gnifetti and Colle del Lys drilling sites (right), from Google Earth

7.3.1 The Colle Gnifetti 2003 ice core

In 2003, a 80-m ice core (CG 2003) was drilled to bedrock on the Colle Gnifetti glacier saddle (45°55' N, 7°52' E), at an altitude of 4455 m a.s.l. The mean annual snow accumulation rate is only ~454 mm w.e., less than half the Ortles accumulation. Due to the preferential wind erosion of light winter snow, this site accumulates snow mainly during summer, permitting the preservation of more than the last 1000 years at a reasonable temporal resolution and, additionally, the presence of more than 10,000 year old ice close to bedrock (Jenk *et al*., 2009). This ice core is the longest climate record ever obtained in the Alps. The $\delta^{18}O$ record (Sigl, 2009; fig. 7.3-2) is believed to go back in time to the last glacial period; the bottom part is characterized by an exceptional thinning of the ice layers, and the most negative isotopic values around 61 m of depth could belong to the last ice age. An increase of the $\delta^{18}O$ signal starts around 7 m and continues until 2 m from the surface, possibly indicating the recent warming trend. The mean $\delta^{18}O$ value is -13.90 ‰ (max: -7.58 ‰; min: -23.37 ‰), compared to the Ortles core #1 mean value of -15.07 ‰ (max: -7.49 ‰; min -26.64 ‰). The higher isotopic mean value is due to the seasonal bias toward more enriched summer precipitation, considering that most of the winter deposition is scoured by wind.

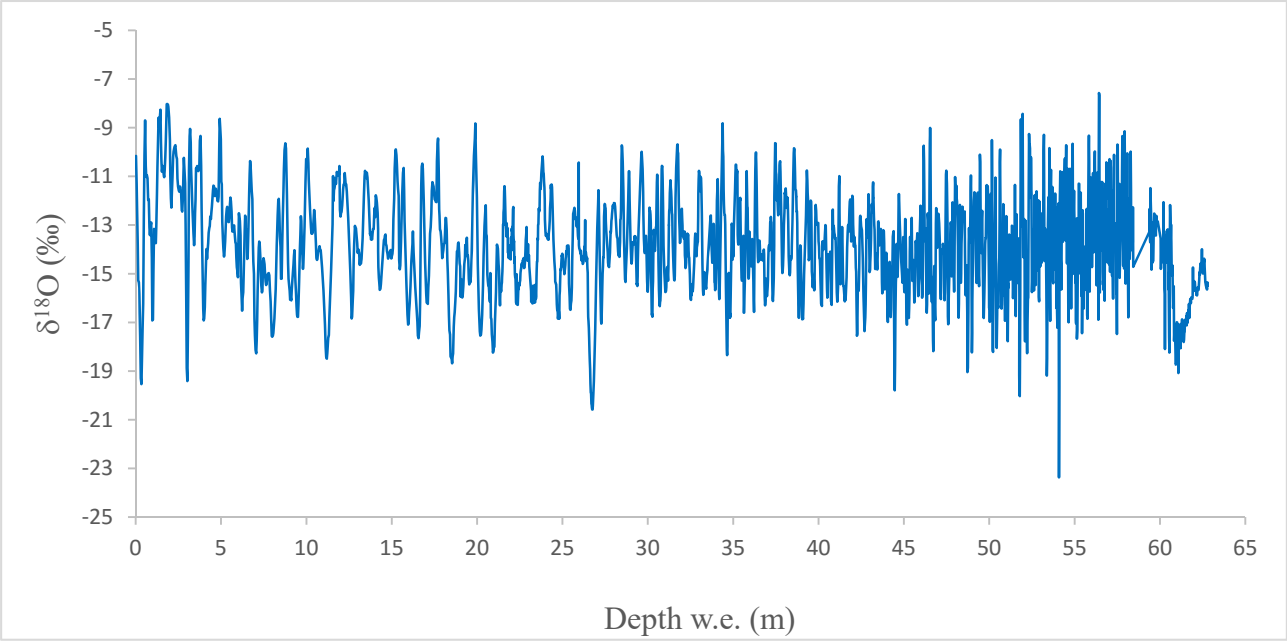

Fig. 7.3-2 CG 2003 $\delta^{18}O$ record vs depth w.e. From Sigl (2009)

The $\delta^{18}O$ profile from CG 2003 can rely on a solid age scale; the preliminary Ortles age scale (see previous section) is considered reliable only for the last century, but is applied to the entire core

length, so it is possible to compare the two Alpine records (CG 2003 and Ortles core #2) for the last millennium. The data have been compared using a 100-point moving average, in order to lower the noise of the $\delta^{18}O$ signal and better capture long-time trends (fig. 7.3-3).

The 1000-year comparison shows surprising results: most of the principal oscillations can be observed in both cores. Between 1000 and 1470 AD there is a clear decrease in both $\delta^{18}O$ records, followed by a ~200-year increase showing discrepancies between the two profiles. Between ~1750 and the beginning of the 20th century higher isotopic values are spotted in both cores, followed by two minima (around 1910 and 1950) and another peak (1960-1970) clearly visible in both profiles. After 1980 the increasing trend, of higher magnitude compared to earlier oscillations, is noticeable in Ortles core #2 and CG 2003. The similarity between these two records is impressive, considering the different altitudes, locations, moisture source patterns and the uncertainties related mainly to the Ortles age scale. The different seasonal distribution of precipitation and the strong effect of wind erosion on Colle Gnifetti, removing the most part of winter accumulation, have also to be taken into account. The good accordance between the isotope profiles of the two cores might suggest the presence of a continuous long climate record (at least 1 ka) stored in the Ortles ice.

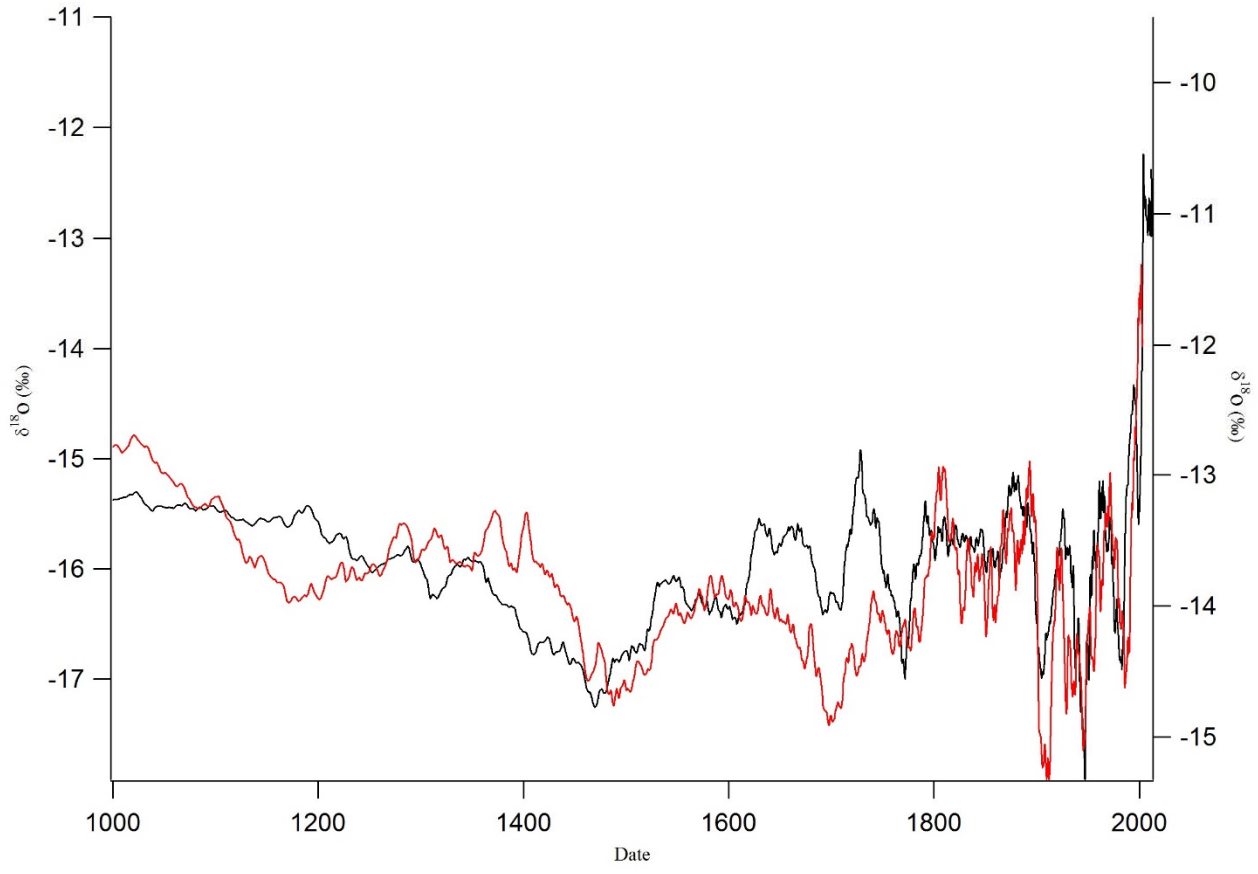

Fig. 7.3-3 Comparison between CG 2003 (red, right y-axis) and Ortles core #2 (black, left y-axis) $\delta^{18}O$ records, using a 100-point moving average, for the last 1000 years

7.3.2 The Colle del Lys drillings

Colle del Lys (45°92'N, 7°86'E), is one of the main drilling sites of the Alpine region; in 1996, a 80-m core was drilled at 4248 m a.s.l. in the framework of the European project ALPCLIM (CdL 1996). The drilling procedure was coordinated by Professor V. Maggi (DISAT-UNIMIB).

Water stable isotopes analyses were carried out for the first 53 m of the core. The estimated accumulation rate (based on the tritium peak of 1963, found at 49.6 m of depth w.e.) is equal to 1.5 m w.e./a; more than three times the estimated accumulation for Colle Gnifetti, despite being less than 2 km away from the other Mt Rosa drilling site. Thanks to the high elevation of this site, and to the high accumulation rate, the isotope signal is well preserved throughout the core. The $\delta^{18}O$ values range from -29.06 to -7.24 ‰, and the mean value is -16.28 ‰. A small warming trend can be deduced by the slight increase of the $\delta^{18}O$ signal (fig. 7.3-4). For comparison, the Ortles core #1 mean $\delta^{18}O$ value is -15.07 ‰ for $\delta^{18}O$ (max: -7.49 ‰; min -26.64 ‰). Assuming an altitude effect of -0.2 ‰/100m (Siegenthaler and Oeschger, 1980; Schürch *et al*., 2003), and an elevation difference between the two drilling sites of ~400 m, the expected mean $\delta^{18}O$ value for the CdL 1996 core should be -15.86 ‰. Considering the distance between the two sites, and the different precipitation influence for the Western Alps, a different value can be expected. It has also to be taken into account that the CdL 1996 does not contain 15 year of increased temperature in its record (1996-2011), which should raise the isotope values.

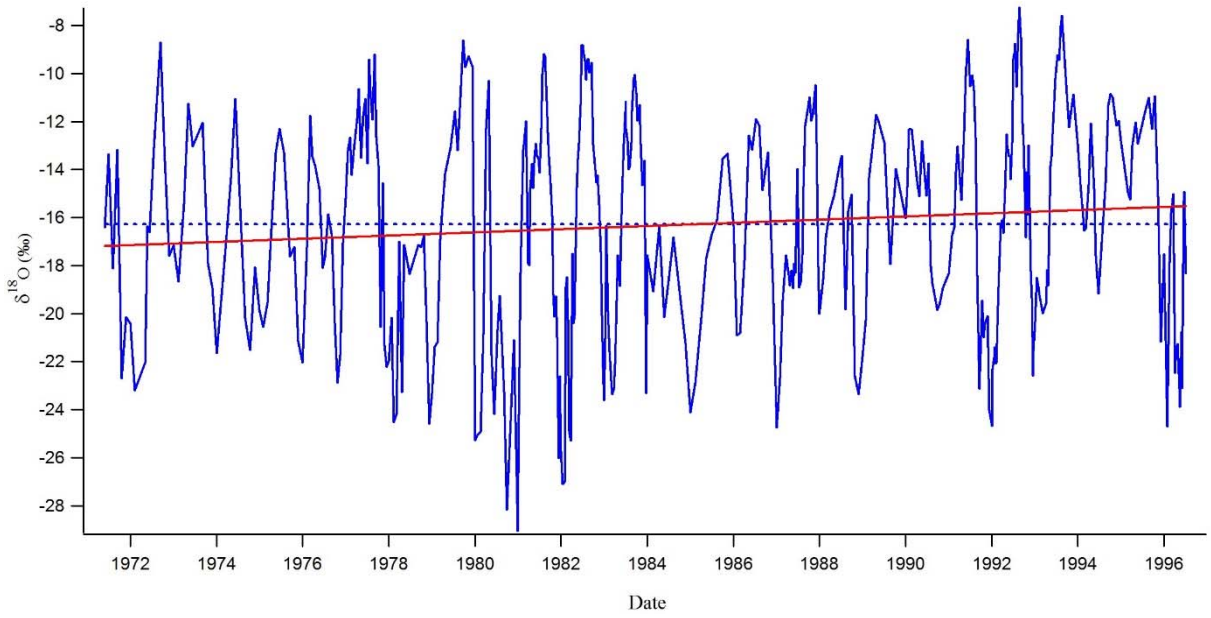

Fig. 7.3-4 CdL 1996 core $\delta^{18}O$ (continuous blue line) vs age; the dotted line represents the average $\delta^{18}O$ value. The red line is the linear trend of the $\delta^{18}O$ signal. (Stenni, personal comm.)

Compared to the Ortles core #1 and #2 profiles, the $\delta^{18}O$ shows ampler seasonal variations, and both summer maxima and winter minima are, on average, higher and lower, respectively, than those found in the Ortles cores, which means that the isotope record has probably not undergone the same smoothing occurred in the Ortles glacier, due to post-depositional processes. In fact, the upper firn part does not present a noticeable reduction of the intra-annual fluctuations, possibly implying that the meltwater seepage was, at least at that time, limited to few centimeters.

Another deep core (106 m) was retrieved on Colle del Lys in July 2003 (CdL 2003), in proximity of the 1996 core, at 4248 m a.s.l.; the drilling was once more coordinated by Professor V. Maggi (DISAT-UNIMIB). $\delta^{18}O$ has been measured for the whole core; the $\delta^{18}O$ record is presented in the graph below (fig. 7.3-5). Tritium analyses indicate a peak at 53.7 m of depth w.e., suggesting a mean annual accumulation rate of 1.34 m w.e. (-0.16 m w.e. with respect to the previous estimate).

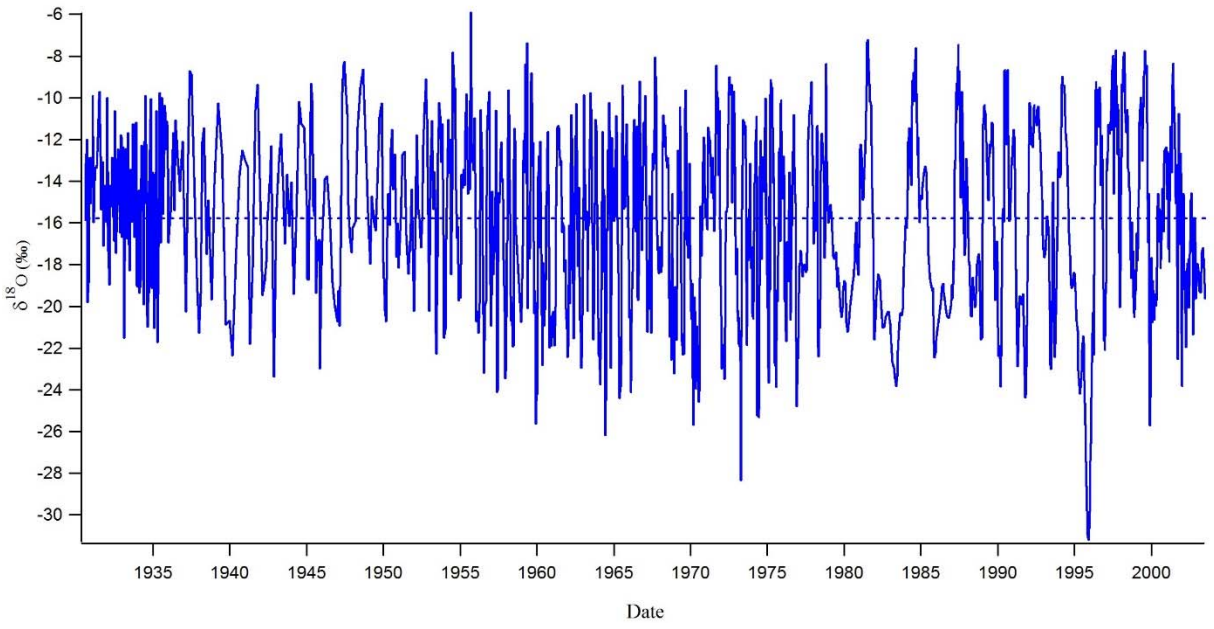

Fig. 7.3-5 CdL 2003 $\delta^{18}O$ profile (solid line) vs age and average $\delta^{18}O$ value (dotted line) (Stenni, personal comm.)

The CdL 2003 core $\delta^{18}O$ profile shows a similar amplitude of seasonal oscillations (compared to CdL 1996), but in the bottom part (approximately the last 7 years) a smoothing of the isotope signal, as well as a significant thinning of the ice layers, can be noticed, in accordance to what was observed for the Ortles cores. The average $\delta^{18}O$ value is -15.78 ‰, +0.50 ‰ with respect to the 1996 core, and very close to the presumed $\delta^{18}O$ value (-15.86 ‰) obtained applying an altitude effect of -0.2 ‰/100 m (Siegenthaler and Oeschger, 1980; Schürch *et al*., 2003) to the Ortles mean

$\delta^{18}O$. This could be due to the positivization of the overall $\delta^{18}O$ induced by the presence of further 7 years of precipitation with respect to the CdL 1996 core (1996-2003); but by looking at the $\delta^{18}O$ profile for the most recent part, this hypothesis seems very unlikely. In contrast to CdL 1996, no trend is detectable for $\delta^{18}O$.

A mean monthly temperature record from the Plateau Rosa AWS (45°56'N, 7°42'E, 3488 m a.s.l.) is available from 1953 to 1991. It is possible to compare these temperature data with $\delta^{18}O$ record from CdL 1996; the old core was chosen because the temperature record ends in 1991 so there was no reason to use more recent isotope data, considering that the 1991 layer was buried deeper in the CdL 2003 core. Given the high resolution of the isotope data, it was possible to resample the isotopic values with a monthly resolution, in order to preserve the seasonal variations.

The linear regression is presented in table 7.3-1.

Interval: 1972-1991	**$\delta^{18}O/T$**	**R^2**
CdL 1996 (depth 1.5-52.3 m)	0.41	0.25

Tab. 7.3-1 seasonal $\delta^{18}O/T$ relationship for CdL 1996 core between 1972 and 1991

The slope is slightly higher than the values found for the Ortles (seasonal scale), and slightly lower than the one found for the Fiescherhorn (Mariani *et al*., 2014). The R^2 though is very low compared to the other Alpine sites. It has to be taken into account that the AWS is located about 10 km away and roughly 800 m below the drilling site.

In order to assess the long-term climate representativeness of Alpine ice cores for a wide area, the CdL 2003 $\delta^{18}O$ record, resampled with a 1-year resolution, was compared to the stacked record of Ortles core #1 and #2 (1-year resolution) and to the temperature (mean annual values) for the Greater Alpine Region (GAR) from the HISTALP gridded-dataset (Auer *et al*., 2007). The GAR goes from 4° to 19° E and from 43° to 49° N. To lower the noise and capture long-term variations, a binomial smoothing (3) was applied to each data series; the comparison starts in 1931 (when the CdL 2003 record begins). The results are presented in fig 7.3-6.

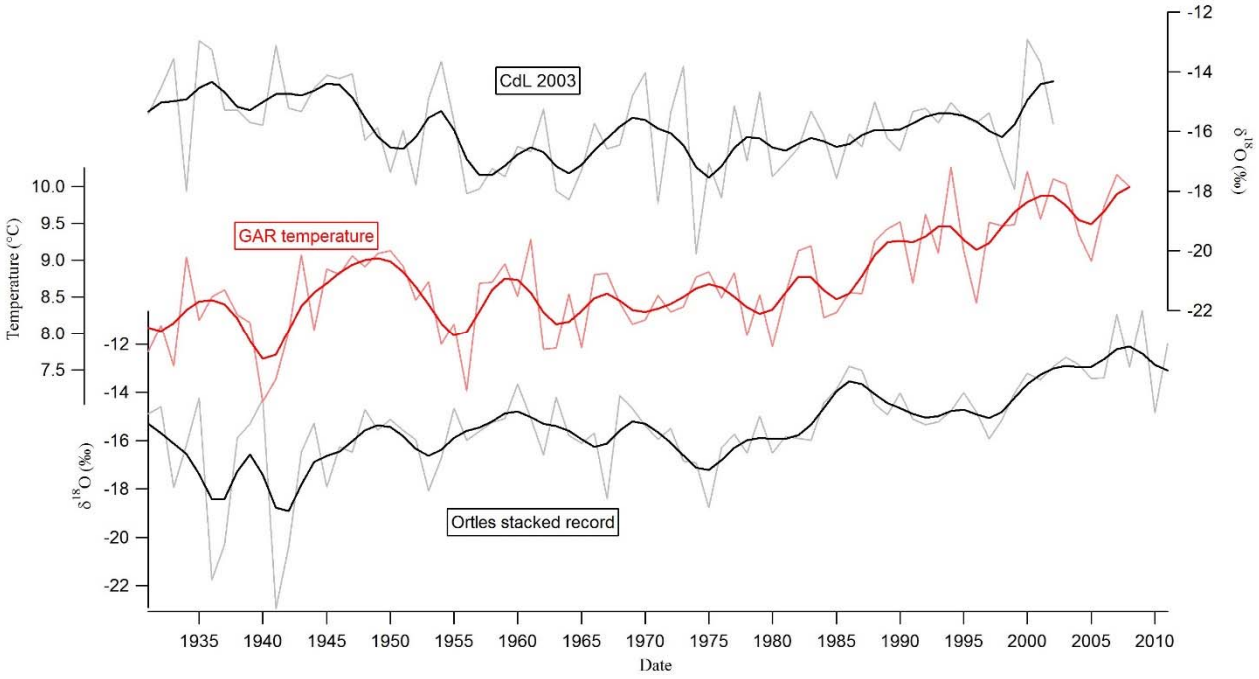

Fig. 7.3-6 CdL 2003 (on top) and Ortles stacked record (at the bottom) $\delta^{18}O$: grey thin line (1-year res.) and black thick line (binomial smoothing: 3), compared with GAR temperature: light red thin line (1-year res.) and red thick line (binomial smoothing: 3) from 1931.

Both $\delta^{18}O$ records show a good overall visual correlation with temperature, especially when considering the smoothed data; the correlation seems better for the Ortles stacked record, in which the temperature increase of the last decades is well represented, as well as some major temperature oscillations from the late 1930s to the early 1960s. Some isotopic data appear in anti-phase with temperature, but the dating uncertainties have to be taken into account, as well as post-depositional processes modifying the pristine isotopic signal, especially in the Ortles cores, located at lower elevation. The CdL 2003, which presents a better-preserved $\delta^{18}O$ seasonality, thanks to the lower temperature and higher accumulation, seems to lag behind the Ortles record in terms of mimicking long-term temperature trends. Overall, the representativeness of temperature variations for the entire Alpine region seems reasonably good for the Ortles stacked isotope profile, despite the high spatial variability of the area. The HISTALP temperature reconstruction for the GAR is based on a dense network of instrumental series for the considered time period (fig. 7.3-6), so it is assumed to be sufficiently reliable.

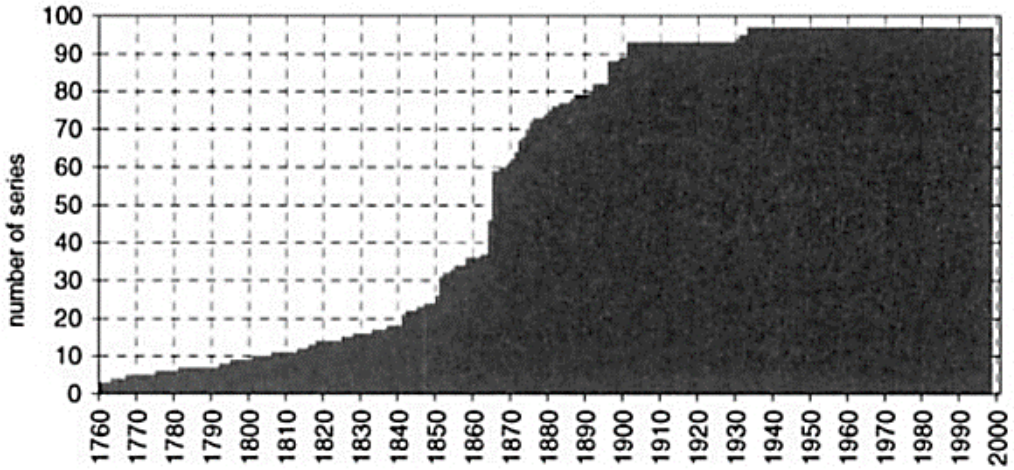

Fig. 7.3-6 Temporal coverage of the instrumental area in the Alps by homogenized temperature records, from Bohm *et al*., 2001

In order to quantify the strength of the isotope-temperature relation for these data, the linear regression was computed between the Ortles $\delta^{18}O$ stacked record and the HISTALP GAR temperature, using a 3-year mean for both datasets. The same was done using the CdL 2003 $\delta^{18}O$ record. The linear regression was carried out between 1931 and 2008 for Ortles and between 1931 and 2002 for CdL 2003. The results are presented in table 7.3-2.

3-year mean	**$\delta^{18}O/T$**	**R^2**
Ortles stacked record	1.78	0.51
CdL 2003	0.17	0.01

Tab. 7.3-2 $\delta^{18}O/T$ relationship between Ortles stacked record and GAR temperature and between CdL 2003 and GAR temperature between 1972 and 1991

The Ortles $\delta^{18}O$ stacked record shows a very good relation with the HISTALP temperature for the Greater Alpine Region when using 3-year mean data, meaning that the isotopic content of the Alto dell'Ortles glacier is representative of the long-term temperature variations for the entire Alpine region; this was also confirmed by the similarities between the Ortles and the Colle Gniffetti isotopic records, which are located in two different sectors of the Alpine mountain range. The slope (1.78) is similar (>1) to those obtained when a more-than-one year mean was used, confirming that the sensitivity of the isotope thermometer decreases when using inter-annual

resolutions instead of seasonal slopes. Surprisingly, the CdL 2003 $\delta^{18}O$ displays a very weak correlation with this temperature dataset.

CONCLUSIONS

The Ortles core #1 (length: ~74 m) was inspected and then processed and analyzed with a high-resolution sampling for $\delta^{18}O$ and δD for the entire length; tritium analyses were carried out in the depth interval between 35 and 55 m, with a 35-cm resolution, in order to find the peak belonging to the maximum of nuclear explosions in the atmosphere (1963), used as an age constraint for the chronological scale of the core. The Core #2 chronology (Gabrielli, personal communication), based on the best polynomial fit of a limited number of age markers, was successfully applied to core #1 (the age scale is assumed to be reliable for the last century only), and the isotope records from the two deep cores were merged into a stacked record in order to improve the signal-to-noise ratio. Isotopic data have been compared to the temperature series in order to assess the sensitivity of isotope variations to surface temperature fluctuations. Furthermore, the isotopic records from snow pits and shallow cores were discussed and compared to temperature data, when possible; the variability of the isotope signal before and after the ablation period (summer) has been quantified using snow pit data; it shows significant inter-annual variations. The post-depositional processes may affect the preservation of the pristine isotopic signal, complicating the climatic interpretation of the isotopic records. It has to be considered that the magnitude of these processes could have been of minor importance in the past, when the drilling site was characterized by lower summer temperatures and the glacier was still cold.

A visual inspection and measurement of the ice lenses of core #1 was carried out as well, without showing any significant trend, but assessing the presence of frequent melt layers throughout the core. This datum confirms that even under colder conditions in the past, the glacier was already experiencing ablation processes during warm summer periods, probably limited to the upper snow portion.

With the intent of characterizing the drilling site from a climatic point of view and the influence of the meteorological parameters on snow isotopic composition, the data from the Ortles AWS station (2011-2014) were presented in this study (Carturan and De Blasi, personal communication). In order to quantify the difference between the isotope content of precipitation and the preservation of that signal in the glacier, the isotope record of precipitation from the Pontresina (Switzerland) station (Meteo Swiss) was presented and compared to the Ortles isotope data.

A comparison with other Eastern and Western Alps ice cores showed a better preservation of isotope records from the Western Alpine sites, normally located at higher altitudes and

characterized by higher snow accumulation rates. Compared to the Ortles cores, the better preservation of the seasonal fluctuations appears evident in the upper part of the cores, in which the Ortles cores also display less negative isotopic values. Conversely, below the firn/ice transition (~30 m of depth for the Alto dell'Ortles glacier) the preservation of the isotope signal in the Ortles deep cores appears to be comparable with the Western Alpine records. The Ortles cores, on the other hand, thanks to the relatively low accumulation rate (~1007 mm w.e./a), are believed to retain a climate archive more extended in time than the majority of Alpine cores. Out of all the considered records, the Ortles core isotope profiles show the clearest growing temperature trend for the last decades, in accordance with the instrumental datasets of the Alpine region. A comparison for $\delta^{18}O$ was carried out between Ortles core #2 and CG 2003 (Sigl, 2009); the Colle Gnifetti core has a solid age scale and is characterized by the most extended temporal record, while the Ortles age scale is preliminary and affected by significant uncertainties, especially in the oldest part. Despite these issues, the two $\delta^{18}O$ profiles show an impressive visual correlation, capturing the main oscillations over the considered 1000-year period. This correlation is the evidence of the presence of a continuous climatic signal in the Ortles cores for at least the last millennium.

The direct comparison of the $\delta^{18}O$ records from the Ortles stacked record and Colle del Lys 2003 (Stenni, personal communication) with the Greater Alpine Region (GAR) temperature, between 1931 and 2008, indicates a better representativeness of large-scale temperature variations for the Ortles profile, meaning that, despite the loss of many intra and inter-annual features due to post-depositional processes, worsened by the steep temperature increase of the last period, the Ortles records are still able to preserve a long-term climatic signal.

Due to the different snow accumulation rates, the CdL 2003 covers ~70 years in 106 m of length, while the Ortles cores cover the same period in less than 50 m (about two third of the cores).

Paradoxically, the intensive post-depositional effects occurring at the Ortles drilling site could somehow help preserving the long-term climate signal of this glacier: as Stichler and Schotterer (2000) reported, the sheltered plateau glacier Plaine Morte, which is today formed by superimposed ice, shows the closest mean $\delta^{18}O$ (-13.3 ‰) to the expected values (compared to some higher elevation ice cores), calculated using the -0.2 ‰/100 m altitude effect (Siegenthaler and Oeschger, 1980; Schürch *et al*., 2003), starting from station collector precipitation values. Although the Plain Morte $\delta^{18}O$ ice core records are severely smoothed by meltwater percolation (no seasonal variations can be observed), the absence of erosive loss (wind scouring) might mean that the glacier may still record some major climatic trends. As in the Ortles case, the shape and magnitude of the tritium peak indicates a good preservation of the isotopic signal. Wind erosion does not affect the $\delta D/\delta^{18}O$ relation, while evaporation (sublimation), condensation and melting

alter that relation, possibly causing the loss of important information on the origin of precipitation given by deuterium excess (Stichler and Schotterer, 2000).

The exact quantification of the sensitivity of the isotope thermometer to temperature variations for the Ortles records was proven not to be feasible at the moment: taking into consideration $\delta^{18}O$ and temperature data on a seasonal scale, the obtained slope is between 0.3 (1953-1965) and 0.4 (2005-2009), but considering an inter-annual resolution (3 or 5 year), the slope is ~1. It has to be taken into account, also, that calculating the δ/T slope for different sections of the cores gives different results, implying a variable sensitivity of the isotope signal retained in the core to temperature variations; so applying a single slope to the whole record, in order to obtain a quantitative temperature reconstruction for the entire period covered by this glacial archive would be a stretch. Using several different slopes for different core sections could be feasible if a high-resolution chronology was available. Given the lack of such a detailed age-scale, beside the one obtained for shallow core 2009 (pollen dating by Festi *et al*., 2015) and the limited portion of clearly detectable annual layers around the 1963 ^{3}H peak in the Ortles deep cores, it is hard to assess the δ/T relation on a seasonal scale. Moreover, the lack of a suitable precipitation series covering a reasonably long time period does not allow to calculate the precipitation-weighted isotopic values, at least for the shallow core 2009 records, which could be more representative of temperature variations.

If we applied the 0.3-0.4 seasonal slope to the entire deep core records, we would obtain a significant overestimation of the temperature increase for the last decades, as well as other overestimated temperature variations in the older parts. If we used the inter-annual slope (~1) instead, we would find a temperature increase probably closer to reality. However, the same temperature data used to assess the isotope/temperature relations cannot be used for validation. In order to try to extend the temperature reconstruction beyond the instrumental data era, a reliable age scale covering the whole core is needed, since the one used in this study is assumed to be reliable for the last century only.

Despite several issues that have emerged from this study, the Mt Ortles ice cores are still believed to retain important climate information, which will be unveiled when a reliable age scale, extending from the surface to the core bottom, is available. The finding of a 2600-year-old larix leaf at the bottom of the glacier indicates the presence of ice from the same period, but the existence of a continuous record, extending from the Bronze Age to the presence, has still to be validated. For these reasons, some samples were recently sent to the Paul Scherrer Institute (PSI) in Bern, Switzerland, for a carbon-14 dating based on particulate and dissolved organic carbon in the ice.

Taking into account the rate at which Alpine glaciers are retreating, and the lack of Eastern Alps sites suitable for ice coring, the archives from the Ortles cores are now more important than ever,

especially considering that the Alto dell'Ortles glacier has been suffering from intense summer melting and meltwater seepage during the last decades, even at high elevation (>3800 m a.s.l.), that have already compromised the integrity of the isotopic signals contained in the upper firn portion.

REFERENCES

Alean J., Haeberli W., Schädler, B. 1983. Snow accumulation, firn temperature and solar radiation in the area of the Colle Gnifetti core drilling site (Monte Rosa, Swiss Alps): distribution patterns and interrelationships. Zeitschrift für Gletscherkunde und Glazialgeologie, 19 (2), 131–147.

Alpine Convention. 2013. Sustainable Tourism in The Alps – Report on The State of The Alps. www.alpconv.org

American Meteorological Society. 2015. State of the Climate in 2014. Special Supplement to the Bulletin of the American Meteorological Society, Vol. 96, No. 7, July 2015.

Arnason B. 1969. The exchange of hydrogen isotopes between ice and water in temperature glaciers. Earth and Planetary Science Letters. Vol. 6, Issue 6, pp 423-430.

Auer I., Boehm R., Schoener W., Hagen M. 1998. 20th century increase of boundary layer turbidity derived from Alpine sunshine and cloudiness series. Preprints of the 8th Conference on Mountain Meteorology, Aug. 98 in Flagstaff, Arizona. AMS, Boston, pp.77-80.

Auer I., Böhm R., Jurković A., Orlik A., Potzmann R., Schöner W., Ungersböck M., Brunetti M., Nanni T., Maugeri M., Briffa K., Jones P., Efthymiadis D., Mestre O., Moisselin J-M., Begert M., Brazdil R., Bochnicek O., Cegnar T., Gajić-Čapka M., Zaninović K., Majstorović Z., Szalai S., Szentimrey T., Luca Mercalli L. 2005. A new instrumental precipitation dataset for the greater Alpine region for the period 1800–2002. Int. J. Climatol., 25, 139–166.

Auer I., Böhm R., Jurkovic A., Lipa W., Orlik A., Potzmann R., Schöner W., Ungersböck M., Matulla C., Briffa K., Jones P.D., Efthymiadis D., Brunetti M., Nanni T., Maugeri M., Mercalli L., Mestre O., Moisselin J-M., Begert M., Müller-Westermeier G., Kveton V., Bochnicek O., Stastny P., Lapin M., Szalai S., Szentimrey T., Cegnar T., Dolinar M., Gajic-Capka M., Zaninovic K., Majstorovic Z., Nieplova E. 2007. HISTALP – Historical instrumental climatological surface time series of the greater Alpine region 1760-2003. International Journal of Climatology 27: 17-46.

Barry R.G., Williams M., Racoviteanu A.E. 2008. Optical remote sensing of glacier characteristics: a review with focus on the Himalaya. Sensors, Vol. 8, pp 3355-3383.

Beck N., Wagenbach D., Münnich K. 1988. Laboratory experiments on the format of solar radiation induced melt layers in dry snow. Zeitschrift für Gletscherkunde und Glazialgeologie, 24 (1), 31–40.

Bell G. and Chelliah M. 2005. Leading Tropical Modes Associated with Interannual and Multidecadal Fluctuations in North Atlantic Hurricane Activity. Journal of Climate, Vol. 19, pp 590-612.

Bigleisen J. 1961. Statistical mechanics of isotope effects on the thermo-dynamic properties of condensed systems. J. Chem. Phys., 34, 1485–1493, doi:10.1063/1.1701033.

Böhm R., Auer I., Brunetti M., Maugeri M., Nanni T., Schöner W. 2001. Regional temperature variability in the European Alps: 1760-1998 from homogenized instrumental time series. Int. J. Climatol. 21: 1779–1801.

Bortolami G.C., Ricci B., Susella G.F., Zuppi GM. 1978. Isotope hydrology of Val Corsaglia, Maritime Alps, Piedmont, Italy. Isotope Hydrology 1976, Vol. 1, IAEA, Vienna, pp 327-350.

Buason T. 1972. Equation of isotope fractionation between ice and water in a melting snow column with continuous rain and percolation. Journal of Glaciology 11(63): 387–400.

Buchan I.E. 2015. StatsDirect statistical tools. http://www.statsdirect.com

Carturan L., Baroni C., Becker M., Bellin A., Cainelli O., Carton A., Casarotto C., Dalla Fontana G., Godio A., Martinelli T., Salvator, M. C., Seppi R. 2013. Decay of a long-term monitored glacier: Careser Glacier (Ortles-Cevedale, European Alps). The Cryosphere, 7, 1819-1838, doi: 10.5194/tc-7-1819-2013.

Carturan L., Dalla Fontana G., Borga M. 2012. Estimation of winter precipitation in a high-altitude catchment of the Eastern Italian Alps: validation by means of glacier mass balance observations, Geogr. Fis. Din. Quat., 35, 37–48, 2012.

Chaplin M. 2015. Water Structure and Science. http://www1.lsbu.ac.uk/water/water_vibrational_spectrum.html

Citterio M., Turri S., Bini A., Maggi V., Pelfini M., Pini R., Ravazzi C., Santilli M., Stenni B., Udisti R. 2005. Multidisciplinary approach to the study of the Lo Lc 1650 “Abisso sul Margine dell’Alto Bregai” ice cave (Lecco, Italy). Theoretical and Applied Karstology, vol. 17, pp 27-44.

Clark I.D. and Fritz P. 1997. Environmental Isotopes in Hydrogeology. CRC Press.

Colucci R.R., Fontana D., Forte E. 2014. Characterization Of Two Permanent Ice Cave Deposits In The Southeastern Alps (Italy) By Means Of Ground Penetrating Radar (Gpr). International Workshop on Ice Caves VI.

Comitato Geografico Nazionale. 1926. Nomi e limiti delle grandi parti del Sistema Alpino. IX Congresso Geografico Italiano.

Commission of the European Communities. 2009. White Paper Adapting to climate change: Towards a European framework for action. Brussels, COM(2009) 147/4.

Coplen T.B., Herczeg A.L., Barnes C. 2000. Isotope engineering: using stable isotopes of the water molecule to solve practical problems, in Environmental Tracers in Subsurface Hydrology. P.G. Cook and Herczeg A.L., Kluwer Academic Publishers, Boston.

Craig H. 1961. Isotopic variations in meteoric waters, Science, 133, 1702–1703, doi:10.1126/science.133.3465.1702.

Craig H. 1966. Isotopic composition and origin of the Red Sea and Salton Sea geothermal brines. Science, 154, pp 1544-1548.

Craig, H. and Gordon L.I. 1965. Deuterium and oxygen 18 variations in the ocean and marine atmosphere. In proc. Stable Isotopes in Oceanographic Studies and Paleotemperatures, Spoleto, Italy. Edited by E. Tongiogi, pp 9-130, V. Lishi e F., Pisa.

Cuffey K.M. and Paterson W.S.B. 2010. The Physics of Glaciers, Fourth Edition. Butterworth-Heinemann, Elsevier.

Dansgaard W. 1953. The abundance of 18O in atmospheric water and water vapour. Tellus, 5, 461–469, 1953.

Dansgaard W. 1964. Stable isotopes in precipitation. Tellus, 16(4), 436–468, doi:10.1111/j.2153-3490.1964.tb00181.x

Dansgaard W., Johnsen S.J., Moller J., Langway C.C.J. 1969. One thousand centuries of climatic record from Camp Century on the Greenland ice sheet, Science, 166, 377–381.

De Angelis M. and Gaudichet A. 1991. Saharan dust deposition over Mont Blanc (French Alps) during the last 30 years. Tellus, 43B, pp 61-75.

Dinçer T., Payne B.R., Florkowski T., Martinec J., Tongiorgi E. 1970. Snowmelt runoff from measurements of tritium and oxygen-18. Water Resources Research, 6, pp 110–124.

Dole M. 1935. The relative atomic weight of oxygen in water and air. J. Am. Chcm. Sot. 57: 2731.

Ebner P.P., Steen-Larsen H.C., Stenni B., Schneebeli M., Steinfeld A. Unpublished. Experimental observation of transient $\delta^{18}O$ interaction between snow and advective airflow.

Eichler R. 1965. Deuterium- Isotopengeochemie des Grund- und Oberflaechenwassers, Geol.Rundschau, vol. 55, pp 144-155.

Eichler, A., Schwikowski M., Gäggeler H.W., Furrer V., Synal H.-A., Beer J., Saurer M., Funk M. 2000. Glaciochemical dating of an ice core from upper Grenzgletscher (4200 m a.s.l.), J. Glaciol., 46, 507–515, doi: 10.3189/172756500781833098.

Eichler A., Schwikowski M., Furger M., Schotterer U., Gäggeler H.W. 2004. Sources and distribution of trace species in Alpine precipitation inferred from two 60-year ice core paleorecords, Atmos. Chem. Phys. Discuss., 4, 71–108, doi: 10.5194/acpd-4-71-2004.

EnvironmentalChemistry.com. 2007. Oxygen Nuclides/Isotopes.

Epstein S. and Mayeda T. 1953. Variation of O18 content of waters from natural sources. Geochemica et Cosmochemica Acta, Voll. 4, pp 213.

Escher-Vetter H., Braun L.N, Siebers M. 2014. Hydrological and meteorological records from the Vernagtferner Basin - Vernagtbach station, for the years 2002 to 2012. doi:10.1594/PANGAEA.829530

European Environment Agency (EEA). Report 2009. Regional climate change and adaptation. The Alps facing the challenge of changing water resources. No 8/2009.

Feng X., Taylor S., Renshaw C.E., Kirchner J.W. 2002. Isotopic evolution of snowmelt: 1. A physically based one-dimensional model. Water Resources Research 38(10): 1217.

Festi D., Kofler W., Bucher E., Carturan L., Mair V., Gabrielli P., Oeggl K. 2015. A novel pollen-based method to detect seasonality in ice cores: a case study from Ortles glacier, South Tyrol, Italy. Journal of Glaciology, Vol. 61, No. 228, 2015 doi: 10.3189/2015JoG14J236.

Fisher D.A. 1991. Remarks on the deuterium excess in precipitation in cold regions. Tellus, 43B, 401-407.

Fischer D.A. 1991. Remarks on the deuterium excess in precipitation in cold regions. Tellus, Vol. 43, pp 401-407.

Fisher D.A., Koerner R.M., Paterson W.S.B., Dansgaard W., Gundestrup N., Reeh N. 1983. Effect of wind scouring on climatic records from ice-core oxygen-isotope profiles, Nature, 301, 205–209.

Fontes J.-Ch. and Olivry J.C. 1977. Composition isotopique des precipitations de la region du Mont Cameroun. ONAREST, Inst. de Recherches sur les Techniques, l'Industrie et le Soussol, 28.

Frei C. and Schär C. 1998. A precipitation climatology of the Alps from high-resolution rain-gauge observations. Int. J. Climatol., 18, 873-900.

Froehlich K. 1996. Deuterium excess and its variation in precipitation. Glaciers from the Alps. Climate and Environmental Archives. Proc. Workshop 21-23 October 1996, Wengen Switzerland. Paul Scherrer Institut, Villingen, Switzerland. pp. 45-47.

Froehlich K., Kralik M., Papesch W., Rank D., Scheifinger H., Stichler W. 2008. Deuterium excess in precipitation of Alpine regions - moisture recycling. Isotopes Environ Health Stud. 2008 Mar; 44(1):61-70. doi: 10.1080/10256010801887208.

Fujita S., Holmlund P., Andersson I., Brown I., Enomoto H., Fujii Y., Fujita K., Fukui K., Furukawa T., Hansson M., Hara K., Hoshina Y., Igarashi M., Iizuka Y., Imura S., Ingvander S., Karlin T., Motoyama H., Nakazawa F., Oerter H., Sjoberg L.E., Sugiyama S., Surdyk S., Strom J., Uemura R., Wilhelms F. 2011. Spatial and temporal variability of snow accumulation rate on the East Antarctic ice divide between Dome Fuji and EPICA DML. The Cryosphere, 5, 1057–1081, doi: 10.5194/tc-5-1057-2011, 2011

Funk M. 1994. Possible alpine ice-core drilling sites: an overview. In Haeberli, W. and Stauffer B., eds. Proceedings of the ESF/EPC Workshop on Greenhouse Gases, Isotopes and Trace Elements in Glaciers as Climate Evidence for Holocene. Zürich, VAW Arbeitsheft, 40–44.

Gabrielli P., Carturan L., Gabrieli J., Dinale R., Krainer K., Helmut H., Davis M., Zagarodnov V., Seppi R., Barbante C., Dalla Fontana G., Thompson L.G. 2010. Atmospheric warming threatens the untapped glacial archive of Mt Ortles, South Tyrol, J. Glaciol., Vol. 56, pp 843–853.

Gabrielli P., Barbante C., Carturan L., Cozzi G., Dalla Fontana G., Dinale R., Dragà G., Gabrieli J., Kehrwald N., Mair V., Mikhalenko V., Piffer G., Rinaldi M., Seppi R., Spolaor A., Thompson L.G., Tonidandel D. 2012. Discovery of cold ice in a new drilling site in the Eastern European Alps. Geogr. Fis. Dinam. Quat. Vol. 35, pp 101-105.

Gat J.R. 1996. Oxygen and hydrogen isotopes in the hydrological cycle. Annual Review of Earth and Planetary Sciences, Vol. 24, pp 225-262. DOI: 10.1146/annurev.earth.24.1.225.

Gat J.R. 2001. Atmospheric water. In Environmental isotopes in the hydrological cycle Principles and applications, Volume II. IHP-V I Technical Documents in Hydrology I No. 39, Vol. II, UNESCO, Paris.

Gat J.R. 2005. Some Classical Concepts of Isotopes Hydrology: Rayleigh fractionation, Meteoric Water Lines, the Dansgaard effects (altitude, latitude, distance from coast and amount effects) and the d excess parameter" Their inception, the role they played in the evolution of the discipline and

how they have stood the test of time. From “Isotopes in the Water Cycle. Past, Present and Future of a Developing Science”, Springer.

Gilbert A. and Vincent C. 2013. Atmospheric temperature changes over the 20th century at very high elevations in the European Alps from englacial temperatures. Gephysical Research Letters, Vol. 40, pp 2102–2108, doi:10.1002/grl.50401.

Giorgi F. and Coppola E. 2007. European climate-change oscillation (ECO). Geophysical Research Letters, Vol. 34 L21703, doi: 10.1029/2007GL031223.

Gobiet A., Kotlarski S., Beniston M., Heinrich G., Rajczak J., Stoffel M. 2014. 21st century climate change in the European Alps - a review. Sci Total Environ 2014.

Gonfiantini R., Roche M-A., Olivry J-C., Fontes J-C., Zuppi G.M. 2001. The altitude effect on the isotopic composition of tropical rains. Chemical Geology, Vol. 181, pp 147–167.

Haeberli, W. and Beniston M., 1998. Climate change and its impacts on glaciers and permafrost in the Alps. Ambio 27: 258–265.

Haeberli W., Noetzli J., Zemp M., Baumann S., Frauenfelder R., Hoelzle M. 2005a. Glacier mass balance bulletin, Bull. 8 (2002 – 2003), 100 pp., World Glacier Monit. Serv., Zurich, Switzerland.

Haeberli W., Zemp M., Frauenfelder R., Hoelzle M., Kääb A. 2005b. Fluctuations of glaciers 1995 - 2000, Volume VIII, report, 288 pp., World Glacier Monit. Serv., Zurich, Switzerland.

Haylock M.R., Hofstra N., Klein Tank A.M.G., Klok E.J., Jones P.D., New M. 2008. A European daily high-resolution gridded data set of surface temperature and precipitation for 1950–2006. Journal of Geophysical Research, Vol. 113, D20119, doi: 10.1029/2008JD010201.

Hindelang M. The Science of Winter Ecology. Michigan, USA: Winter Ecology Institute, Michigan Technological University. [Cited on 13 March 2004]. Available from World Wide Web: (http://www.ed.mtu.edu/esmis/winter/ecology.html)

Hoefs J. 1997. Stable Isotope Geochemistry, 4th ed., Springer-Verlag, Berlin.

Hoefs J., 2009. Stable Isotope Geochemistry 6th Edition. Springer.

Hoffmann G., Cuntz M., Jouzel J., Werner, M., 2005. How much climate information do water isotopes contain? A systematic comparison between the IAEA/GNIP Isotope Network and the ECHAM4 Atmospheric General Circulation Model. In: Isotopes in the Water Cycle. Springer Verlag, Niederlande. doi: 10.1007/14020-3023-1.

Horita J. 1988. Hydrogen isotope analysis of natural waters using an H2-water equilibrium method: A special implication to brines. Chem. Geol. (Isotope Geosc. Sec.), Vol. 72, pp 89-94.

Horita J. 2005. Stable isotope thermometry: There is more to it than temperature. Geochemical Journal, Vol. 39, pp 481-496.

Horita J. and Wesolowski D.J. 1994. Liquid-vapour fractionation of oxygen and hydrogen isotopes of water from the freezing to the critical temperature, Geochim. Cosmochim. Ac., 58, 3425–3437, doi:10.1016/0016-7037(94)90096-5.

Hughes P.D. 2011. Mediterranean Glaciers and Glaciation. In Encyclopedia of Snow, Ice and Glaciers, edited by Singh V.P., Singh P., Haritashya U.K. Springer.

Hurrell J.W. 1995. Decadal Trends in the North Atlantic Oscillation: Regional Temperatures and Precipitation. Science: Vol. 269, pp.676-679.

IAEA. http://www-naweb.iaea.org/napc/ih/documents/userupdate/description/Precip6.html

Intergovernmental Panel on Climate Change (IPCC). 2007. Fourth Assessment Report (AR4).

Intergovernmental Panel on Climate Change (IPCC). 2014. Fifth Assessment Report (AR5).

Jenk, T.M. 2006. Ice Core Based Reconstruction of Past Climate Conditions and Air Pollution in the Alps Using Radiocarbon, PhD thesis, Departement für Chemie und Biochemie, Univ. of Bern, Bern, Switzerland.

Jenk T.M., Szidat S., Schwikowski M., Gäggeler H.W., Brütsch S., Wacker L., Synal H.-A., Saurer M. 2006. Radiocarbon analysis in an Alpine ice core: record of anthropogenic and biogenic contributions to carbonaceous aerosols in the past (1650–1940). Atmos. Chem. Phys., Vol. 6(12), pp 5381–5390.

Jenk T.M., Szidat S., Bolius D., Sigl M., Gaggeler H.W., Wacker L., Ruff M., Barbante C., Boutron C.F., Schwikowski M. 2009. A novel radiocarbon dating technique applied to an ice core from the Alps indicates late Pleistocene ages. J. Geophys. Res., 114, D14305, doi: 10.1029/2009JD011860.

Johnsen S.J. 1977. Stable isotope homogenization of polar firn and ice, in Isotopes and Impurities in Snow and Ice, Proceeding of the Grenoble Symp.

Johnsen S.J., Dansgaard W., Clausen H.B., Langway C.C. 1972. Oxygen isotope profiles through the Antarctic and Greenland ice sheets. Nature, 235, 429–434, 1972.

Johnsen S.J., Clausen H.B., Cuffey K.M., Hoffman G., Schwander J., Creyts T. 2000. Diffusion of stable isotopes in polar firn and ice: The isotope effect in firn diffusion, in Physics of Ice Core Records, edited by T. Hondoh, 121–140, Hokkai-do Univ. Press, Sapporo, Japan.

Jouzel J. 2013. A brief history of ice core science over the last 50 yr. Clim. Past, Vol. 9, pp 2525–2547.

Jouzel, J., Merlivat, L. and Pourchet, M. 1977. Deuterium, tritium, and β activity in a snow core taken on the summit of Mont Blanc (French Alps): determination of the accumulation rate. J. Glaciol. 18 (80), 465-470.

Jouzel J., Legrand M.R., Pinglot J. F., Pourchet M., Reynaud L. 1984. Chronologie d'un carottage de 20 m au Col du Dome (Massif du Mont-Blanc). Houille Blanche 1984, 491–497.

Jouzel J. and Merlivat L. 1984. Deuterium and oxygen 18 in precipitation: modeling of the isotope effects during snow formation, J. Geophys. Res., 89, 11749–11757, 1984. 4754, 4759.

Jouzel J., Masson-Delmotte V., Cattani O., Dreyfus G., Falourd S., Hoffmann G., Minster B., Nouet J., Barnola J.M., Chappellaz J., Fisher H., Gallet J.C., Johnsen S., Leuenberger M., Loulergue L., Luethi D., Oerter H., Parrenin F., Raisbeck G., Raynaud D., Schilt A., Schwander J., Selmo E., Souchez R., Spahni R., Stauffer B., Steffensen J.P., Stenni B., Stocker T.F., Tison J.L., Werner M. & Wolff E.W., 2007. Orbital and millennial Antarctic climate variability over the past 800,000 years. Science, 317, 793-796. Doi: 10.1126/science.1141038. Published on line 5 July 2007.

Kendall C. and Coplen T.B. 2001. Distribution of oxygen-18 and deuterium in river waters across the United States. Hydrological Processes Special Issue: Water Quality of Large US Rivers: Results from the US Geological Survey's National Stream Quality Accounting Network, Vol. 15, Issue 7, pp 1363–1393.

Koerner R.M. 1997. Some comments on climatic reconstructions from ice cores drilled in areas of high melt. Journal of Glaciology, Vol. 43 (143), pp 90-97.

Langway C.C. 2008. The history of early polar ice cores, Cold Reg. Sci. Technol., 52, 101–117, 2008.

Loewe F. 1970. Screen temperatures and 10 m temperatures. J. Glaciol., 9 (56), 263-268.

Longinelli A. and Selmo E. 2003. Isotopic composition of precipitation in Italy: a first overall map. Journal of Hydrology, 270, pp 75–88.

Luterbacher J., Dietrich D., Xoplaki E., Grosjean M., Wanner H. 2004. European seasonal and annual temperature variability, trends, and extremes since 1500, Science, 303, 1499.

Lüthi M. and Funk M. 2001. Modelling heat flow in a cold, high-altitude glacier: Interpretation of measurements from Colle Gnifetti, Swiss Alps. J. Glaciol., 47, 314 – 324.

Marazzi S. 2006. (IT) Suddivisione Orografica Internazionale Unificata del Sistema Alpino (SOIUSA); (DE) Internationale vereinheitlichte orographische Einteilung der Alpen (IVOEA); (FR) Subdivision Orographique Internationale Unifiée du Système Alpin (SOIUSA); (SL) Enotna Mednarodna Orografska Razdelitev Alp (EMORA).

Mariani I. 2013. Water stable isotopes in Alpine ice cores as proxies for temperature and atmospheric circulation. PhD Thesis. University of Bern, Switzerland.

Mariani I., Eichler A., Jenk T.M., S. Brönnimann S., Auchmann R., Leuenberger M.C., Schwikowski M. 2014. Temperature and precipitation signal in two Alpine ice cores over the period 1961–2001. Clim. Past, Vol. 10, pp 1093–1108.

Martinec J., Moser H., de Quervain M.R., Rauert W., Stichler W. 1977. Assessment of processes in the snowpack by parallel deuterium, tritium and oxygen-18 sampling. In: Proc. Symposium Isotopes and Impurities in Snow and Ice, Grenoble 1975. IAHS Publ. No.1 18: 220- 231.

Matulla C., Schöner W., Alexandersson H., von Storch H., Wang X.L. 2007. European storminess: late nineteenth century to present. Climate Dynamics, DOI 10.1007/s00382-007-0333-y.

Meyer B.S. (September 19- 21, 2005). Nucleosynthesis and Galactic Chemical Evolution of the Isotopes of Oxygen (PDF). Workgroup on Oxygen in the Earliest Solar System. Proceedings of the NASA Cosmochemistry Program and the Lunar and Planetary Institute (Gatlinburg, Tennessee). 9022. Retrieved January 22, 2007.

MeteoSwiss - Federal Office of Meteorology and Climatology.

Molion, L. 1987. Micrometereology of an Amazonian rain forest. In Dickinson R. (ed.), The Geophysiology of Amazonia. Wiley. New York.

Moser H. and Stichler W. 1974. Deuterium and oxygen-18 contents as an index of the properties of snow covers. Snow Mechanics (Proceedings of the Grindelwald Symposium, Switzerland, April 1974), IAHS Publ., 114, pp 122–135, 1974.

Nakawo M, Chiba S, Satake H, Kinouchi S. 1993. Isotopic fractionation during grain coarsening of wet snow. Annals of Glaciology 18: 129–134.

Nakazawa F., Fujita K.; Takeuchi N., Fujiki T., Uetake J., Aizen V., Nakawo M. 2005. Dating of seasonal snow/firn accumulation layers using pollen analysis. Journal of Glaciology, Vol. 51, N. 174, pp 483-490.

Nakazawa F., Miyake T., Fujita K.,Takeuchi N., Uetake J., Fujiki T., Aizen V., Nakawo M. 2011. Establishing the timing of chemical deposition events on Belukha Glacier, Altai Mountains, Russia, using pollen analysis. Arct. Antarct. Alp. Res., 43(1), 66–72. doi: 10.1657/1938-4246-43.1.66.

National Accademy of Sciences and The Royal Society. 2014. Climate Change: Evidence & Causes.

National Institute of Standard & Technology (NIST). 2005. Report of Investigation (in cooperation with the International Atomic Energy Agency).

National Snow & Ice Data Center. 2015. https://nsidc.org/cryosphere/seaice/processes/albedo.html

Niels Bohr Institute. http://www.iceandclimate.nbi.ku.dk

Nier A.O. 1937. A Mass-Spectrographic Study of the Isotopes of Hg, Xe, Kr, Be, I, As, and Cs. Phys. Rev. 52, 933.

Oerter H. 1977. Wasserbewegung in einem Gletscher, dargestellt an den Feldarbeiten auf dem Vernagtferner. In: Vortragsveranstaltung 9. Febr. 1977 (Sonderforschungsbereich 81, Techn. Univers. Müchen, Ed.), München: 67-92.

Oerter H., Neuherberg O., Rufli H. 1982. Core drilling through a temperate alpine glacier (Vernagtferner, Oetzal Alps) in 1979. Zeitschrift fur Gletscherkunde und Glazialgeologie. Band 18 (1982), Heft 1, Seite 1-11.

Oerter H., Baker D., Stichler W., Rauert W. 1985. Isotope studies of ice cores from a temperate Alpine glacier (Vernagtferner, Austria) with respect to the meltwater flow. Annals of Glaciology Vol. 7, pp 90-93.

Oeschger H., Schotterer U., Stauffer B., Haeberli W., Roethlisberger H. 1977. First results from Alpine core drilling projects. Z. Gletscherkd. Glazialgeol. 13, 193-208.

Orombelli G. 2004. Il ghiaccio nelle Alpi. Istituto Nazionale della Montagna. Bononia University Press.

Palmer A.S., Schwikowski M., Gaeggeler H.W. 2003. A Sub-Seasonal Trace Chemical Ice Core Record from Piz Zupo, Swiss Alps. EGS - AGU - EUG Joint Assembly, Abstracts from the meeting held in Nice, France, 6 - 11 April 2003, abstract #1331.

Paterson W.S.B. 1994. The Physics of Glaciers. 3rd ed. Pergamon, Terrytown, N.Y.

Payne B.R. and Yurtsever Y. 1974. Environmental isotopes as a hydrological tool in Nicaragua: Isotope Techniques in Groundwater Hydrology. International Atomic Energy Agency Symposium, Vienna, Austria, 193 pp.

Pecci M., Rinaldini A., Smiraglia C., D'Agata C., Diolaiuti G., Maggi V., Marinoni A., De Amicis M., Filippazzi M., Polesello S., Valsecchi S. 2005. Glacialism and the cryosphere in the Mediterranean area: indicators of the effects of industrial activities on living environments.

Persson A., Langen P.L., Ditlevsen P., Vinther B.M. 2011. The influence of precipitation weighting on interannual variability of stable water isotopes in Greenland, J. Geophys. Res., 116 (D20), D20120, doi:10.1029/2010JD015517.

Pierre C., Vergnaud Grazzini C., Thouron D., Saliège J.-F. 1986. Compositions isotopiques de l'oxygène et du carbone des masses d'eau en Méditerranée: Memorie della Societa Geologica Italiana, Vol. 36, pp 165–174.

Pfahl S. and Sodemann H. 2014. What controls deuterium excess in global precipitation? Clim. Past Discuss., 9, 4745–4770.

Pohjola V.A., Moore J.C., Isaksson E., Jauhiainen T., van de Wal R.S.W., Martma T., Meijer A.J. and Vaikmäe R. 2002. Effect of periodic melting on geochemical and isotopic signals in an ice core from Lomonosovfonna, Svalbard. Journal of Geophysical Research, Vol. 167, NO. D4, 4036.

Preunkert S., Wagenbach D., Legrand M., Vincent C. 2000. Col du Dome (Mt Blanc Massif, French Alps) suitability for ice-core studies in relation with past atmospheric chemistry over Europe. Tellus (2000), 52B, 993–1012

Rank D. and Papesch.W. 2005. Isotopic composition of precipitation in Austria in relation to air circulation patterns and climate. From "Isotopic composition of precipitation in the Mediterranean Basin in relation to air circulation patterns and climate", IAEA-TECDOC-1453.

Ronseaux F. and Delmas R.J. 1988. Chemical Composition of Bulk Atmospheric Deposition to Snow at Col De La Brenva (Mt Blanc Area). Vol. 252 of the series NATO ASI Series pp 491-510.

Rozanski K., Araguás-Araguás L., Gonfiantini R. 1993. Isotopic patters in modern global precipitation, in Climate Change in Continental Isotopic Records. Geophys. Monogr. Ser., 78, ed. by P.K. Swart, et al, pp. 1-36, AGU, Washington, DC, 1993.

Rufli H., Stauffer B., Oeschger H. 1976. Lightweight 50-meter core drill for firn and ice. Reproduced from Ice-Core Drilling edited by John F. Splettstoesser by permission of the University of Nebraska Press. Copyright 1976 by the University of Nebraska Press. Copyright renewed 2004 by the University of Nebraska Press.

SAHRA. 2005. http://web.sahra.arizona.edu

Scripps Center for Metabolomics and Mass Spectrometry. https://masspec.scripps.edu

Sharp Z. 2007. Principles of Stable Isotope Geochemistry. Pearson Prentice Hall.

S. Terzer L.I., Wassenaar L., Araguás-Araguás J., Aggarwal P. K. 2013. Global isoscapes for $\delta^{18}O$ and $\delta^{2}H$ in precipitation: improved prediction using regionalized climatic regression models. Hydrol. Earth Syst. Sci., 17, 1–16.

Schotterer U., Haeberli W., Good W., Oeschger H., Rothlisberger H. 1978. Datierung von kaltem Firn und Eis in einem Bohrkern vom Colle Gnifetti, Monte Rosa. In: Jb. Schweiz. Naturf. Ges., wiss. Teil: 48- 57. Verlag Birkhauser, Basel.

Schotterer U., Oeschger H., Wagenbach D., Munnich K. 1985. Information on paleo-precipitation on a high-altitude glacier Monte Rosa, Switzerland, Z. Gletscherkd. Glazialgeol., 21(85), 379 – 388.

Schotterer U., Fröhlich K., Gäggeler H.W., Sandjordj S., Stichler W. 1997. Isotope records from Mongolian and Alpine ice cores as climate indicators. Clim. Change, Vol. 36(3-4), pp 519–530, doi: 10.1023/A:1005338427567.

Schotterer U., Stichler W., Graf W., Burki H.-U., Gourcy L., Ginot P., Huber T. 2002. Stable isotopes in Alpine ice cores: do they record climate variability? IAEA-CN-80/83.

Schürch M., Kozel R., Schotterer U., Tripet J.P. 2003. Observation of isotopes in the water cycle – the Swiss National Network (NISOT), Environ. Geol., 45, 1–11.

Schwikowski M. 2006. Paleoenvironmental reconstruction from Alpine ice cores. PAGES Past Global Changes. http://www.pages-igbp.org/

Schwikowski M., Brutsch S., Gaggeler H.W., Schotterer U. 1999. A high-resolution air chemistry record from an Alpine ice core: Fiescherhorn glacier, Swiss Alps. Journal of Geophysical Research, Vol. 104, NO. D11, pp 13,709-13,719.

Schwikowski M., Eichler A., Jenk T.M., Mariani I. 2014. Annualy resolved climate signal in high-alpine ice cores. Pages Magazine, Vol. 22, No. 1.

Serot O., Wagemans C., Heyse J. 2005. New Results on Helium and Tritium Gas Production from Ternary Fission. International conference on nuclear data for science and technology. AIP Conference Proceedings 769: 857–860. doi:10.1063/1.1945141.

Siegenthaler U. and Oeschger H. 1980. Correlation of ^{18}O in precpitation with temperature and altitude. Nature, 285, pp 314-317.

Sigl M. 2009. Ice core based reconstruction of past climate conditions from Colle Gnifetti, Swiss Alps. PhD Thesis. University of Bern, Switzerland.

Sodemann H., Schwierz C., Wernli H. 2008. Inter-annual variability of Greenland winter precipitation sources: Lagrangian moisture diagnostic and North Atlantic Oscillation influence. Journal of Geophysical Research 113(D03): D03107, doi: 10.1029/2007JD008503.

Sodemann H. and Zubler E. 2010. Seasonal and inter-annual variability of the moisture sources for Alpine precipitation during 1995-2002. International Journal of Climatology. 30: 947-961.

Stahl W., Aust H., Dounas A. 1974. Isotope Techniques in Groundwater Hydrology. IAEA, Vienna. Vol. 1, pp 317-339.

Steen-Larsen H.C., Masson-Delmotte V., Hirabayashi M, Winkler R., Satow K., Prié F., Bayou N., Brun E.,. Cuffey K. M, Dahl-Jensen D., Dumont M., Guillevic M., Kipfstuhl S., Landais A., Popp T., Risi C., Steffen K., Stenni B., Sveinbjörnsdottir A.E. 2014. What controls the isotopic composition of Greenland surface snow? Climate of the Past, Vol. 10, pp 377–392.

Stichler W. 1987. Snowcover and snowmelt process studies by means of environmental isotopes. In: H.G. Jones and W.J. Orville-Thomas (Eds.), Seasonal Snowcovers: Physics, Chemistry, Hydrology D. Reidel Publishers, pp 673-726.

Stichler W, Rauert W, Martinec J. 1981. Environmental isotope studies of Alpine snowpack. Nordic Hydrology 12: 297–308.

Stichler W., Baker D., Oerter H., Trimborn N. 1982. Core Drilling on Vernagtferner (Oetzal Alps, Austria) in 1979: deuterium excess and oxygen-18 contents. Zeitschrift fur Gletscherkunde und Glazialgeologie. Band 18 (1982), Heft 1, Seite 23-35.

Stichler W. and Schotterer U. 2000. From accumulation to discharge: modification of stable isotopes during glacial and post-glacial processes. Hydrol. Process., Vol. 14, pp 1423-1438.

Stichler W., Schötterer U., Frohlich K., Ginot P., Kull C., Gäggeler H., Pouyaud B. 2001. Influence of sublimation on stable isotope records recovered from high-altitude glaciers in the tropical Andes. Journal of Geophysical Research, Vol. 106, pp 22,613-22,620.

Suter S., Hoelzle M., Ohmura A. 2004. Energy balance at a cold Alpine firn saddle, Seserjoch, Monte Rosa. International Journal of Climatology, 24, 1423–1442

Suzuki K. 1993. Oxygen-18 of snow meltwater and snow cover. Seppyo, 55(4): 335–342 (in Japanese with English summary).

Swiss Federal Institute of Technology Zurich. Glaciological activities at Jungfraujoch.

Tarussov A., 1992. The arctic from Svalbard to Severnaya Zemyla: Climatic reconstructions from ice cores. Climate Since A.D. 1500, edited by Bradley R.S. and Jones P.D., Routledge, New York, 1992.

Trueba G.J.J, Moreno M.R., de Pisón M.E., Serrano E. 2008. 'Little Ice Age' glaciation and current glaciers in the Iberian Peninsula. The Holocene 18: 551-568.

Uetake J., Kohshima S., Nakazawa F., Suzuki K., Kohno M., Kameda T. 2006. Arkhipov, S.; Fujii, Y. others. 2006. Biological ice-core analysis of Sofiyskiy glacier in the Russian Altai. Ann. Glaciol., 43, 70–78, doi: 10.3189/172756406781811925.

United Nations Environment Programme (UNEP). 2010. UNEP 2009 Annual Report.

Van de Velde K., Boutron C., Ferrari C., Bellomi T., Barbante C., Rudnev S., Bolshov M. 1998. Seasonal variations of heavy metals in the 1960s Alpine ice: sources versus meteorological factors, Earth Planet. Sci. Lett., 164, 521–533.

van Trigt R. 2002. Laser Spectrometry for Stable Isotope Analysis of Water Biomedical and Paleoclimatological Applications. PhD Thesis. University of Groningen. Netherlands.

Vincent C., Vallon M., Pinglot J.F., Funk M., Reynaud L. 1997. Snow accumulation and ice flow at Dome du Gouter (4300 m), Mont Blanc, French Alps. J. Glaciol., 43, 513 – 521.

Vincent C., Le Meur E., Six D. 2005. Solving the paradox of the end of the Little Ice Age in the Alps. Geophysical Research Letters, Vol. 32, L09706, doi: 10.1029/2005GL022552.

Vogel J.C., Lerman J.C., Mook W.G. 1975. Natural isotopes in surface and groundwater from Argentina. Hydrological Science Bulletin, 20, pp 203-221.

Von Gunten H.R., Elfriede Rossler W., Gaggeler H. 1982. Dating of ice cores from Vernagtferner (Austria) with fission products and lead-210. Zeitschrift fur Gletscherkunde und Glazialgeologie. Zeitschrift fur Gletscherkunde und Glazialgeologie. Band 18 (1982), Heft 1, Seite 37-45.

Wagenbach D. 2003. Alpine ice cores as climate proxies. Wien, ALP-IMP Kick-off 5.5.03.

Wagenbach D., Bohleber P., Preunkert S. 2012. Cold, alpine ice bodies revisited: what may we learn from their impurity and isotopic content? Geografiska Annaler: Series A, Physical Geography © 2012 Swedish Society for Anthropology and Geography DOI:10.1111/j.1468-0459.2012.00461.x

Wang Q., Fan X., Wang M. 2014. Recent warming amplification over high elevation regions across the globe. Clim. Dyn., Vol. 43, pp 87-101.

WeatherOnline. 2015. http://www.weatheronline.co.uk

Werner M., Langebroek P. M., Carlsen T., Herold M., Lohmann G. 2011. Stable water isotopes in the ECHAM5 general circulation model: Toward high-resolution isotope modeling on a global scale, J. Geophys. Res., 116, D15109, doi: 10.1029/2011JD015681.

Yoshimura Y., Kohshima S., Takeuchi N., Seko K., Fujita K. 2000. Himalayan ice-core dating with snow algae. J. Glaciol. 46(153), 335–340 (doi: 10.3189/172756500781832918)

Young P.G. and Foster D.G. 1972. An Evaluation of the Neutron and Gamma-ray Production Cross Sections for Nitrogen. Los Alamos Scientific Laboratory.

Yu.B. Gurov D.V., Aleshkin M.N., Behr S.V., Lapushkin P.V., Morokhov V.A., Pechkurov N.O., Poroshin,V.G., Sandukovsky M.V., Telkushev B.A., Chernyshev T.D.Shchurenkova. 2004. Spectroscopy of superheavy hydrogen isotopes in stopped-pion absorption by nuclei. Phys.Atom.Nucl., Vol. 68, pp 491-497.

Zagorodnov V., Thompson L. G. and Mosley-Thompson E. 2000. Portable system for intermediate-depth ice-core drilling. J. Glaciol., 152, 167-172.

Zemp M., Haeberli W., Hoelzle M. Paul F. 2006. Alpine glaciers to disappear within decades? The Cryosphere, Vol. 33, issue 13.

Zemp M., Frey H., Gärtner-Roer I.,1 Nussbaumer S.U., Hoelze M., Paul F., Haeberli W., Denzinger F., Ahlstrom A.P., Anderson B., Bajracharya S., Baroni C., Braun L.N., Bolívar E. Caceres B.E., Casassa G., Guillermo Cobos G., Davila L.R., Delgado Granados H., Demuth M.N., Espizua L., Fischer A., Fujita K., Gadek B., Ghazanfar A., Hagen J.O., Holmlund P., Karimi N.,21 Li Z., Pelto M., Pitte P., Popovnin V.V., Portocarrero C.A.,Prinz R., Chandrashekhar V. Sangewar C.V.,

Severskiy I, Sigurdsson O., Soruco A., Usubaliev R., Vincent C. 2015. Historically unprecedented global glacier decline in the early 21st century. Journal of Glaciology, Vol. 61, No. 228, 2015 doi: 10.3189/2015JoG15J017.

Zhou S., Nakawo M., Hashimoto S., Sakai A., Nairta H., Ishikawa N. 2000. Isotopic fractionation and profile evolution of a melting snowcover. Science in China (Series E), Vol. 44 Supp.